

A Study in the Cutting of Copper Cylinders Using High Explosive
Detonation Wave Interactions

by

Eugene Lee

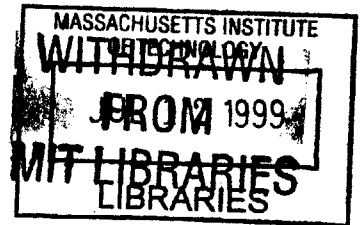
Submitted to the Department of Mechanical Engineering
in Partial Fulfillment of the Requirements for the Degree of
Master of Science and Bachelor of Science in Mechanical Engineering

at the

Massachusetts Institute of Technology

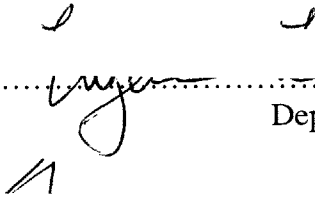
June 1999

© 1999 Eugene Lee
All rights reserved




ENG

The author hereby grants to MIT permission to reproduce
and to distribute publicly paper and electronic
copies of this thesis document in whole or in part.

Signature of Author..... 
Department of Mechanical Engineering
May 20, 1999

Certified by..... 
Lallit Anand
Professor of Mechanical Engineering
Thesis Supervisor

Accepted by..... 
Ain A. Sonin
Chairman, Department Committee on Graduate Students

A Study in the Cutting of Copper Cylinders Using High Explosive Detonation Wave Interactions

by

Eugene Lee

Submitted to the Department of Mechanical Engineering
on May 20, 1999 in Partial Fulfillment of the
Requirements for the Degree of Master of Science
and Bachelor of Science in Mechanical Engineering

ABSTRACT

When two high explosive (HE) detonation waves collide, they interact constructively and result in a local high pressure spike in the region of interaction. This shock wave interaction phenomenon is applied to the cutting of copper cylinders in order to better understand the metal cutting process and how geometry, in particular, radius of curvature, influences the process. The first experiment run, the convergent system, consists of a copper tube with an annulus of high explosive on the outside of the tube. The second experiment, the divergent system, consists of the same tube but with the HE on the inside of the tube. In both cases, the HE is ring-lighted on the ends and the detonation waves run down the walls of the tube and collide in the middle. This creates approximately a 600 kBar shock which results in a large shear stress that attempts to cut the copper tube in half. Data is collected using high energy, pulse x-ray machines to take dynamic radiographs of the shots, and this data is subsequently analyzed using tomographic reconstruction.

Numerical modeling of the experiments was performed using a 2D hydrocode called MESA. These calculations were compared to the experimental results in order to determine which set of strength and fracture models most accurately describes the physical metal cutting process.

Thesis Supervisor: Lallit Anand
Title: Professor of Mechanical Engineering

Table of Contents

1 INTRODUCTION.....	4
2 CONSTITUTIVE MODELS.....	7
2.1 Strength Models.....	7
2.1.1 Hydrodynamic.....	7
2.1.2 Elastic-Perfectly-Plastic.....	9
2.1.3 Johnson-Cook Strength Model.....	9
2.2 Fracture Models.....	13
2.2.1 Johnson-Cook Fracture Model.....	13
2.2.2 Johnson Spall Model.....	14
2.3 Equation of State.....	17
2.4 Cases to Examine.....	19
3 EXPERIMENTAL DESIGN AND SETUP.....	20
3.1 Copper.....	20
3.2 Shot Geometry Selection and Design.....	21
3.3 Experimental Setup.....	23
4 RESULTS AND ANALYSIS.....	30
4.1 Radiographs.....	30
4.2 Tomographic Reconstructions.....	30
4.3 Numerical Analysis.....	32
4.4 Qualitative Analysis.....	36
4.5 Quantitative Analysis.....	37
5 DISCUSSION.....	41
5.1 Strength Models.....	41
5.2 Fracture Models.....	44
5.3 Other Considerations.....	47
5.3.1 High Explosive Burn Models.....	47
5.3.2 Mesh Resolution.....	49
5.3.3 Ring Lighting System Effects.....	50
5.4 Influence of Curvature.....	52
6 CONCLUSIONS.....	54
7 LIST OF FIGURES.....	59
8 REFERENCES.....	116
9 APPENDIX.....	118

1.0 Introduction

Many aspects of the use of high explosives to deform materials at high strain rates has long been studied, but the examination of the actual metal cutting process using detonation wave interaction has relatively recently been of interest. The direct application and primary motivation for this research will be for the multi-mode warhead program at the Los Alamos National Laboratory (LANL). The goal is to gain a better understanding of a process rather than to solve a specific problem.

Current multi-mode warheads consist of a concave metal liner with high explosive (HE) behind it. One of the modes that the warhead can be fired is by an array of detonation points right behind the liner which causes the liner to be cut in multiple locations by the numerous shock wave interactions. The liner fragments and diverges, throwing a blast of shrapnel, similar to that of a shotgun. Another mode is single point detonation point on the back of the HE, which will cause the liner to deform into an armor-penetrating slug. More concave liners can result in better slugs. However, the more concave the liner is, the harder it is for the liner to fragment in the divergent mode. The concave geometry tends to counteract the cutting action of the multiple shock wave interactions due to the resulting convergent velocity vectors. The goal is not to address this problem in particular, but rather, to characterize the metal cutting process as the curvature is varied and to determine which material computer models and fracture criterion best describe the process.

In order to accomplish this, two main types of experiments were conducted: 1) A copper tube filled with an annulus of HE, PBX-9501, and detonated using a ring-lighting system at both ends, and 2) A copper tube with the annulus of HE on the outside which is also ring-lighted simultaneously from both ends. Drawings of these setups can be seen in Figures 3.4 and 3.5. From here on in, the first case will be referred to as the divergent system and the second as the convergent system. In both cases, shock waves will propagate from each end, interact constructively, and the resulting local radial pressure increase of approximately 600 kbars will create a large shear stress that will attempt to cut the cylinder right in the middle. The geometries and dimensions for the experiments were chosen to enhance the features of interest, namely the cutting region, and to facilitate the analysis of the experimental data. For both experiments, detailed radiographs were taken of the shot at a primary time of interest using high powered pulse x-ray machines. The convergent shot was radiographed using the Pulsed High Energy Radiographic Machine Emitting X-rays (PHERMEX), and the divergent shot was captured using a less powerful 2.3 MeV machine due to the unavailability of PHERMEX.

Previous work has been done examining the cutting of flat copper and tantalum plates using the interaction of two spherically expanding PBX-9501 detonation waves at the Los Alamos National Laboratory's Dynamic Experimentation Division by Dr. Larry Hull [1]. The positive radius of curvature geometry of the copper liner in the divergent system, and the negative radius of curvature geometry in the convergent system, will hopefully lead to insightful conclusions and statements about the nature of metal cutting using HE and the influence of curvature on the process.

In order to determine the set of constitutive equations to best simulate and characterize the cutting process, it was necessary to use numerical simulation since a closed-form solution to the problem is impossible. The particular code employed was a 2D Eulerian hydrocode very commonly used for explosive/metal applications called MESA [2]. Five combinations of strength and fracture models were applied to the copper in the calculations, and the MESA results for each case were analyzed using two methods. First, the calculations were qualitatively compared to the reconstructed radiographic data by graphically overlaying the two sets of data. Second, the stress-strain histories for regions of interest in the copper were plotted to quantify the calculations and to help explain the differences between the models observed in the overlays. Through these two methods, conclusions can be drawn on what kind of improvements can be expected by using different sets of strength and fracture models, and to explain why this is so. Further modeling issues concerning HE burn models, mesh resolution, and effects of the ring-lighting systems on the experiment are also explored.

2.0 Constitutive Models

2.1 Strength Models

2.1.1 Hydrodynamic:

One of the primary goals of this research is to understand the improvements gained in modeling the cutting process as more refined and detailed constitutive models are used. As a zeroth order base case, a MESA calculation was run which assumed no strength in any of the materials, including the copper tube. This provided a look at the most simple model in which everything in the experiment was allowed to flow in a completely hydrodynamic fluid manner.

The stress tensor, σ_{ij} , in a material can be broken up into two components: a volumetric stress component ($P\delta_{ij}$), and a deviatoric stress component (σ'_{ij}) such that

$$\sigma_{ij} = P\delta_{ij} + \sigma'_{ij}. \quad (2.1)$$

where P , the volumetric or mean stress, is defined as

$$P = -\frac{1}{3}\sigma_{kk} \quad (2.2)$$

with σ_{kk} being the trace of the stress tensor. In the hydrodynamic model, all deviatoric components of the stress tensor are fixed to zero, thus the material will not support a

shear and only has volumetric strength. Therefore, what is left is $P\delta_{ij}$, which is also known as the hydrostatic pressure. Hence, in the hydrodynamic case

$$\sigma_{ij} = P\delta_{ij}. \quad (2.3)$$

The pressure in the MESA code is defined by the Equation of State (EOS), which will be discussed later in detail in Section 2.3. The EOS defines the pressure as a function of density (ρ) and internal energy (E):

$$P = f(\rho, E). \quad (2.4)$$

Therefore, since the stress deviators are zero, the EOS drives the volumetric response of the hydrodynamic material.

In all the strength models, a P_{\min} can also be specified, which defines a pressure threshold that must be exceeded before the material is allowed to expand, and thus dropping the density below the EOS-predicted value. P_{\min} is often set negative to mimic the behavior of a compressible fluid. When the spherically tensile state of P_{\min} is reached, additional mass flow divergence will cause the pressure to stay at P_{\min} , and the density will be reduced to satisfy mass conservation until the material is recompressed.

It was important to examine this hydrodynamic case because it gave us a standard to which subsequent cases using various strength and fracture model could be compared.

2.1.2 Elastic-Perfectly Plastic:

This strength model simply assumes that the material has a constant yield strength. In the stress-strain plane, the material has an elastic and a plastic region, both of which are linear as shown in Figure 2.1. The models allow the copper to strain elastically up to a certain yield strength. In this region, a material can be strained, relieved, and still return to its original shape. However, once the yield strength is surpassed and the plastic region is reached, the material will always have a constant level of stress independent of strain. Once relieved, it will have the same elastic recovery, but also have a permanent deformation associated with it.

2.1.3 Johnson-Cook Strength Model:

To understand this model better, it is necessary to begin with the deviatoric strain rate which is equal to an elastic component and a plastic component:

$$\dot{\epsilon}'_{ij} = \dot{\epsilon}'_{ij}{}^{e'} + \dot{\epsilon}'_{ij}{}^p. \quad (2.5)$$

The elastic and plastic components are,

$$\dot{\epsilon}'_{ij}{}^{e'} = \frac{\dot{\sigma}_{ij}}{2G} \quad (2.6)$$

and

$$\dot{\epsilon}_{ij}^p = \frac{3}{2} \dot{\epsilon}^p \left(\frac{\sigma'_{ij}}{\sigma} \right) \quad (2.7)$$

respectively, where $\dot{\sigma}'_{ij}$ is the stress rate, G is the shear modulus, $\dot{\epsilon}^p$ is the equivalent plastic strain rate, σ'_{ij} is the deviatoric stress, and σ is the equivalent flow stress:

$$\sigma = \sqrt{\frac{3}{2} \sigma'_{ij} \sigma'_{ij}}. \quad (2.8)$$

Solving Equation 2.7 in terms of σ'_{ij} yields,

$$\sigma'_{ij} = \frac{2}{3} \left(\frac{\sigma}{\dot{\epsilon}^p} \right) \dot{\epsilon}_{ij}^p. \quad (2.9)$$

The equivalent stress, σ , is also a function of the plastic strain, ϵ^p , the plastic strain rate, $\dot{\epsilon}^p$, and the temperature, T .

$$\sigma = f(\epsilon^p, \dot{\epsilon}^p, T) \quad (2.10)$$

Therefore, the deviatoric stress components also become a function of plastic strain, plastic strain rate, and temperature.

Of the strength models used in the calculations, the Johnson-Cook strength model is the only one that takes into account strain hardening, strain rate, and temperature

effects. The Johnson-Cook equation is the specific form of Equation 2.10, and it relates the equivalent flow stress, σ , to the equivalent plastic strain, ϵ^p . It is expressed as:

$$\sigma = [A + B\epsilon^{p^n}][1 + C \ln \dot{\epsilon}^{p*}][1 - T^{*m}], \quad (2.11)$$

where A, B, C, n, and m are material constants, $\dot{\epsilon}^{p*} = \dot{\epsilon}^p / \dot{\epsilon}_0^p$ is a dimensionless strain rate, and $T^* = (T - T_{\text{room}}) / (T_{\text{melt}} - T_{\text{room}})$ is a dimensionless temperature for $0 \leq T^* \leq 1.0$.

The expression in the first brackets of Equation 2.11 incorporate the strain-hardening effect. The constant, A, is equal to the material yield strength while B and n determine the influence of strain hardening. This reveals the primary disadvantage of the model which is that it is empirical and therefore has no sound physical basis. Also, as will be discussed later, there is no one set of material constants that will accurately model behavior through the whole spectrum of strains, strain rates, and temperature. For example, one set of constants might model the low strain rate behavior very accurately, but then completely over-predict for large strains. What makes the Johnson-Cook strength model so popular and desirable is that it is simple to implement in a computer code and does not require excessive computing time or memory. Constants for a variety of materials can be obtained through a limited number of laboratory tests, and the effects of the important variables can be identified and separated easily. The constants A, B, and n are usually obtained through numerous isothermal torsion and tension tests at strain rates below 1.0 s^{-1} . The second bracketed expression represents the strain-rate effect. Through torsion tests at various strain rates, quasi-static tensile tests, and Hopkinson Bar

tensile tests at a strain rate of about 400 s^{-1} , the constant C was determined. Finally, the third bracket representing temperature dependence contains the thermal softening constant, m . It was calculated through more Hopkinson bar tests done at different temperatures [3].

For OFHC copper, these constants have been determined by researchers at Los Alamos, and an independent check for high strain rate validity of the constants and of the model was done by comparing high strain rate copper cylinder impact tests to numerical simulations using the EPIC-2 hydrocode. These impact test, or Taylor-Anvil tests, provided strains in excess of 2.0 and strain rates in excess of 10^5 s^{-1} . The results showed a fairly good agreement between the data and the calculation, and were deemed acceptable for most applications. The cylinder impact test data was not incorporated into the model, but rather used as a check for high strain rate cases [4]. However, in a study done about five years later, Johnson and Holmquist attempt to modify the constants to the Johnson-Cook strength equation for higher strain and strain rate applications. Using copper cylinder impact test data again, the five constants (A, B, C, m, n) are iterated through until the model achieved an exact fit with the experimental data. It was concluded that these new, revised set of constants could be used with confidence for applications with maximum equivalent plastic strains of about 0.6 and strain rates around 10^4 to 10^6 s^{-1} . Despite the fact that maximum plastic strains of around 2.0 were reached in the impact tests, it was found that the majority of the cylinder experienced strains of 0.6 or less. Consequently, the fitting process reflected the low strain regime (<0.6) well, but do not necessarily provide a good representation for larger strains [5].

2.2 Fracture Models

2.2.1 Johnson-Cook: Fracture Model

This model, also known as the Johnson-Cook Damage model, introduces a new damage variable. Damage is defined as

$$D = \sum \frac{\Delta \epsilon}{\epsilon_f} \quad (2.12)$$

where $\Delta \epsilon$ is a small increment of equivalent plastic strain per time step and ϵ_f is the equivalent strain to fracture for a given strain rate, temperature, pressure, and equivalent stress. As the plastic strain increases, the damage accumulates until it reaches a value of 1.0, at which point the material “fails” and all stress tensors are set to zero. The equivalent strain to fracture can be expressed in a similar form to that of the Johnson-Cook strength equation and is given by

$$\epsilon_f = [D_1 + D_2 e^{D_3 \sigma^*}] [1 + D_4 \ln \dot{\epsilon}^*] [1 + D_5 T^*] \quad (2.13)$$

where D_1 through D_5 are experimentally determined material constants, and where $\dot{\epsilon}^*$ and T^* are the same as those used in Equation 2.11 for the Johnson-Cook strength model. The σ^* is a dimensionless pressure-stress ratio also known as triaxiality. It is defined as the average of the three normal stresses divided by the von Mises equivalent stress,

$$\sigma^* = \frac{-\frac{1}{3}\sigma_{kk}}{\sqrt{\left(\frac{3}{2}\right)s_{ij}s_{ij}}} \quad (2.14)$$

where σ_{ij} and s_{ij} represent the stress and stress deviator tensors. For the two dimensional, axi-symmetric copper tubes in particular, Equation 2.14 can be expanded out to

$$\frac{-\frac{1}{3}(\sigma_{rr} + \sigma_{\theta\theta} + \sigma_{zz})}{\sqrt{\frac{3}{2}[s_{rr}^2 + s_{zz}^2 + s_{\theta\theta}^2 + 2s_{rz}^2]}} \quad (2.15)$$

In Equation 2.13, the first three constants, D_1 , D_2 , and D_3 , are determined through isothermal torsion, notched quasi-static tension, and unnotched quasi-static tension tests. The last two constants, D_4 and D_5 were obtained from the unnotched tension tests and the Hopkinson bar tension tests at various temperatures [3].

2.2.2 Johnson Spall Model

The Johnson Spall, or Johnson Void Growth, model assumes that spallation in a ductile material is due to localized plastic deformation around small voids present in the material which grow and eventually coalesce to form a spall plane. Voids in the material are assumed to be spherical and evenly distributed throughout the material in order to simplify the derivation. Furthermore, in the spallation process nearly all the volume change is associated with hole growth rather than density reduction in the solid

constituent surrounding the voids. One of the first conclusions reached is that void growth in a material begins at a mean tensile stress of

$$p_{eq} = -\frac{a_s}{\alpha_0} \ln \frac{\alpha_0}{\alpha_0 - 1} \quad (2.16)$$

where a_s is an experimentally determined constant and α_0 is the initial distention. The distention is defined as $\alpha = V/V_s$, where V is the total volume of a given porous material, and V_s is the volume of solid material within V . Further, the porosity of the material is defined as $\phi = (\alpha - 1)/\alpha$. The material begins with an initial porosity and as a mean tensile stress is applied to it, the porosity does not change until it reaches this p_{eq} , at which point void growth begins. Once growth does begin, another relationship is derived to describe the rate at which the voids grow, and that is given by

$$\begin{aligned} \dot{\alpha} &= 0, \Delta p \geq 0 \\ \dot{\alpha} &= -\frac{(\alpha_0 - 1)^{2/3}}{\eta} \alpha (\alpha - 1)^{1/3} \Delta p, \Delta p < 0 \end{aligned} \quad (2.17)$$

$$\Delta p \equiv \bar{p} - p_{eq}, \bar{p} = -\frac{1}{3} \sigma_{kk}$$

where α is the distention, η is a viscosity-like parameter that gives the materials resistance to the rate of void growth, and \bar{p} is the externally applied pressure (negative in tension). Equation 2.17 tells us that there will be void growth and that the voids will grow at a rate of $\dot{\alpha}$ only if the material is in tension and the applied tensile pressure is greater

than p_{eq} . If the material is in compression, or if the mean tensile pressure applied is less than p_{eq} , then there will be no void growth. The particular version of the spall model used does not allow for void closure. The derivations for Equations 2.16 and 2.17 can be found in Jim Johnson's paper on dynamic fracture and spallation in ductile solids [6].

The material constants for copper such as η and a_s were determined using a copper flyer plate experiment. This consisted of a 0.6 mm thick copper plate striking a 1.6 mm thick copper target backed with a thick plate of PMMA (polymethylmethacrylate) at an impact velocity of 0.016 cm/ μ s and creating a peak tensile stress of about 15 kbars. Calculations using the model and the determined material parameters were found to predict the spall plane and the target porosity very well. To prove the model's generality with regards to the dynamic ductile fracture of copper, a second experiment was conducted which produced much higher tensile pressures in the copper. A 25 mm thick plate of copper was placed in contact with a 12.7 mm thick piece of composition B-3 which was initiated with a P-40 plane wave generator. This generated a peak tensile stress of close to 100 kbars in the copper plate and a radiograph of the experiment showed multiple spall layers present. A calculation done using the numerical finite-difference code SIN and implementing the Johnson Spall model not only gave the correct spall locations and thicknesses, but it also showed the unusual way in which porosity changes with time by accurately predicting the order in which the spall layers were produced. Therefore, the Johnson Spall model and the referenced constants used for the calculations have both low and high pressure validity [6].

2.3 Equation of State

It should also be noted that in all cases the linear U_s - U_p (Mie-Gruneisen) model was used for the copper's equation of state (EOS). In examining a shock wave running through a material, the velocity of the shock can be defined as U_s , and the velocity of the material particles at the shock front and behind it can be defined as U_p . The particle velocity ahead of the shock, relative to the shock velocity, is zero assuming that the shock is supersonic. The material ahead of the shock, or pre-shocked material, exhibit the initial conditions of pressure P_o , density ρ_o , and energy E_o . At and behind the shock, the conditions have changed and are at pressure P , density ρ , and energy E . Performing a conservation of mass, momentum, and energy between the shocked and pre-shocked material regions the following three equations,

$$\rho_o U_s = \rho(U_s - U_p) \quad (2.18)$$

$$(P - P_o) = \rho_o U_s U_p \quad (2.19)$$

$$E - E_o = \frac{1}{2}(P + P_o)(V_o - V), \quad (2.20)$$

are arrived at respectively. There are three equations and five unknowns (U_s , U_p , ρ , P , and E) which means that an additional equation is needed to be able to determine all parameters as a function of one of them. This fourth equation is known as the U_s - U_p EOS and for most metals has the form

$$U_s = c_o + sU_p \quad (2.21)$$

where c_o is the material sound speed at zero pressure, and s is a constant. This is an empirically based relationship and both constants have been experimentally determined for numerous materials [8]. Now, various curves like pressure versus specific volume, or pressure vs. particle velocity can be plotted, and these curves, known as Hugoniot, define a locus of all shocked states in a material.

For many applications, such as shock wave impedance matching calculations involving rarefaction waves, the relationships above are not sufficient. The shock wave data can be extended off the Hugoniot by applying the Mie-Gruneisen EOS,

$$P = P_H(V) + \frac{\Gamma(V)}{V} [E - E_H(V)], \quad (2.22)$$

where the Gruneisen Gamma

$$\Gamma(V) = V \left(\frac{\partial P}{\partial E} \right)_V \quad (2.23)$$

and P_H and E_H are points off the Hugoniot. The Mie-Gruneisen EOS relates a (P, V, E) state to the pressure and internal energy off the Hugoniot shock curve at the same volume. Therefore, using the U_s-U_p and Mie-Gruneisen EOS's, it is possible to numerically and adequately model the state of a shocked material [7][8].

2.4 Cases to Examine

It was not practical to examine additional constitutive models or even all possible combinations of the strength and fracture models listed above. Instead, five combinations were chosen that would best depict change in the calculated results as the models used became more and more refined. The cases chosen to be examined were:

Table 2.1: Five Combinations of Available Models for the Copper Used in Simulations of the Cylinder Cut Experiments

Case #	Strength Model	Fracture Model
1	Hydrodynamic	None
2	Elastic-Perfectly-Plastic	None
3	Johnson-Cook	None
4	Johnson-Cook	Johnson Spall
5	Johnson-Cook	Johnson-Cook Damage

There are numerous other constitutive models available such as the Mechanical Threshold Stress (MTS) model [9] and a more recently developed crystal plasticity based model that was shown to satisfactorily predict the behavior of commercially pure b.c.c. tantalum under a wide range of strains and strain-rates [10]. These and other pertinent models were not included in the study as they were not readily available for implementation into the MESA hydrocode.

3.0 Experimental Design and Setup

3.1 Copper

In designing the experimental setup it was desirable to keep as many variables constant between the divergent and convergent systems, and to have as many material parameters known as possible in order to make any meaningful comparisons. One of the many aspects of the design that especially required this level of attention was the copper tubing. The copper that was eventually used in the experiments initially came in the form of 3" thick hot rolled plate from Eglin Airforce Base in Florida. The stock is nominally 0.9999 pure copper with a grain size on the order of several hundred microns. The copper is highly controlled and characterized, and has had many low and high strain rate tests done on it. To form the plate stock into tubes, it is first upset forged, then clock-rolled to a final thickness of 0.2". The method employed does not result in any planar anisotropies even though the texture is not isotropic in the through-thickness direction. Next, the thin plate is rolled into cylindrical form and the seam is e-beam welded together. The cylinder is then pressed through a die to form the outer diameter and to ensure adequate roundness. Finally, the copper tube is annealed at 300°C for one hour and then machined down to final specifications. After all this processing, the copper has a fairly fine grain structure with an average grain size on the order of 20 microns, as can be seen in Figure 3.1. The micrograph is oriented such that the horizontal direction in the picture corresponds to the circumferential direction of the cylinder.

3.2 Shot Geometry Selection and Design

The most important part of the shot setup selection was the choice of wall thickness and radius of curvature for the copper cylinders. It was desirable to choose a geometry which would result in a full or semi-complete cut. Through two preliminary divergent shots it was learned that a 1.2"OD, 0.1" wall thickness tube filled with PBX-9501 was cut rather easily. The setup and resulting radiographs can be seen in Figures 3.2 and 3.3, and it is rather obvious from inspection that the cylinder did cut cleanly. In these small experiments the 9501 was detonated from both ends simultaneously and the radiographs were taken using 450 keV x-ray machines. The 9407 in Figure 3.2 represents a PBX-9407 booster pellet and the SE1 is the detonator used. Employing these ensure a reliable, symmetric detonation of the 9501.

However, in examining the MESA calculations for the same geometry in the convergent system, it seemed that the copper tube would collapse on itself well before it was cut. Therefore, after performing several subsequent calculations on MESA, it was found that a OD of 6" and wall thickness of 0.1" could possibly allow the convergent system enough time to experience the full effect of the shock wave interaction. As radius of curvature is increased, the tube begins to approximate a flat plate and the cutting process becomes much easier, and there is much more time for it to cut. However, it was the largest geometry that fit easily within the copper and 9501 manufacturing constraints. The largest diameter 9501 parts that could be conveniently fabricated was 8" and so 6"OD on the copper seemed reasonable enough to leave sufficient room for a ring-

lighting system on the ends of the tube. As for the 0.1" wall thickness, the copper could not be rolled much thinner without running into problems with getting it perfectly round.

Having chosen the geometry of the copper tubing, it was then necessary to design a convergent and a divergent system which would drive the copper tubes with about the same forces and under similar conditions. Figures 3.4 and 3.5 show the shot designs for both these systems.

The PBX-9501 annulus on both systems had a wall thickness of 0.75" and a length of 4". This is to ensure that the copper tube is driven out with the same radial force. To demonstrate this, the dynamic variable of radial velocity of a particle in the middle of the copper wall at $z=0$ (r-z coordinate system as defined in Figures 3.4 and 3.5) was compared between the convergent and divergent systems. The graph derived from MESA, in Figure 3.6, shows how closely the systems compare in this regard. In order to facilitate the visual comparison, the divergent velocity curve was inverted.

The next consideration in the design was to implement a ring-lighting system which would effectively detonate the 9501 annulus symmetrically and simultaneously. This end cap, ring-lighter would also have to 1) stop HE products from shooting into the copper tube, 2) attenuate any shock waves propagating into the inside of the tube, and 3) prevent the HE annulus from being shock desensitized before it is detonated. In both designs, there are polyethylene and stainless steel end caps which physically prevent HE products from entering the tube. These particular materials were chosen for their very different values of impedance, polyethylene having a low impedance and stainless steel having a high impedance. When a shock travels across an interface of two materials with

dissimilar impedance, the shock gets attenuated to a certain degree. This is called impedance mismatching attenuation and the larger the difference between the two values, the more attenuation that occurs. Finally, the reason polyethylene was put in contact with the 9501 ring-lighter was because it has a slow sound speed, allowing the detonation wave to reach the 9501 annulus before the shock waves could travel out through the polyethylene and desensitize the 9501 annulus. Therefore, the polyethylene and stainless steel caps on the convergent system and the discs on the divergent system accomplished all three requirements mentioned above. The tapered shape of the convergent system HE ring-lighter was designed to allow the detonation wave to more easily traverse the 90° direction change in the corner. In both systems, the contact region between the HE ring-lighter and the HE annulus was 1/8" on the radius, about 2mm more than the minimum needed for the detonation wave to jump across the interface.

3.3 Experimental Setup

The convergent experiment was run at the PHERMEX facility at the Los Alamos National Laboratory in the Dynamic Experimentation (DX) Division. In order to produce such high energy x-rays a conical beam of electrons, of at least 1000 amps, is first produced by a sintered-tungsten cathode, and then run through six magnetic focusing lenses which control the diameter and convergence angle of the beam. Next, the electron beam goes through three high-energy, rf amplifier driven accelerator cavities. Upon exiting the third cavity, the beam energy is at least 30 MeV. The beam is then collimated through two more sets of magnetic lenses into a spot size of typically 3mm which finally

hits the tungsten target producing high energy x-rays. The beam passes through a set of rough, half-angle collimators, and usually have a dose of 350 R at 1m and have a pulse width of approximately 200 ns. For the experiment in particular, PHERMEX was not at peak performance and the spot size was at 4.5mm. Therefore, a 1.7mm spot size collimator was used and even though that reduced the dose to about 100 R at 1m, that was enough to penetrate the relatively thin walled copper cylinder.

On the firing point, the shot was oriented vertically and placed on a shot stand at 4 m away from the tungsten target on axis with the beam. The film pack was positioned behind the shot at 8 m away from the tungsten target, also on axis. This set of distances was chosen to optimize resolution while keeping the entire image on the film and not over exposing, or saturating, the film. For a 1.7 mm spot, the resolution increases in a linear fashion up until approximately a magnification factor of 1.75 where it then continues to increase but at a decreasing rate [11]. The magnification factor is equal to the distance from the tungsten target to the film divided by the distance from the tungsten target to the shot. Therefore, in the experiment the standoff distance from target to shot was chosen to be equal to the distance from shot to film in order to get a magnification factor of 2, which would result in a high resolution radiograph while allowing the entire copper cylinder to fit on 14"x17" film. The second, perhaps more important issue was that of not saturating the film with too much dose. From the source on the tungsten target, the dose was 100 R at 1m and falls off as the inverse of distance squared. Therefore, the dose that the film sees taking into account distance and attenuation through the shot is equal to:

$$I_{film} = I_o \left(\frac{1}{r^2} \right) \left[e^{-\left(\frac{\mu}{\rho} \right) (\rho l)} \right] \quad (3.1)$$

where I_o is equal to the dose produced by PHERMEX at 1m, r is the distance from the tungsten target to the film pack, μ/ρ is equal to approximately 0.318 for copper, and ρl is the path length through the object which was calculated to have a maximum value of about 41 g/cm². Inserting these values into Equation 3.1 gives an estimated dose of 420mR at the film pack. As a result of the actual densities of the shot varying quite a bit, this value was only meant to give an idea of the range of film that should be used. Four different types of film were put into the film pack in order to cover the large dynamic range of the shot. In ascending film speed and sensitivity, AA, F, DEF, and storage phosphors were used to cover anything from about 1R to several milliR of dose. The storage phosphors were the most sensitive, yet also had the largest dynamic range, being able to take up to several hundred milliR before saturating. The phosphors were chosen to be the primary film for that reason and because they have a linear response, have no background fog, and are more easily processed using a laser scanner rather than the conventional chemical baths.

Having designed the film packs and chosen standoff distances, the shot was setup on the PHERMEX firing mound. Figure 3.8 shows the setup for the convergent system. An additional film pack was put at 3 meters in front of PHERMEX, between the target and the shot, in order to photograph the dynamic beam profile. This information would be used later to aid in the reconstruction of the data because the x-ray beam is not a uniform

distribution. Rather, it is most intense in the center and weakens as you go further out. Half inch thick pieces of glass were placed in front of both film packs to slow down any fragments thrown at them. This prevented the aluminum casing of the pack from being punctured and ruining the film. Statics were taken of the shot assembly on to the film pack at 8 meters simply to verify alignment and proper exposure.

Unfortunately, after completing the convergent experiment, PHERMEX became unavailable due to mechanical failure of the electron gun and therefore the divergent shot had to be conducted elsewhere. The second best option available was using a 2.3 MeV x-ray machine despite the fact that its dose output is significantly lower, about 100 mR at 1 meter, and that its spot size is significantly larger, measuring at least 5mm in diameter. This loss in performance resulted in less x-ray penetration through the shot and increased x-ray scatter which decreased the resolution and increased the noise of the data. In order to counter the effect of lost dose the film pack was moved slightly closer to the x-ray source and more sensitive film was used. Again, storage phosphors were chosen to be the primary film because of their ability to detect even a several hundred μ R dose signal. The other two types of film put into the film pack were Biomax and XAR, both of which are used commonly in the medical industry. They are highly sensitive and require light screens to be placed in between the films rather than lead. In the effort to increase resolution, the magnification factor was reduced by placing the shot further away from the source and closer to the film. Since blur is equal to the spot size times the magnification factor minus one, the increased spot size needed to be offset by lowering the magnification factor. With such a big spot on the 2.3 MeV, scatter of the x-rays

presented a problem to resolution. The beam comes out at a relatively large divergence angle and x-rays tend to scatter off of the air and any surrounding objects onto the film, making the data extremely noisy. To counteract this scatter, two lead collimators, shown in Figure 3.7, were used. The first stage of collimation was accomplished by placing the two inch thick lead doughnut directly over the 2.3 MeV spot with the center of the doughnut in line with the center of the beam. The second stage of collimation consisted of a lead brick wall built in a similar fashion to the one in Figure 3.7 and placed one meter in front of the shot. The bricks were approximately 3" thick and the 6" x 8.5" window was calculated to just be big enough to capture the entire experiment at the time of interest. Finally, a thin sheet of lead was placed directly behind the 14x17" film pack to prevent x-rays from bouncing off objects behind the film and exposing the film from behind. The shot was done at a firing point called Meenie Site and the setup was done as shown in Figure 3.9. The standoff distances chosen were 6 meters from source to shot and 1 meter from shot to film pack, giving a magnification factor of 1.167. For protection from the ensuing copper fragments, half inch plates of aluminum and lexan were placed at an angle in front of the 2.3 MeV and the film pack. Once again, statics were taken of the shot to ensure proper alignment of the shot and exposure of the films.

In assembling the shots, both were put together and placed on the shot stand vertically, meaning the z-axis was perpendicular to the table. The convergent system was all dry fit together with each piece simply fit and stacked onto the rest of the assembly. In the divergent case, only the top polyethylene and stainless steel discs inside the 9501 annulus were glued into place so that they would not slide down inside. In both

assemblies, vacuum grease was put in between the 9501 end cap and inner polyethylene interface to ensure that there were no air gaps caused by imperfections in the parts from machining. Air gaps would cause the shock wave to run up faster in those parts along the gaps and this would result in an asymmetrical lighting of the 9501 annulus.

As mentioned in Section 3.1, the copper tubes used in these experiments were manufactured with weld lines in them which have much larger and varying grain sizes, resulting in unpredictable behavior in that small region. Therefore, the position of the line was kept track of and when placed on the shot stand, was oriented 45 degrees off the beam axis as shown in Figure 3.10. This was thought to be the optimal position so that it would not be in the two critical places on the radiograph, namely the tube wall and right in the middle of the picture. These are at 0 and 90 degrees so 45 appeared to be a good choice, the furthest away from both areas.

The final issue in the shot setup was timing. For the convergent case, it was desirable to photograph the tube when the cutting region was the most under-dense, and when that particular feature was the largest. Using MESA, it was observed that this occurred at approximately 38 μs and, therefore, PHERMEX was pulsed at exactly that time. In order to make the divergent experiment as comparable to the convergent as possible, it was necessary radiograph the experiment at an “equivalent” time. To find this equivalent time, the time at which the detonation waves first collide at the middle of the copper cylinder was defined as t_0 . Setting the wave collision time, t_0 , as the reference time in both experiments effectively eliminated the difference in ring-lighting systems. Looking at the MESA calculations for both cases, this t_0 time was found to be

approximately $24.3 \mu\text{s}$ for the convergent case and $16.7 \mu\text{s}$ for the divergent case.

Therefore, a Δt can now be defined as the radiographic time minus t_0 . The radiographic time for the convergent system was $38 \mu\text{s}$, so Δt was $13.7 \mu\text{s}$. Once this Δt was added to the divergent t_0 , it told us that a radiographic time of about $30.4 \mu\text{s}$ was needed for the divergent experiment to make adequate comparisons. The actual radiographic times that these shots were taken at were $37.995 \mu\text{s}$ and $30.340 \mu\text{s}$ for the convergent and divergent experiments respectively.

4.0 Results and Analysis

4.1 Radiographs

After each experiment, the film packs were recovered and taken to be processed. The hard films were developed using the traditional chemical baths and then the images were scanned in on a microdensitometer at a resolution of 200 micron pixels. The Fuji storage phosphors were simply scanned with a Fuji scanner built specifically for that purpose at the same 200 micron pixel resolution. Through careful comparison of the resulting radiographs in each experiment, it was determined that the phosphors gave the best results in terms of exposure level. It should be noted that in the divergent experiment, there was a small light leak into the film pack which ruined the hard films, but seemed to have little or no effect on the phosphors as they are relatively insensitive to sunlight. The light leak was caused by improper taping of the film pack. Figure 4.1 shows these radiographs obtained from the storage phosphors for each experiment. The radiographs show the cylinders standing on end and the dark trapezoidal shapes are the stainless steel end caps.

4.2 Tomographic Reconstructions

In order to better visualize the copper tubes, a tomographic reconstruction was performed on the radiographs. This is the method used to obtain the cross-section of a three-dimensional, axially symmetric object from a radiograph of the object oriented with its axis of symmetry perpendicular to the radiographic axis. It is the extension of the

Abel inverse, determined by N.H. Abel in 1826 [12] in order to reconstruct the profile of a 2-D, circularly symmetric object from its projection. The benefits in using tomographic reconstruction are improved delineation of material boundaries, enhanced display of minor variations from axial symmetry, and often times revealing features in the object too subtle to be seen from the radiograph. In general, it effectively removes the overlying material from the radiograph and increases the contrast. The optical density given by the radiograph is assumed to be a function of the exponential of the pathlength. The axially symmetric object is then considered to be composed of a series of nested, concentric annuli whose amplitudes are to be determined from the pathlengths. Using the bowtie method, the amplitudes of each annuli is determined by working inwards from the outermost annuli by assuming that the pathlength is equal to a bow-tie structured matrix, called the measurement matrix, multiplied by the amplitude. The details of the reconstruction theory and process can be found in Hanson's paper on tomographic reconstruction [13]. The reconstructions of the radiographs for the two experiments can be seen in Figure 4.2.

As witnessed by comparing Figures 4.1 and 4.2, the walls of the copper tubes become much easier to see with sharper definition and contrast. One drawback to this type of tomographic reconstruction is the large amount of noise associated with the axis of symmetry. This is caused by the fact that the image is resolved from outside to inside, and each successive iteration through the annuli carries over error which builds up and causes poor signal-to-noise quality in the middle. The cylindrical geometry was chosen particularly for this reason so that the regions of interest would be as far off the center

axis as possible. All radiographic manipulation and reconstruction were done on a software package.

4.3 Numerical Analysis

In order to examine the effects of different strength and fracture models with respect to the process of cutting copper tubes, numerical simulations were run using a hydrocode. Since the experiments were axially symmetric, only a two-dimensional code was needed and the choice was MESA 2-D, a standard and much used code for these types of applications. The MESA 2-D code is a collection of programs typically used for hydrodynamic calculations and applied to high explosive systems involving materials such as various metals, plastics, and gases. Originally developed for armor anti-armor applications, it's strength lies in compressible flow and "fluid like" metal deformation problems. The code also has various fracture, strength, spall, and void growth models to accurately simulate dynamic material behavior, especially at extremely high strain rates. The main program in the hydrocode is a second order, Eulerian, explicit finite difference code. It establishes a fixed mesh of cells and allows the various material region to move through them while keeping track of the conditions inside and around the boundaries of the cells. In addition, a very attractive feature of the code is the ability to place massless tracer particles in any cell. These tracer particles are Lagrangian and record up to twenty-two variables (velocity, pressure, density, etc.) over time. After running these calculations using various strength and fracture models, images can be produced of the experiments at the exact times the radiographs were taken. These calculated images were then

qualitatively compared to the reconstructions of the data in order to examine the effect of using different constitutive models. For each case, a history of the conditions in the cut region and off of the cut region of the copper can be plotted to help quantify the results and provide some explanation for the qualitative differences.

The five cases examined, listed back in Chapter 2, all required having the correct material constants to be used in the MESA input files. Table 4.1 shows a list of the copper alloy 101 constants used for all the major variables required for each material model. The full input files can be found in the Appendix, which contain all of the material parameters for all materials.

Table 4.1: MESA Input Parameters for Copper Alloy 101

Model	Parameter	Symbol	Value [Units]
U _s /U _p EOS [14]	Sound Speed	C _o	0.394 [cm/μs]
	Slope of U _s /U _p Curve	S	1.489
	First Gruneisen Ratio	Γ _o	0.0
	Second Gruneisen Ratio	Γ ₁	2.02
Elastic-Perfectly-Plastic Strength [14]	Density	ρ	8.93 [g/cc]
	Yield Strength	Y _o	1.2 [kbars]
	Shear Modulus	G _o	477 [kbars]
Johnson-Cook Strength [16]	Yield Strength	A	0.35 [kbars]
	Strain Hardening Coefficient	B	3.75 [kbars]
	Strain Rate Coefficient	C	0.0175
	Strain Hardening Exponent	n	0.3
	Thermal Softening Exponent	m	1.2
	Melt Temperature	T _{melt}	1356 [K]
	Room Temperature	T _{room}	298 [K]
Johnson Spall Fracture [6]	Initial Distention Ratio	α _o	1.0003
	Defines Strength at which Void Growth Begins	a _s	1.7 [kbar]
	Defines Resistance to Void Growth (Viscosity-like)	η	10 [P]
	Poisson's Ratio	ν	0.345
Johnson-Cook Damage [3]	First Fracture Constant in Strain to Failure Relation	D ₁	0.54
	Second Fracture Constant	D ₂	4.89
	Third Fracture Constant	D ₃	-3.03
	Fourth Fracture Constant	D ₄	0.014
	Fifth Fracture Constant	D ₅	1.12
	Damage Level at which Failure Occurs	D _{failure}	1.0

The Johnson-Cook strength constants were derived from work done recently at the Los Alamos National Laboratory by Shuh-Rong Chen and George T. Gray III of the Materials Science and Technology division. Copper alloy 101, from the same stock and in the same condition as was used for the copper cylinder experiments, was put through a series of mechanical testing under varying temperatures and strain rates. The stress-strain

data from these tests were plotted and a set of Johnson-Cook strength constants were found that best fit the data for the high strain application of cylinder cutting. This meant over-predicting at low strains so that the high strain regions, about 30% and higher, the Johnson-Cook fit would be accurate. The actual mechanical property measurement and fitting procedure can be found in Chen and Gray's paper [15]. Seen in Figure 4.3 is data from three of the tests and their respective fits. There were actually 12 separate tests done, but the three shown are representative of the varying strain rate and temperature ranges.

Two sets of constants were actually derived by Chen, one being the set that was used in the modeling and one for even higher strain and strain-rate applications. The set that was used is mainly applicable to strain ranges of 0.1-1.5 at rates of less than $10^4/s$. This was a refinement of the constants that Johnson and Cook first derived using the method described in Chapter 2. These constants were later modified by Johnson by fitting the model to Taylor cylinder impact tests to capture high strain and strain rate behavior [5]. The second fit derived by Chen was a refinement of this second set by Johnson. It attempted to predict the greater than $10^4/s$ region by over-predicting anything below $10^3/s$. In order to decide which set of Chen's constants to use, calculations were done using both sets of constants and the results were compared to the experimental data using the overlaying method described in the next section, 4.4. It was found that Chen's first set fit better despite the fact that the strain rates in the experiments were found to be in the 10^4 to $10^5/s$ region. One reason for this may be due to the fact that these fits were done on constant temperature experiments. In reality, the copper cylinders undergo adiabatic

heating and this causes the stress-strain curves to increase slower than predicted at constant temperatures in the higher strain regimes. Thus, in Chen's second, high-rate fitting, the constants derived may be over-predicting at high strains too and thus resulting in a calculation that is not accurate. Therefore, the lower strain rate constants do a better job in predicting at high strains [16].

4.4 Qualitative Analysis

In order to best compare the experimental data to the calculations, it was necessary to manipulate them such that the two could be overlaid on one another. First, a surface reconstruction was done on the experimental data such that the edges of the copper tube were extracted from the tomographic reconstruction and plotted out. Next, a MESA output file containing detailed density information of the simulation at the experimental time, is read and transformed into a synthetic radiograph. Finally, the experimental edge fit and the MESA calculation could then be overlaid for each of the material model cases and give a good representation of how well the two match. Figures 4.4 and 4.5 show these overlays for all five model cases for the convergent and divergent experiments respectively.

It can be easily seen that in the divergent overlays, the edge fit is both lower resolution and not quite as symmetric as the convergent case. Recall that the divergent experiment was radiographed using a 2.3 MeV x-ray machine as compared to the convergent which was done on the 30 MeV PHERMEX. The lower energy of the 2.3 MeV x-rays and the machine's bigger spot size resulted in lower resolution and increased

noise. Therefore, the edge fit becomes thicker and noisier, but is still usable data. The convergent edge fit is higher fidelity and in the analyzing the overlays they will be considered first, while using the divergent overlays as a secondary measure to estimate how close the experiment was to the calculation. The asymmetries associated with divergent shot may be due to air gaps in between the PBX-9501 end cap disc and polyethylene end cap parts. These 9501/Polyethylene interfaces were filled with a thin layer of vacuum grease, but if any air gaps existed, this would cause the detonation wave to travel faster through the gap region and thus cause asymmetries in the experiment. Both the convergent and divergent experiments required the use of vacuum grease, but the air gap problem appears to have only occurred in the divergent case. Perhaps in the future, redesigning the ring-lighting systems to avoid these explosive/material interfaces would result in more consistent and symmetric wave propagation. Despite this fact causing the right side of the reconstruction to be off, the left side matches fairly well, and the most important region, the cut region, on the left side matches well enough to use for analysis. From a cursory glance at the overlays, it appears that there are no drastic changes as one iterates through the models. All of them seem to match the experimental data fairly well. However, upon closer examination, there are more subtle differences between each model and these will be discussed in the next chapter.

4.5 Quantitative Analysis

After examining the qualitative differences between the models, it was desirable to somehow quantify the calculations in order to understand better why the models

behaved as they did. Massless tracer particles were placed in various parts of the copper wall in the MESA calculations to record the conditions of the region as a function of time. Using this information, it was possible to construct stress-strain graphs for each of the cases and attempt to use the stress-strain behavior to explain the qualitative results. The two areas of particular interest were right in the middle of the cut region and far off the cut region. Figure 4.6 shows that the particles were placed right in the middle of the wall thickness to avoid any edge effects.

Once the calculations were run with the particles, it was possible to obtain both the equivalent plastic strain and the overall stress state, or triaxiality. Recall from Chapter 2 that the triaxiality is simply the mean normal stress divided by the von Mises equivalent stress. One advantage to using these variables is that it is possible to plot Johnson-Cook failure curves onto the same graph when using the Johnson-Cook Damage model as those curves are plotted on a triaxiality vs. plastic strain plane for various materials in Johnson-Holmquist's paper [3]. Another advantage to using triaxiality is that it is easy to calculate, given the stress tensors and mean pressure from the MESA particle output file. Figures 4.7 and 4.8 show the results of the particle plots varying quite a bit as compared to the qualitative overlays throughout the different model cases.

The most noticeable aspect of the triaxiality vs. plastic strain plots is the large variance in stress-strain history between the various models. These plots truly accentuate and magnify the subtle differences seen in the qualitative overlays and help provide an explanation for some of those differences. In the Johnson Spall Fracture and the Johnson-Cook Damage plots, additional information was added to the graphs to show the specific

failure criterion associated with that model. On each curve in the spall model, markers were plotted representing levels of porosity. At 30% porosity, the material is assumed to have failed and so these porosity levels were plotted up to 30% or to the highest porosity reached for the particular particle as seen in Figures 4.7(c) and 4.8(c). For the Johnson-Cook Damage model recall from Equation 2.12 that a damage variable is defined as the sum of small increments of plastic strain over time divided by ϵ_f , the equivalent strain to fracture for the current conditions of triaxiality, strain-rate, and temperature. When the damage, D , equals one, then the material is failed. So, from this it is possible to write that

$$D_c(t) + D_f(t) = 1 \quad (4.1)$$

where $D_c(t)$ is the current damage level and $D_f(t)$ is the additional damage needed to be done to reach failure. This equation can be rewritten as

$$D_c(t) + \frac{\Delta\epsilon_f(t)}{\epsilon_f(t)} = 1 \quad (4.2)$$

where $\Delta\epsilon_f(t)$ is the additional equivalent plastic strain needed to be done to reach failure. This equation was used to construct the failure curves seen above in the Johnson-Cook Damage plots. For each discrete point in time the current damage level is noted and ϵ_f is calculated from Equation 2.13 in order to get a $\Delta\epsilon_f(t)$. This additional strain to failure is

then added on to the current plastic strain to construct the failure curves seen above.

Therefore, the failure curve strain, ϵ_{fc} can be represented as

$$\epsilon_{fc}(t) = \epsilon_p(t) + \epsilon_f(t)[1 - D_c(t)] \quad (4.3)$$

where $\epsilon_p(t)$ is the current equivalent plastic strain. For each point in time, the failure curve strain is plotted versus the corresponding triaxiality. The points generated are then curve fit with an exponential form and those fits are overlaid onto the triaxiality vs. plastic strain graphs as shown in Figures 4.7(d) and 4.8(d). If and when one of the stress-strain curves hits one of these curves, the material is said to have failed under the model.

5.0 Discussion

5.1 Strength Models

As was mentioned before, upon a quick observation of Figures 4.4 and 4.5, all five model iterations seem to fit the experimental data with a fair amount of accuracy. This seems to suggest that the largest part of the degree of accuracy in simulating the experiment lies in getting the hydrodynamic part of the model correct. The strength and fracture models still play a role in determining the solution, but the overall shape and timing of the simulation appear to be somewhat insensitive to variations in the modeling. However, upon examining Figures 4.4 and 4.5 more closely, one sees that the hydrodynamic and elastic-perfectly-plastic (EPP) strength models do not predict the shape as well as the cases when the Johnson-Cook strength model was used. In the convergent overlays, small bulges of material can be seen around the cut region on the outside edge of the copper wall which are not in the data for the hydrodynamic and EPP cases. The predicted shape of the outer wall in the cut region is also slightly wider than the data. As for the divergent overlays, the left side of the overlays show similar results. In the hydrodynamic and EPP cases, the calculations predict more material in the cut region than in the experimental data or the Johnson-Cook strength cases. The EPP model gives a slight improvement over the hydrodynamic case, but the more refined Johnson-Cook strength model contributes a significant improvement and predicts the data very well. This can be explained by examining the triaxiality versus plastic strain plots in Figures 4.7 and 4.8. The EPP model shows much higher amplitudes of fluctuation in

triaxiality and allow higher strains to be reached. This is due to the Johnson-Cook model accounting for strain hardening, strain-rate effects, and temperature dependencies.

From this, the question arises as to how much influence the strength modeling has on the fracture models. If a simple strength model like EPP can predict relatively the same shape and have little influence over the fracture modeling as compared to a more refined strength model like Johnson-Cook, then that would translate into significant cost and time savings. Designers would need only a few simple mechanical tests of an uncharacterized material to use EPP, and thus would avoid the numerous tests needed to obtain Johnson-Cook parameters. To resolve this, two new sets of calculations were run. One set used EPP strength and Johnson Spall models, and the other set used EPP strength and Johnson-Cook Damage models. The results could then be compared to cases #4 and #5 from Table 2.1 where the Johnson-Cook strength model was used along with the same fracture models. In Figures 5.1-5.4, the two strength models are compared while varying the fracture model and system geometry (convergent or divergent) using MESA contour plots at the radiographic times.

In Figures 5.1, 5.2 and 5.4 the trend is clear. The choice of strength model does have an influence over the evolution of damage and porosity in the cases mentioned. With the convergent geometry (Fig. 5.1 and 5.2), using EPP over Johnson-Cook strength results in larger and more developed damage and porosity contours. Similarly, in the divergent mode using Johnson-Cook Damage (Fig. 5.4), there is a noticeable increase in damage when using the EPP model. This trend makes sense since the Johnson-Cook strength model is in theory “stronger” than EPP. It takes into account strain-hardening

and strain-rate effects which the constant yield surface of EPP does not. Therefore, the copper under the Johnson-Cook model would not be as prone to developing damage or porosity. The one case that does not appear to follow this trend is Figure 5.3, a divergent system using Johnson Spall. There exists more porosity growth in the regions around the cut axis using EPP as expected, but on the very tip of the cut area right on the cut axis, there is more porosity growth in the Johnson-Cook case. A 30% contour actually started to grow there whereas in the EPP case there was none. One explanation for the trend going in the opposite direction for this particular case may be because in the EPP model, the copper around the cut will tend to flow more easily into the cut region thus restricting under-densification. The initial colliding shock waves force the copper to flow towards the cut axis, counteracting the divergent velocity vectors from the geometry. The reason this did not happen in the convergent system may be that this effect was made negligible from the convergent velocity vectors imposed by geometry. All the material is being pushed into the cut axis already and the higher strength of the copper in the cut region outweighed the convergent flow effect. The Johnson-Cook Damage cases were unaffected because the damage variable is not based on regional densities, but rather on the strain history. In order to make sure that this one case was not an artifact due to effects like mesh resolution, a further calculation was run in the divergent mode using EPP and Johnson Spall. In the case, however, the yield strength, Y_0 , was set to 3.75 kbar which is over three times the previous yield strength used. This was done to effectively make the material stronger, and see whether the trend of higher strength, more porosity in the divergent mode continued. The result in Figure 5.5 shows that it did.

One final observation to be made from Figures 5.1-5.4 is that the difference in the shape of the cut region is quite noticeable. The EPP cases have strained more judging from its position and shape. The cases using the Johnson Spall model seem to show larger changes in shape and that is due to mass conservation because larger, more porous regions are going to take up more volume.

5.2 Fracture Models

Trying to evaluate the two fracture models was a slightly more arduous task given the quality of the data. At first, it seemed that the Johnson-Cook Damage (JCD) model was better predicting the convergent experiment simply because it was showing from Figure 4.7, that the copper would come close to failing, but never actually fail. This seemed reasonable given that the reconstruction of the convergent experiment was showing full density throughout the wall in the cut region. The Johnson Spall (JS) model, however, was predicting 25% porosity in the cut region and eventual failure not too far after the radiographic time. The divergent radiograph and reconstruction show that the wall had broken through most of the way and would eventually cut successfully. Both the JCD and JS models predicted this accurately although in the JCD model, the region had not failed yet (90% damage), while the JS model predicted failure in most of the region at the radiographic time. What seemed to differentiate the two models most was the fact that the JCD model was not capturing the right physics of the cutting process. The model might be able to predict *when* a material will fail, but it will not dynamically describe the way the density changes in the material as it is approaching failure. This can

easily be observed from the divergent shot. At the radiographic time, the JCD model claims that the cut region is at full density which it is obviously not. It does claim that the material is 90% damaged, but this damage variable is simply a ratio of strains and is not physically based. For that reason, the JS was further examined and an attempt was made to explain why it seemed to be over-predicting the density reduction in the convergent case.

In order to compare densities between the calculation and the experiment, a better reconstruction of the experimental data needed to be implemented. A forward model, known as the Bayesian Inferencing approach, was used by Gregory Cunningham, a member of the image analysis team, to better resolve the radiograph. The essence of the Bayesian approach is to incorporate prior information of the structure radiographed by using a random selection from an identifiable ensemble of similar images to reconstruct the data [17]. By using the Bayesian Inferencing Engine, and eliminating the motion blur, blur caused by the spot size of the x-ray machine, and scatter, a higher quality reconstruction was produced of the convergent experiment. Due to much lower resolution, higher scatter, the thinness of the copper wall, and time constraints, an attempt to reconstruct the divergent data in this manner was not made. Figure 5.6 shows a line plot of density through the copper wall on the cut axis resulting from this Bayesian reconstruction. The same plot from the MESA calculation using the Johnson Spall model is shown in Figure 5.7.

Both the calculation and the experiment show a small low density region along the inner wall of the cut region, but the JS model predicts approximately a 40% density

reduction while the data is showing only a 20% reduction. In order to resolve this difference, the porosity failure criterion was taken out of the model. This criterion set all stress tensors to 0 when the porosity in the local area reached 30%. The 30% criterion was originally inserted into the model as a result of Jim Johnson's findings that in copper, pores spall planes generally formed at a porosity of about 30% [6]. These finding, however, were based on uniaxial, one-dimensional flyer plate tests. What is going on with the cylinder cutting is a much more complicated 3-D process. A region that has reached 30% porosity probably doesn't have much strength left in it, but there are compressive forces acting on the cut region which can heal the material, by closing up voids and spall planes. The failure criterion irreversibly fails the material and thus results in over-predicting the density reduction. Therefore, another calculation was run using a modified JS model without the failure criterion. The resulting convergent overlay and triaxiality plots are shown in Figures 5.8 and 5.9.

The calculation still fits extremely well with the experimental edge fit and shows a smaller density gradient in the cut region. With the failure criterion taken out, the convergent system is no longer predicted to fail. It reaches and levels off at a porosity of about 16.4% while the divergent system predicts failure eventually, but not complete failure at the radiographic time. It is still possible to say that copper at 30% porosity is failed with the modified model because at that point, the material doesn't have much strength left. However, this model works better because it doesn't permanently fail a region like before. Getting rid of the failure criterion also eliminated the spall bubbles on the ends of the cylinder that show up in Figure 4.4(d). A line plot similar to the ones in

Figures 5.6 and 5.7 can be done with the modified JS model and this shows in Figure 5.10, that the density through the cut region matches up much better with the experimental results in Figure 5.6.

The density profile is still not perfect, but it does begin to approximate the experiment better. The low density ridge on the inside wall is now about a 30% reduction at the lowest part, but the ridge is smoother than before. Therefore, the Johnson Spall model without the 30% failure criterion is more accurate than the Johnson Spall model with the criterion, and for that reason, was used in all calculations in Chapter 5 where the spall model was implemented. One cause of the slight over-prediction in the model might be from other effects like the burn model which will be discussed in detail later in the next section.

5.3 Other Considerations

5.3.1 High Explosive Burn Models

In all of the MESA calculations performed the standard HE burn model known as Program Burn was employed to predict the shape and speed of the explosive detonation waves. The model assumes a spherical detonation wave which expands at a constant velocity, D_{CJ} , the Chapman-Jouguet velocity. A more refined burn model that is still in the developmental phase is the Detonation Shock Dynamics (DSD) burn model. This model assumes that the detonation wave velocity, D_n , is a function of the curvature, κ , of the wave [18].

$$D_n = D_{CJ} - \alpha(\kappa) \quad (5.1)$$

Therefore, when the wave is a flat, plane wave it is travelling at its fastest and as the wave front gets more curved it begins to propagate slower through the explosive. DSD was not implemented because the version available in the code could only handle a limited number of material regions and a limited type of high explosives. However, in order to gain some insight into how using the DSD model instead of the Program burn model would effect the numerical results, a handful of simplified cylinder cut experiments were simulated. These simplified calculations consisted solely of the original copper cylinder and the annulus of PBX-9501. All of the polyethylene, stainless steel, PBX-9501, and PBX-9407 parts which made up the ring lighting system were taken out. The 9501 annulus that remained was ring-lit in the same location as with the ring-lighting system. Therefore, the number of material regions and explosives were minimized to the essential parts of the experiment. Both divergent and convergent systems were run using Program burn and DSD burn. Figure 5.11 shows four particle plots illustrating some of the differences between the two burn models when applied to the convergent system.

The most noticeable effect that implementing DSD has is that the copper cylinder gets driven less hard, both radially and axially, which results in less porosity at the cut region. The peak shock pressures seen in 5.11(a) differ by approximately 40 kbars, and 5.11(b) shows about a 3% reduction in radial velocity. What was most surprising was the huge reduction in axial velocity 1" off the cut axis and porosity on the cut axis associated with the DSD model. They dropped around 25% and 13.7% respectively from the

Program burn values. The reduction in driving force of the explosive makes sense since there was a fair amount of curvature in the detonation waves and therefore, under DSD, would travel slower than predicted in Program burn and thus cause less density reduction in the cut region. As for the divergent system, similar results were observed except in the case of porosity which actually seemed to increase slightly at late times using DSD.

These plots are seen in Figure 5.12.

In the divergent case, switching to DSD produced pretty much the same effects in terms of reducing pressures and velocities, but the magnitude of the reductions was slightly less. The peak pressure reduction was down to only 13 kbar while the cut region radial velocity and off-axis axial velocity were only down 2.5% and 20% respectively. However, the porosity levels seemed to follow each other fairly well until late times where the DSD model, unpredictably, becomes more porous than the Program burn model.

An explanation for these effects will not be attempted, but it can be concluded from the above calculations that the choice of burn model can have a significant impact. For the most part, the DSD model shows a reduction in shock pressures and velocities as compared to Program burn, but the effects are dependent on system configuration as can be observed best by the porosity plots.

5.3.2 Mesh Resolution

Whenever numerical simulations are performed which involve the problem being broken into a finite mesh of cells, the question of whether the calculation is mesh

resolved or not is always an issue. Being mesh resolved means having the individual cell size be small enough such that the solution to the calculation has converged to a single, unique answer. Therefore, if the cell size is further reduced, the solution will not change. In all of the calculations run, square cells of 0.05 x 0.05 cm were used as the mesh. Through several iterations, this was found to be the smallest cell size that could be used without causing the MESA program to crash often. For that reason it was not possible to check for mesh resolution by examining cases with a finer mesh. Two calculations where the cell size was increased were run, both on a convergent system since it's bigger features would accentuate any changes between calculations. One case used a 0.1cm cell and the other a 0.075cm cell. The resulting overlays with the data for both these cases and the 0.05cm cell case are shown in Figure 5.13.

From Figure 5.13 it is not possible to say for certain whether or not calculations using a 0.05 cell size are mesh resolved because there is a noticeable difference between the three cases. The fact that the 0.05cm calculation matches the experimental data extremely well in the cut region suggests that this mesh resolution is either fully resolved or very close to being so. Again, it is impossible to state with absolute certainty that a 0.05cm mesh is fully resolved from the three cases performed, but it appears likely that it is or is close to resolved.

5.3.3 Ring Lighting System Effects

The final issue that needs to be addressed is the effect of the ring-lighting system. Ideally, the copper cylinder experiments would be run with simply the copper tube and

the annulus of PBX-9501. This would ensure that there would be no external effects from additional parts on the system that would need to be accounted for. However, this was not feasible since the HE annulus needed to be ring-lit simultaneously from both ends. The ring-lighting system used, comprising of the polyethylene, stainless steel, and PBX-9501 end caps on both sides of the copper cylinder, was designed to minimally interfere with the experiment as a whole and the cut region in particular. To examine the effects of the ring-lighting system, a calculation was run using a “simplified” geometry as discussed in 5.2.1 where only the copper tube and the 9501 annulus are involved. The result was overlaid with the experimental data in Figure 5.14.

The ring-lighting system certainly does make a difference as the simplified calculation did not match the experimental data as well as with a full system calculation. However, the area in which the quality of the match decreases is on the ends of the cylinder, and this is not the area of interest. The critical region of interest is right in the middle of the cylinder in the cut region. It still matches the experimental data very well which allows the conclusion to be reached that the cutting process was largely unaffected by the ring-lighting system. This allows time and CPU memory savings as further iterations on MESA for the cylinder cut experiments can be run with reasonable confidence using only the simplified system as long as the region of interest remains in the vicinity of the cut axis.

5.4 Influence of Curvature

In an attempt to better understand the influence of radius of curvature of the copper cylinder in the convergent geometry, a simplified calculation was run with a 25" outer diameter cylinder. The only change from the 6" OD calculations was in the diameter. The copper wall thickness, HE annulus thickness, and cylinder length were all kept at 0.1", 0.75", and 4" respectively. Hence, the copper was driven under the same loading conditions and inward at the same radial velocity. Both simulations were run with the Johnson-Cook strength and Johnson Spall (without the 30% failure criterion) models. Upon comparing the two cases, it was first noted that the curvature had very little effect on the initial shock response of the copper around the cut region. A mass-less tracer particle was placed 0.15" off the cut axis and Figure 5.15 shows that the initial shock and release waves drove the particles at the same axial velocity profile despite the difference in curvature.

To answer the more important question of how curvature affects the cutting process, it was necessary to look at the porosity in the cut region as a function of the relative deformation done to the copper cylinders. The reason for using the relative deformation is that in order to make meaningful comparisons between the two cases one must examine them at similar points in their hoop strain histories, not time histories. For example, at 30 μ s, the 6" cylinder has deformed to the point where it is about to collapse on itself whereas the 25" cylinder has deformed to only about 80% of its initial size. Therefore, a dimensionless radius, the current cylindrical radius divided by the initial radius (R/R_0), was used to define the relative deformation or hoop strain of the cylinder.

From Figure 5.16, it can be observed that the porosity in the cut region asymptotically approaches about the same value, thus showing that curvature has little effect on the ultimate porosity in the cut region. However, it is also observed that the porosity in the 25" case does grow at a faster relative rate than in the 6" case. This means that with a lower radius of curvature, the copper is likely to break earlier in its strain history.

One final observation that can be made is that at late deformation stages the axial velocity of particles near the cut region for the 6" OD calculation becomes non-negative. In this case, negative velocity denotes movement towards the center cut axis and positive denotes movement away from it. Looking at Figure 5.17, this means that for most of the time the copper is converging into the cut region due to the convergent geometry of the system. However, at R/R_0 of 0.4, this convergence slows down and at 0.3, the copper around the cut is actually beginning to diverge. If one believes the trend for the 25" OD curve, it appears that the cross into positive axial velocity will occur much sooner, perhaps around an R/R_0 of 0.5. This also suggests that reducing the radius of curvature allows the copper wall to cut earlier in its strain history, assuming that divergent axial flow of material around the cut region tends to break the copper more than convergent flow does.

6.0 Conclusions

- *The radius of curvature of the copper cylinder liner has a tremendous influence over the cutting process.*

Through the convergent and divergent copper cylinder cut experiments performed, it can be concluded that a change of sign in the radius of curvature does have a tremendous influence on the cutting process of a copper liner. Examining the radiographic data shows that the divergent, positive curvature, system clearly had a cut developing which was characterized by high levels of density reduction on the cut axis, while the convergent, negative curvature, system exhibited no signs of cutting. Even after applying a BIE reconstruction and accounting for blur and scatter variations, the convergent radiograph showed only a 1-2 mm wide 20% density reduction in the tip of the cut. Having been driven with the same load, this difference was due to the velocity vectors created by geometry. In the convergent system, the detonation wave interaction attempts to drive the copper apart but the velocity vectors force the material to flow in on itself counteracting the cutting. The exact opposite occurs in the divergent system where the velocity vectors of the material assist cutting by forcing the material to flow away from itself. This effect is also what causes the walls in the convergent system to thicken with time and causes the divergent system walls to thin.

The influence of the magnitude of the radius of curvature also seems to follow a predictable trend. After running a calculation with a 25" OD cylinder, it can be justifiably said that increasing the radius of curvature in the convergent system does allow the

cylinder to cut faster with respect to the relative deformation. The late time, or ultimate porosity of the cut was not influenced much by the change in curvature, but the porosity did grow at a faster rate when plotted against the relative deformation or radial strain of the cylinder. Also, it was found that a larger curvature in the convergent system allows the material around the cut region to begin diverging axially at an earlier point in the relative deformation history, thus helping the copper to cut easier. If the 6" and 25" diameter calculations run are seen as extremes in curvature space, the 25" being a high radius of curvature, and the 6" being a low radius of curvature, the trend is obvious. Increasing radius of curvature in a convergent system allows faster and easier cutting of the metal.

- *From the five models studied, the Johnson Cook strength model and the Johnson Spall fracture model (without the failure criterion) best simulate the experimental data, however, the modeling of the hydrodynamics plays the dominant role in accurately modeling the experiments.*

In modeling the experiments using MESA, it is concluded that the majority of the solution in predicting the right shape and timing is dependent on getting the hydrodynamics correct. All five cases with varying strength and fracture models showed fairly good agreement with the experimental data. This demonstrated the relative insensitivity of the experiments to strength and fracture models, and the ability of MESA to simulate the hydrodynamics accurately.

Yet, while hydrodynamics does play the dominating role, strength does influence the simulation to a certain degree. A closer examination of the cut region shape does show a improvement as the model is changed from no strength to Elastic-Perfectly-Plastic, and finally to Johnson-Cook. Each model is successively stronger than the previous one, which allows the material to strain least in the Johnson-Cook case giving it the best fit. A more detailed comparison between EPP and Johnson-Cook show that the models also have an effect on the fracture model predictions. For the most part, the EPP model does result in noticeably higher porosity contours when using the Johnson Spall fracture model, and higher damage contours when applying Johnson-Cook Damage. This makes sense as the strain-hardening effects in Johnson-Cook strength does not allow the copper to strain as much thus reducing damage and porosity growth. However, the exception to this conclusion is in the divergent mode using Johnson Spall where porosity growth in the tip of the cut is actually higher for the Johnson-Cook strength case. This is probably due to the weaker EPP model allowing more convergent axial flow of material into the cut region thus reducing porosity growth. This was backed up by a subsequent calculation using an EPP model with a higher yield strength that displayed the same trend.

In terms of fracture models, it initially appeared that the Johnson-Cook Damage model performed the best. It predicted that the divergent experiment was very close to cutting while the convergent experiment would never cut. Judging by the radiographs, this seemed an accurate statement. The Johnson Spall model was predicting failure in both cases. One drawback to the damage model though is that while it may be able to

predict when the copper will break, the damage variable in the model is based on strain history and did not predict any density reductions in the material. It had the cut region in the divergent experiment at full density at radiographic time, which is obviously inaccurate. In other words, the damage model does not dynamically predict the physics of the experiment correctly. The spall model does, however, dynamically grow pores and thus reduces the density, although it appeared to be over-predicting the density reduction in the convergent case. Therefore, a revised Johnson Spall model was used which did not include the 30% porosity failure criterion where all stress tensors are set to zero when the material in a cell reached 30% porosity. The spall model without the criterion showed a significant improvement coming much closer to reasonably predicting the correct density profile through the cut axis of the convergent system. Therefore, out of the fracture models examined, the Johnson-Spall model without the 30% failure criterion appeared to be the best model. This, however, by no means concludes that the spall model can accurately predict when a cut occurs. There is still much work to be done in the area of fracture and perhaps a model that combines both the porosity growth of Johnson-Spall and the strain history based damage of Johnson-Cook Damage might come closer to solving that problem.

- *There exists a significant difference between using Program Burn and DSD Burn in modeling these types of experiments, and much more attention must be paid to the choice of burn models in the future.*

In running hydrocodes involving the detonation of explosives, it is necessary to understand the impact of the burn model. From the small amount of analysis done here can be concluded that there exists a significant difference between using DSD or Program Burn. The simpler Program burn was used in all the calculation done iterating through constitutive models because DSD could not be implemented on such experiments involving so many parts. However, DSD is believed to be more refined and accurate. It was found that DSD drives the copper less hard both radially and axially, and thus for the most part, causing less porosity damage. These differences ranged from a few percent to almost 30% in some cases. The only exception to the rule was in porosity growth in the divergent case. This was not as much of a surprise as expected as a similar prediction occurred when comparing the EPP model to the Johnson-Cook model and it can be explained in a similar fashion. Program burn drove the copper harder axially causing more material to flow into the cut and counteract the porosity growth due to diverging radial velocity vectors, which allowed the divergence it less hard in all cases, causing less porosity damage. Regardless, switching to DSD from Program burn does make a significant impact and one needs to pay much attention to explosive burn modeling. Once a more useful DSD model can be implemented into the code, it will be possible to make statements about the accuracy of it.

7.0 List of Figures

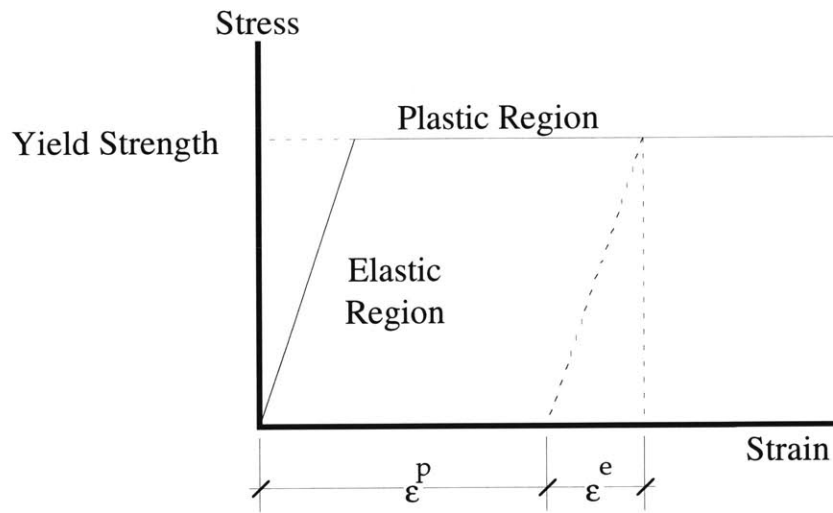


Figure 2.1: Elastic-Perfectly-Plastic Stress Strain Curve

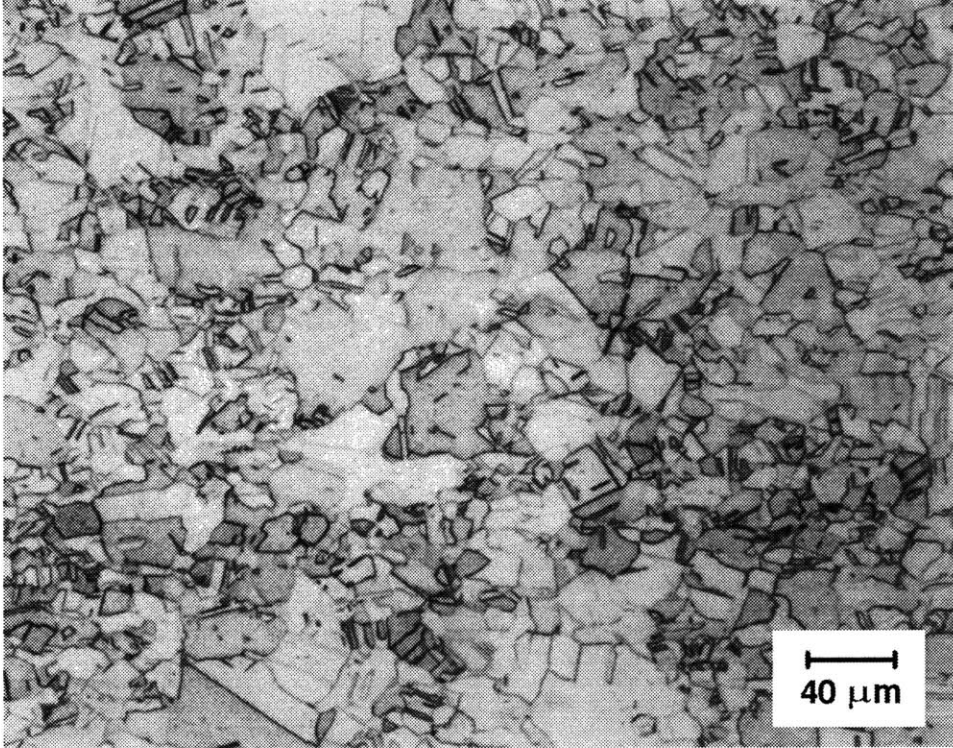


Figure 3.1: Micrograph of Post-Processed Copper Tube

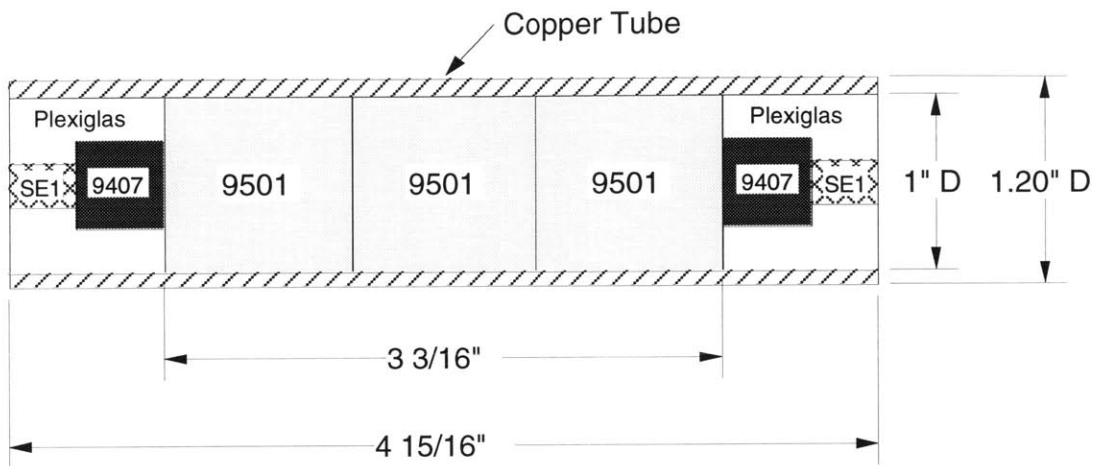


Figure 3.2: Design of a 1.2" OD Preliminary Copper Cylinder Cut Shot

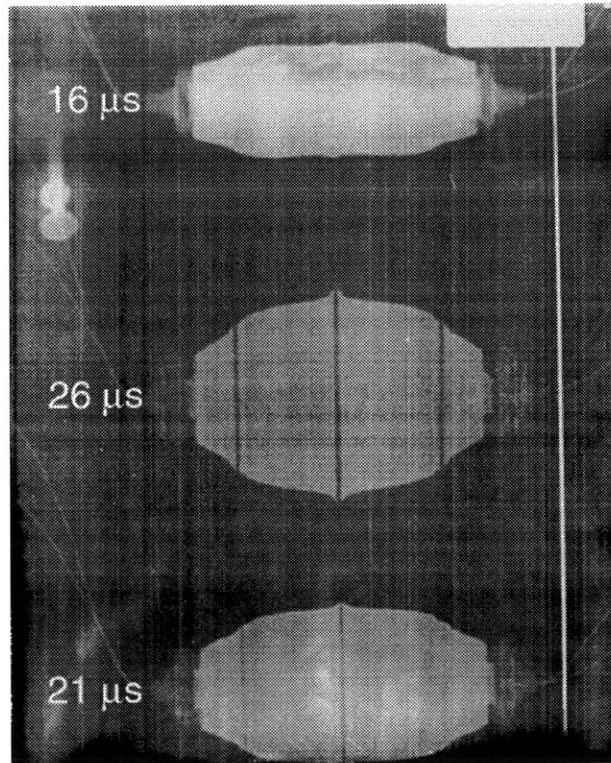


Figure 3.3: Resulting Radiograph from the Preliminary Cylinder Cut Shot

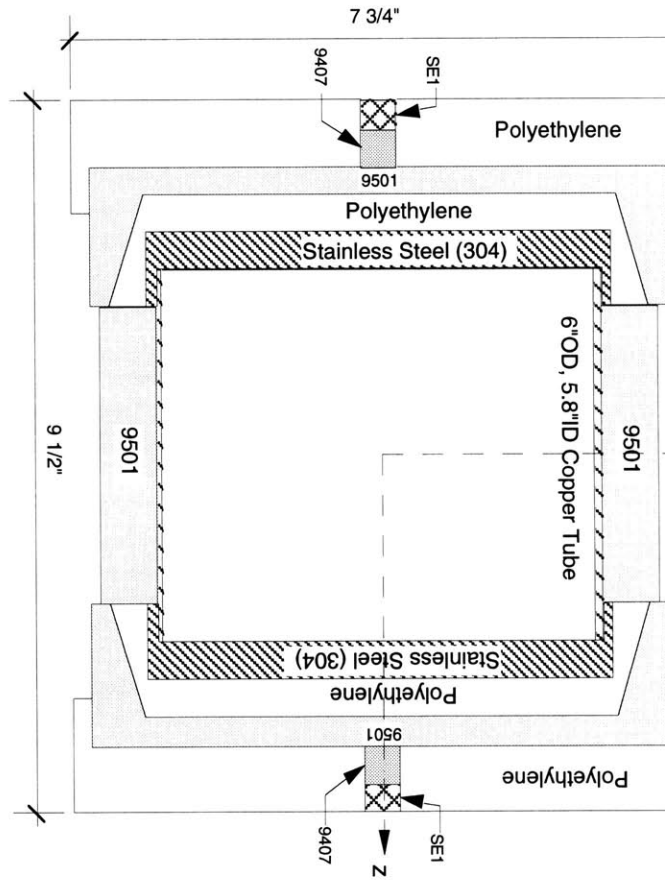
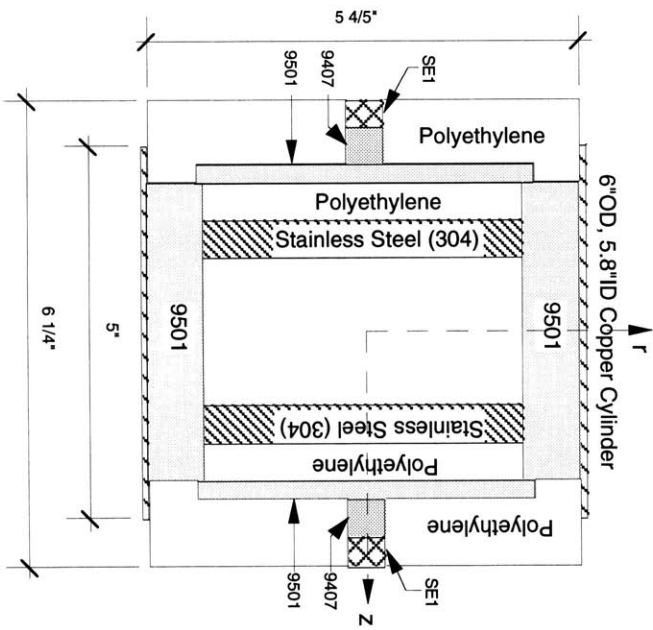


Figure 3.4: Convergent System Shot Design

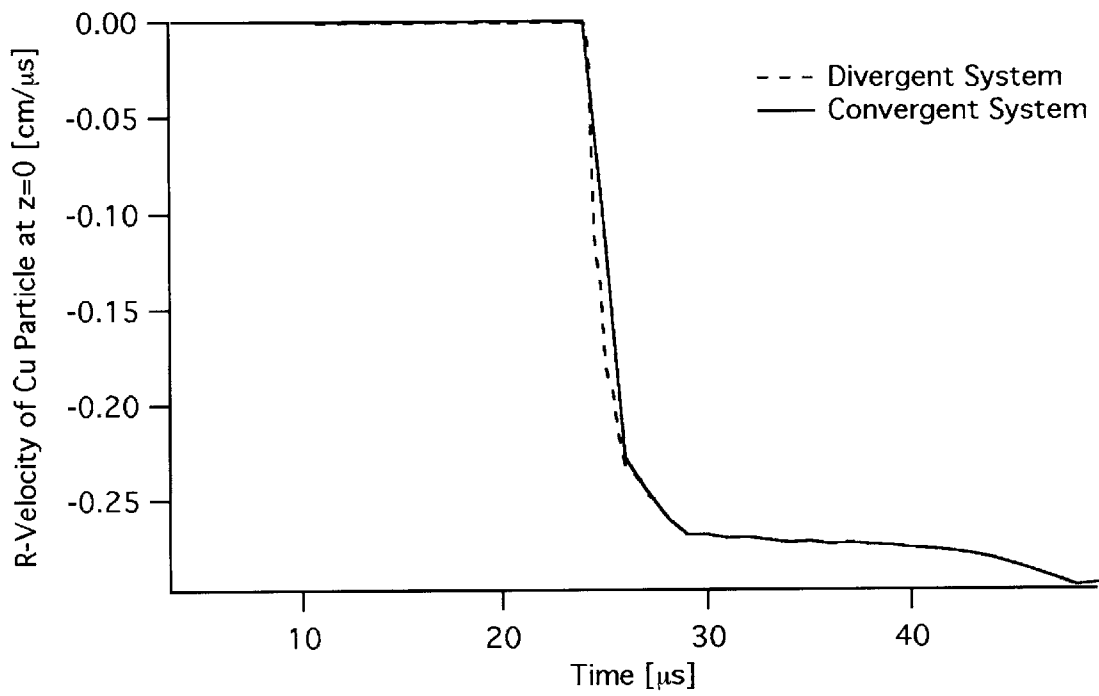
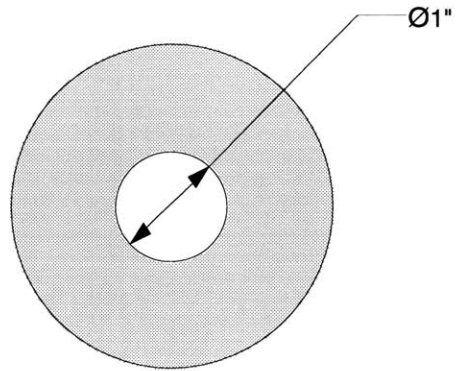
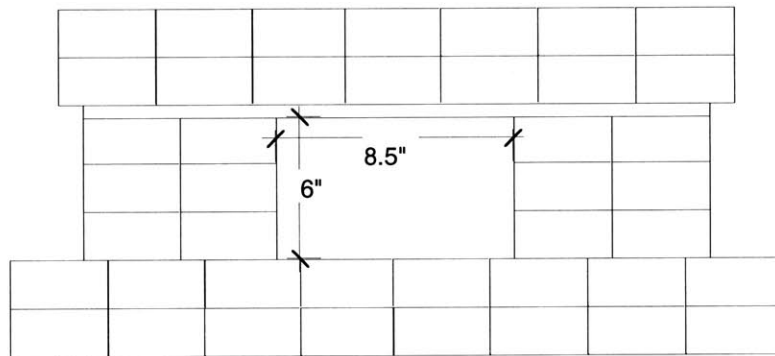


Figure 3.6: MESA Calculation Showing Convergent and Divergent Copper Tubes Driven with same Radial Velocity Profiles



(a)



(b)

Figure 3.7: (a) Lead Doughnut Collimator, (b) Lead Brick Wall Collimator used in Divergent Experiment to Reduce X-ray Scattering

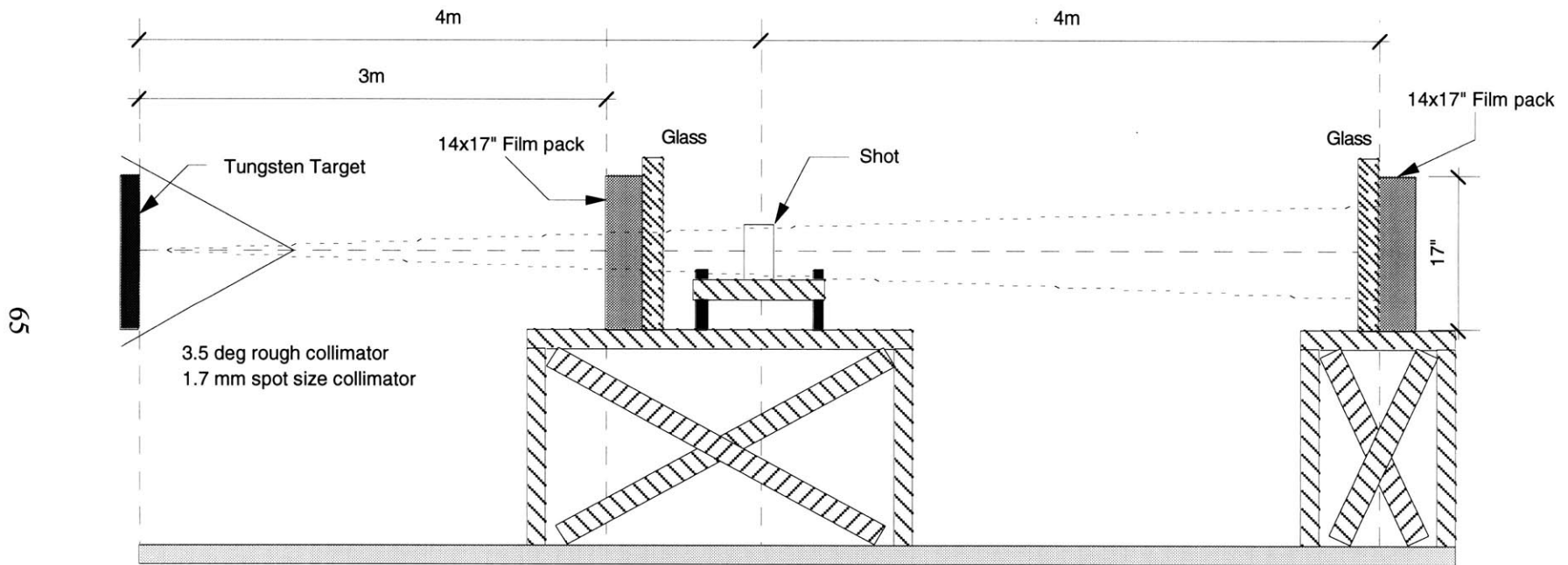


Figure 3.8: Shot Setup on PHERMEX Firing Point for Convergent System

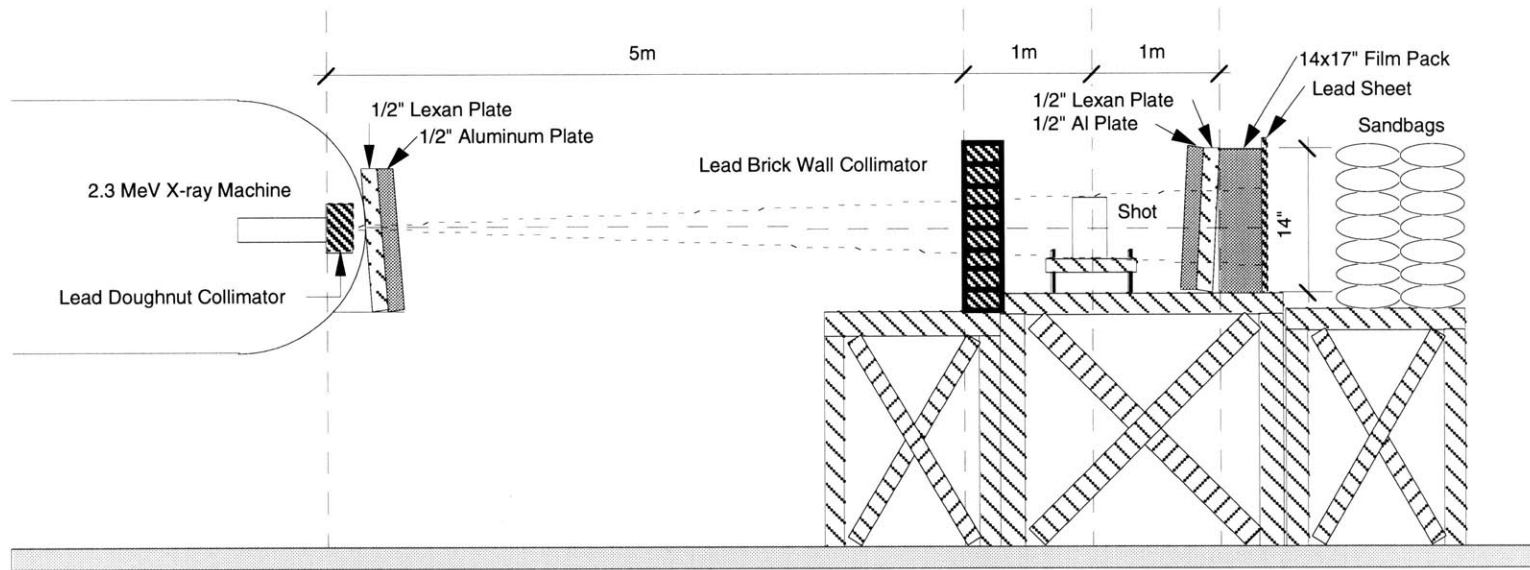
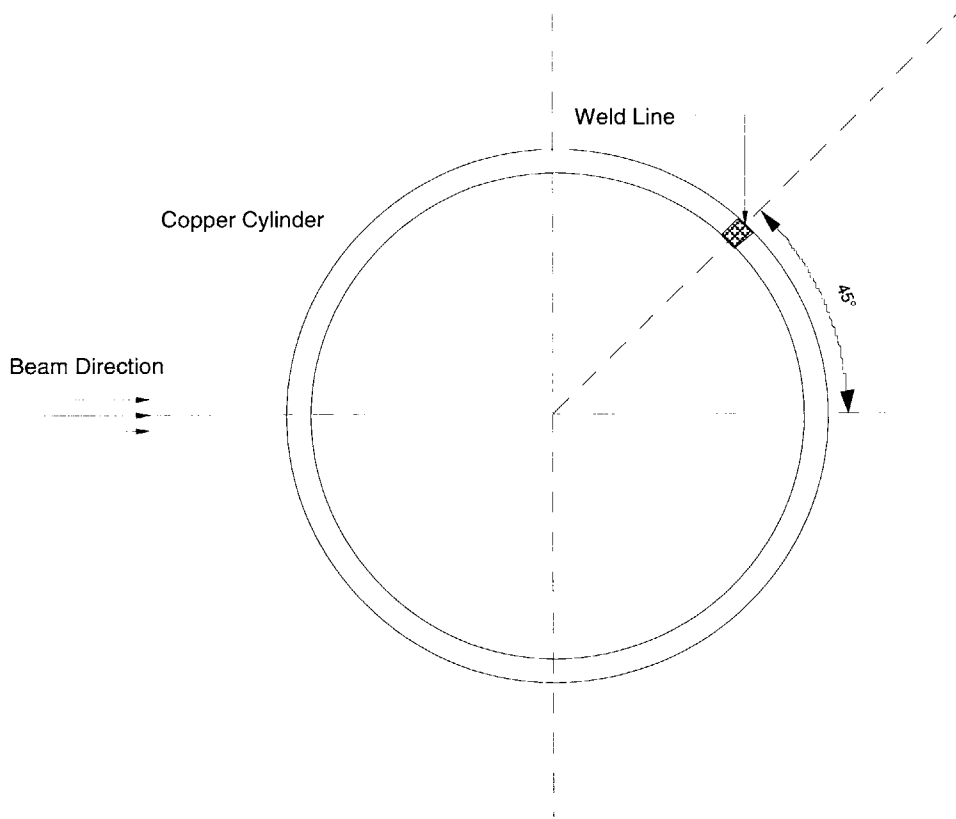


Figure 3.9: Shot Setup at Meenie Firing Point for Divergent System



**Figure 3.10: Copper Tube Weld Line Placed 45° Off Beam Axis
(Top View of Copper Tube on the Shot Table)**

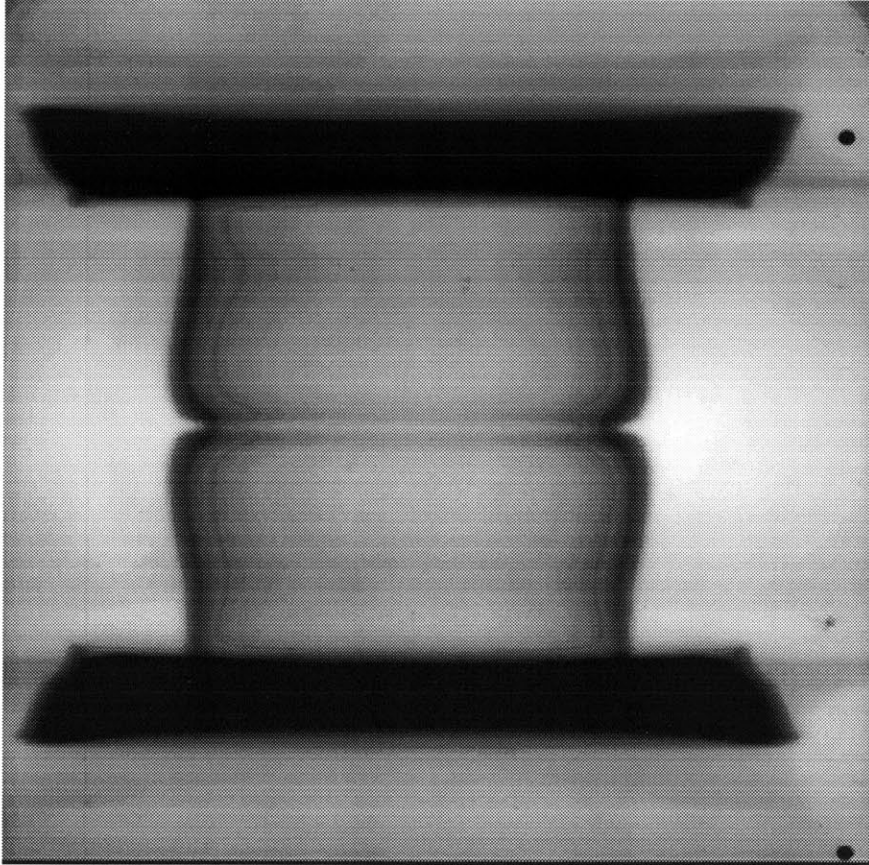


Figure 4.1(a): Convergent Radiograph

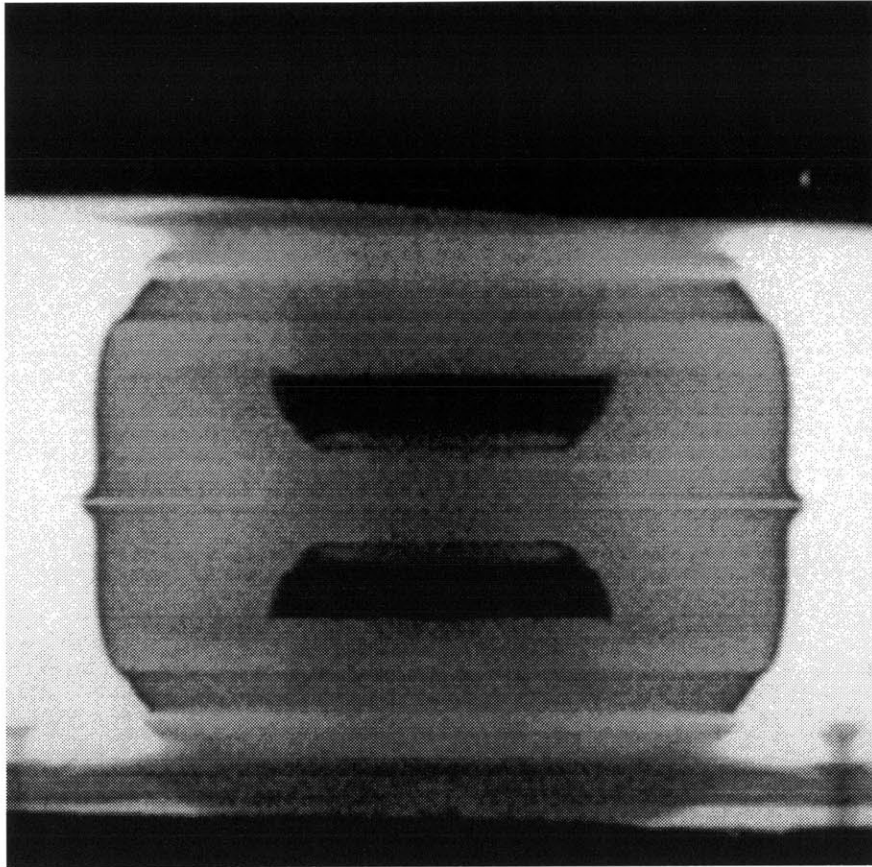


Figure 4.1(b): Divergent Radiograph

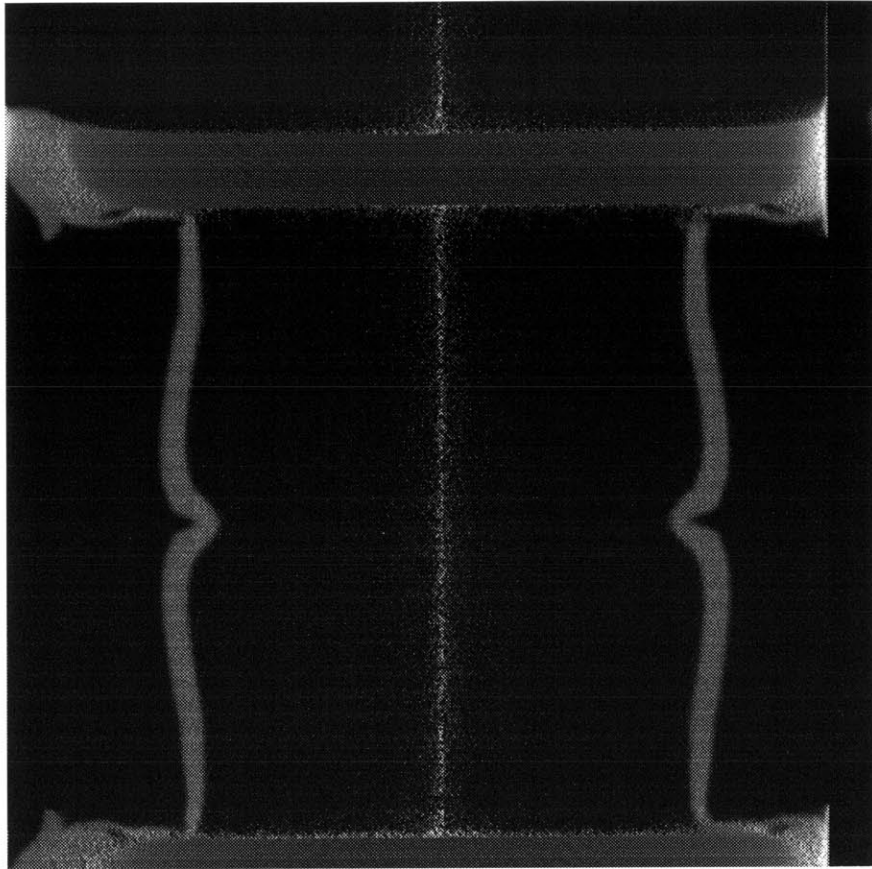


Figure 4.2(a): Convergent Reconstruction

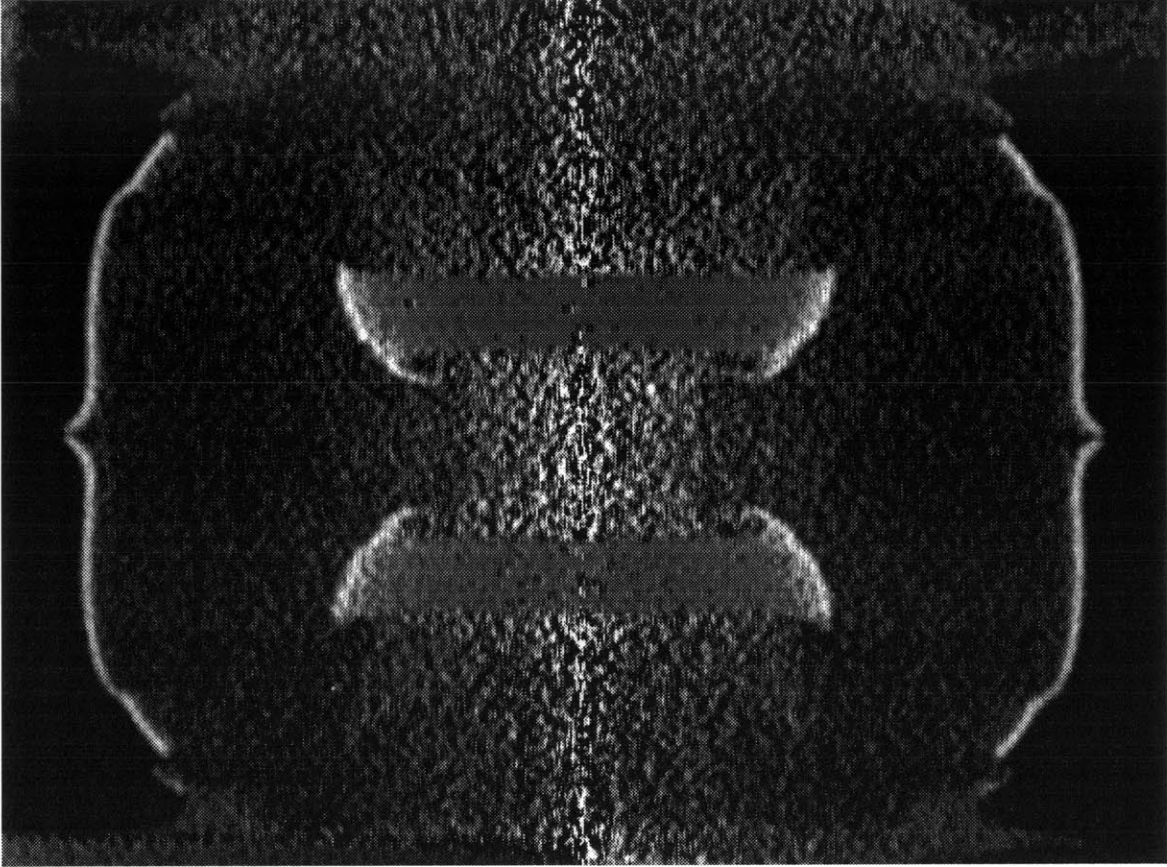


Figure 4.2(b): Divergent Reconstruction

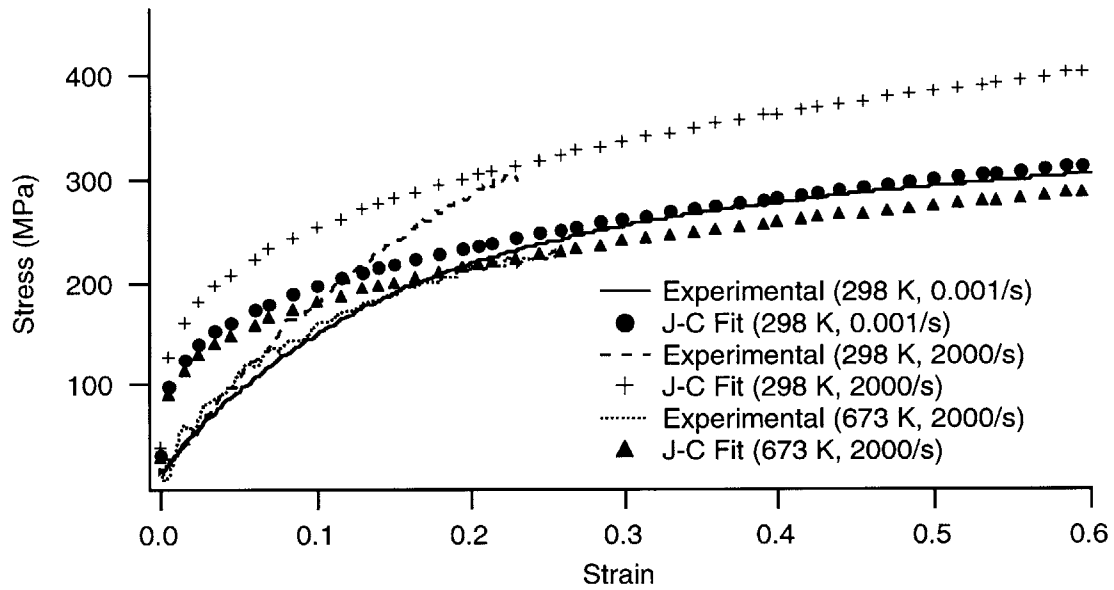
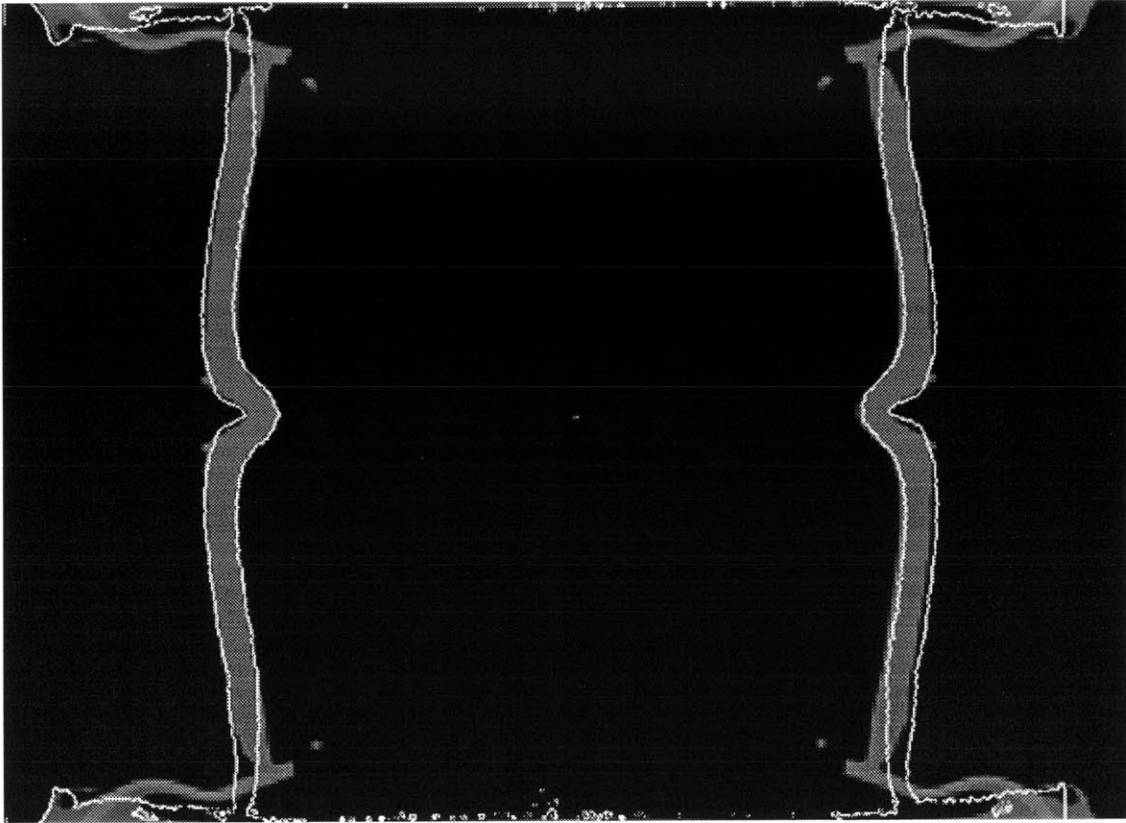
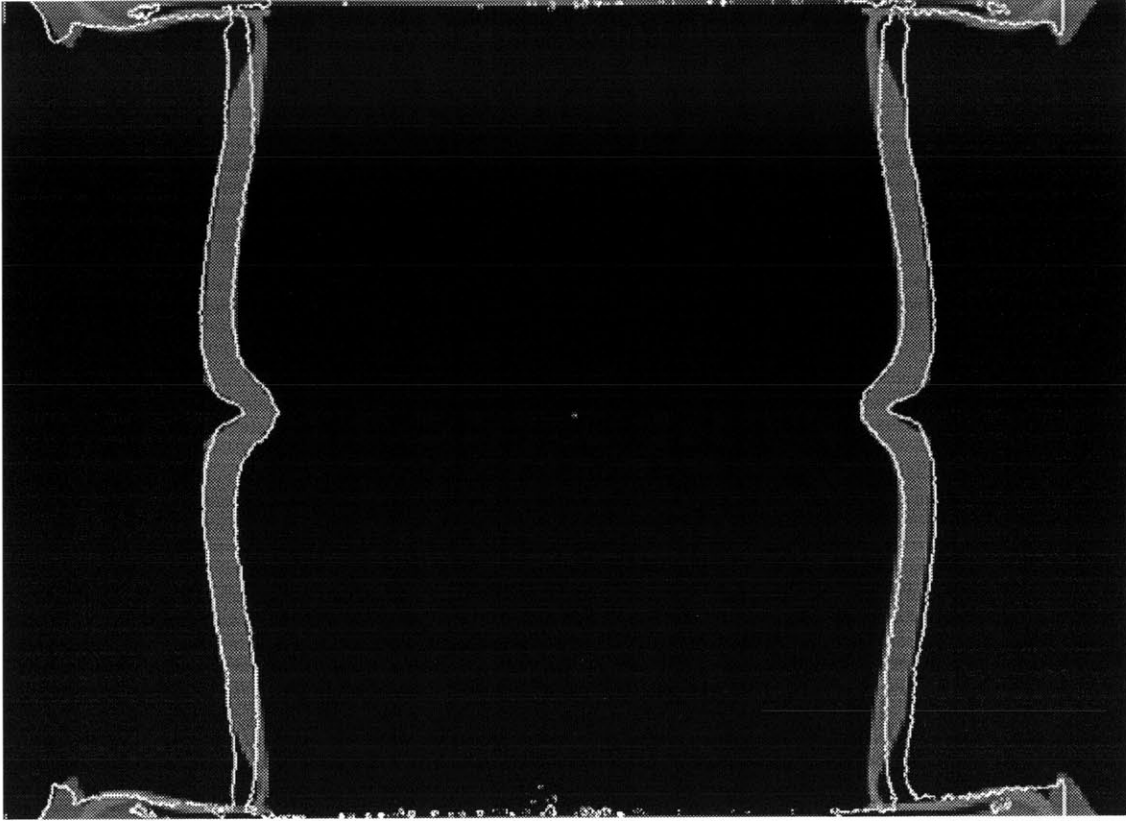


Figure 4.3: Stress-Strain Data on Copper Alloy 101 with Corresponding Johnson-Cook Strength Model Fits



**Figure 4.4(a): Hydrodynamic, Convergent Overlays;
White Outline = Experiment,
Shaded Region = MESA Calculation**



**Figure 4.4(b): Elastic-Perfectly-Plastic, Convergent Overlays;
White Outline = Experiment,
Shaded Region = MESA Calculation**

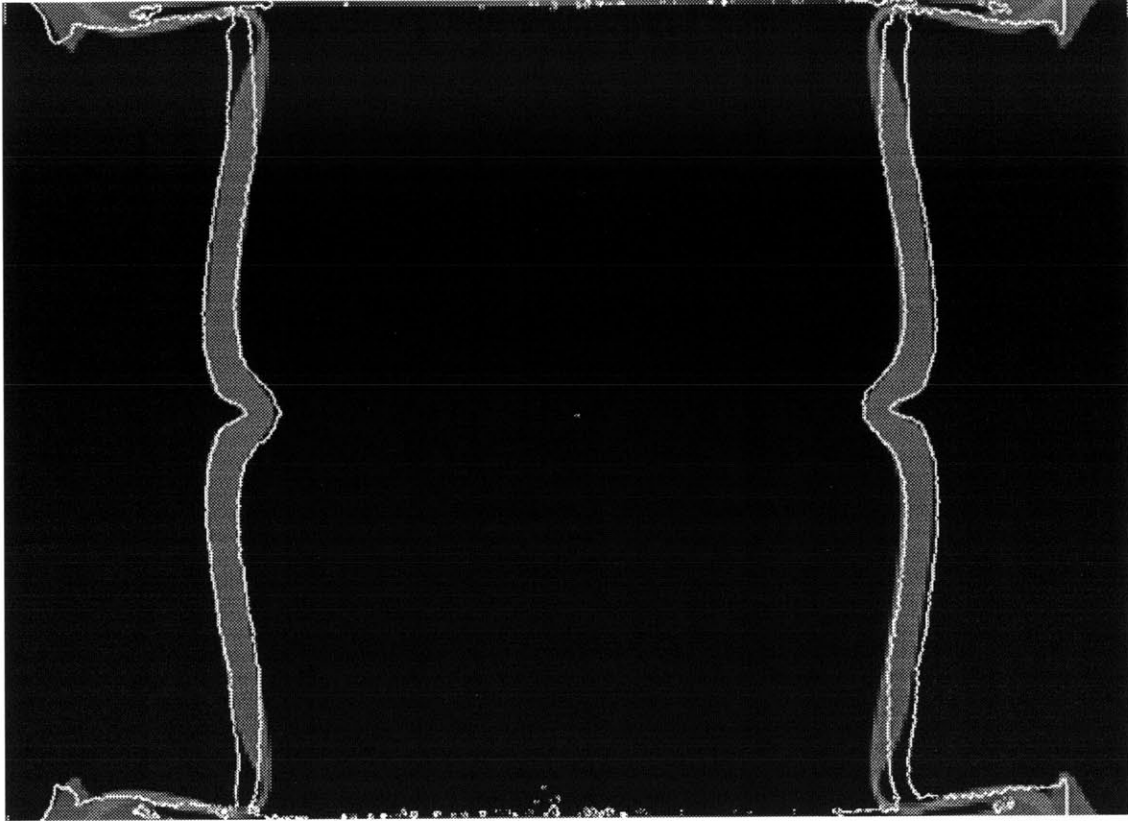


**Figure 4.4(c): Johnson Cook Strength, Convergent Overlays;
White Outline = Experiment,
Shaded Region = MESA Calculation**

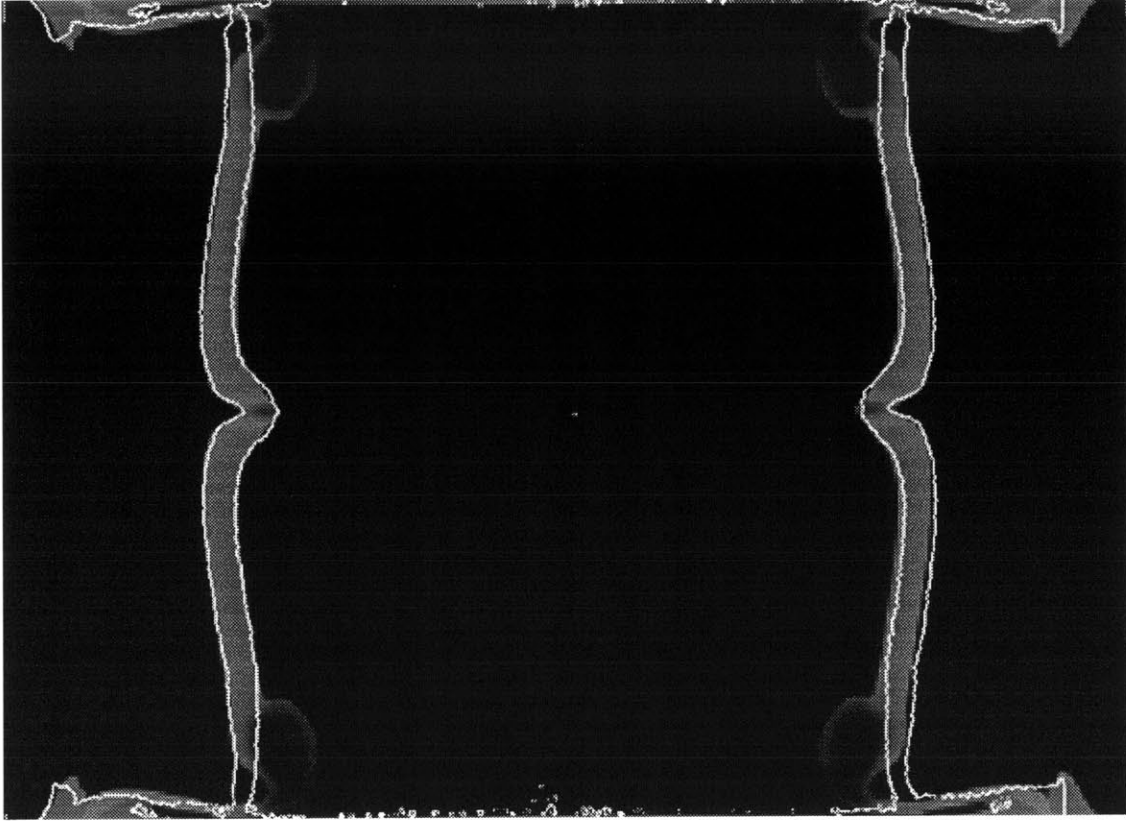


**Figure 4.4(d): Johnson Cook Strength / Johnson Spall Fracture,
Convergent Overlays; White Outline = Experiment,
Shaded Region = MESA Calculation**

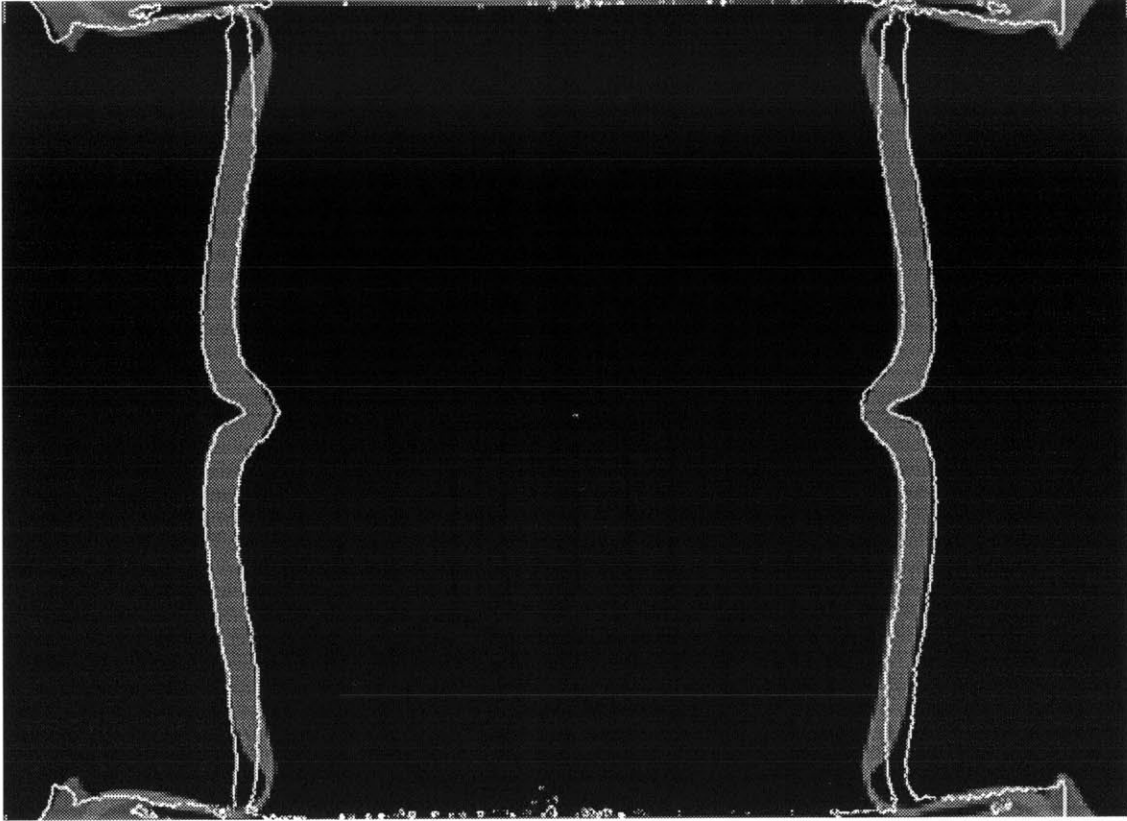


**Figure 4.4(e): Johnson-Cook Strength / Johnson-Cook Damage,
Convergent Overlays; White Outline = Experiment,
Shaded Region = MESA Calculation**

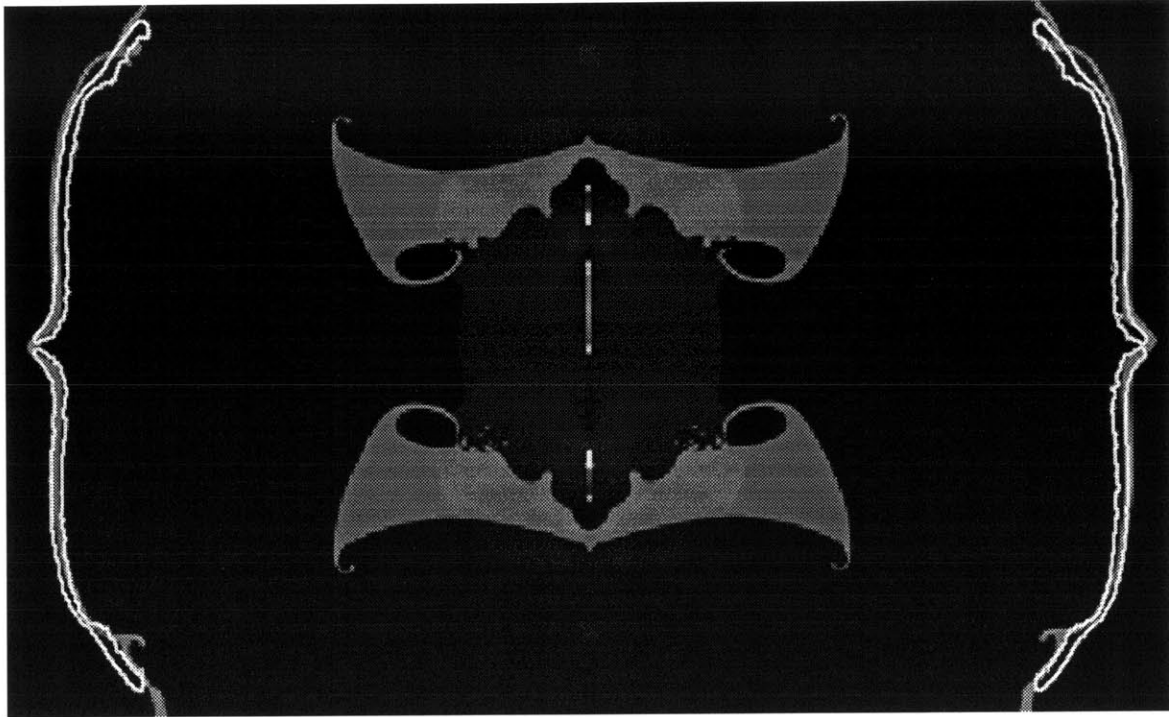


**Figure 4.5(a): Hydrodynamic, Divergent Overlays;
White Outline = Experiment,
Shaded Region = MESA Calculation**

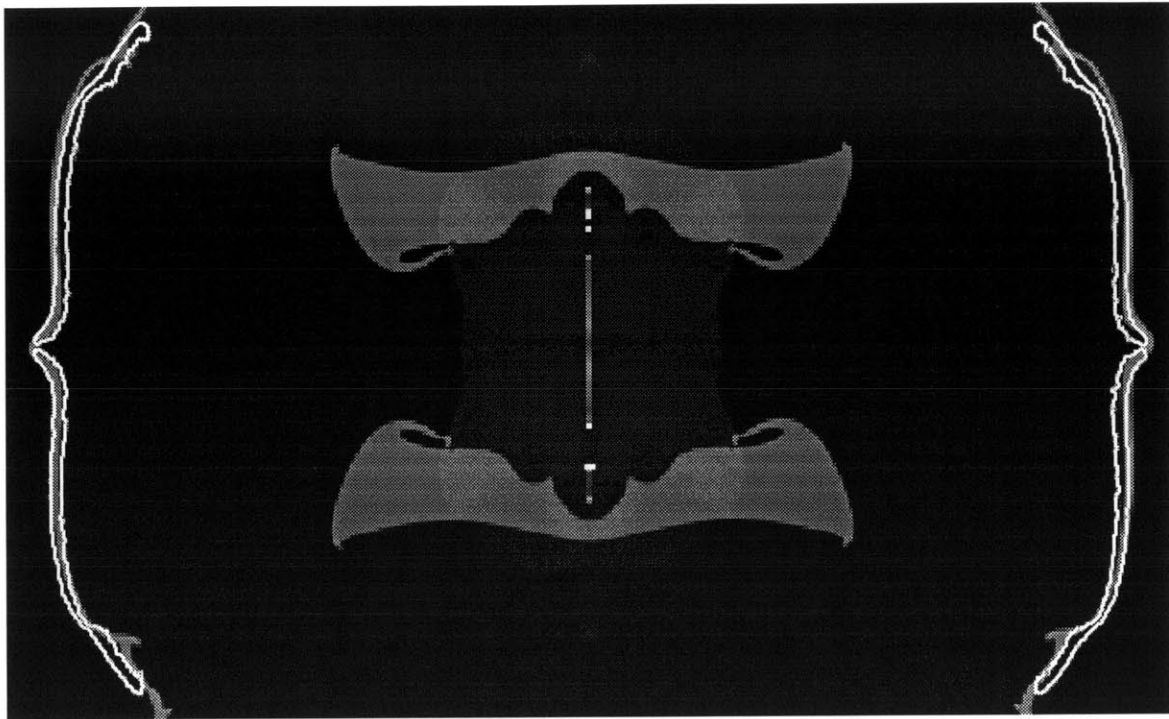


**Figure 4.5(b): Elastic-Perfectly-Plastic, Divergent Overlays;
White Outline = Experiment,
Shaded Region = MESA Calculation**

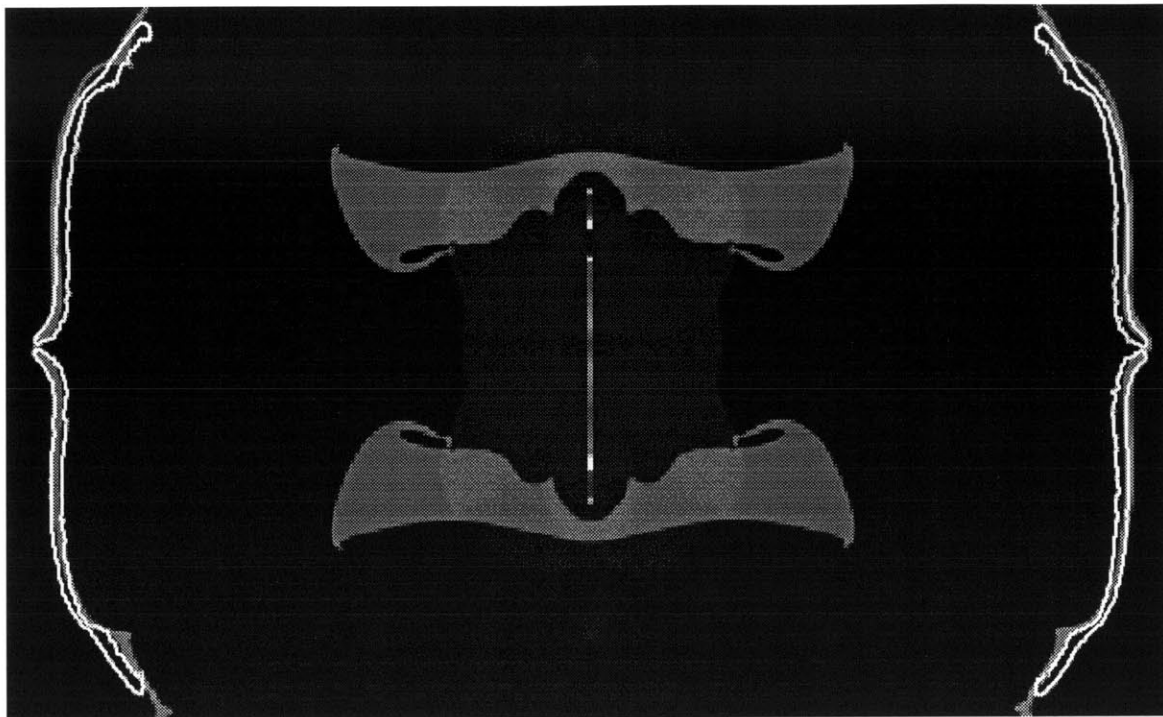


**Figure 4.5(c): Johnson-Cook Strength, Divergent Overlays;
White Outline = Experiment,
Shaded Region = MESA Calculation**

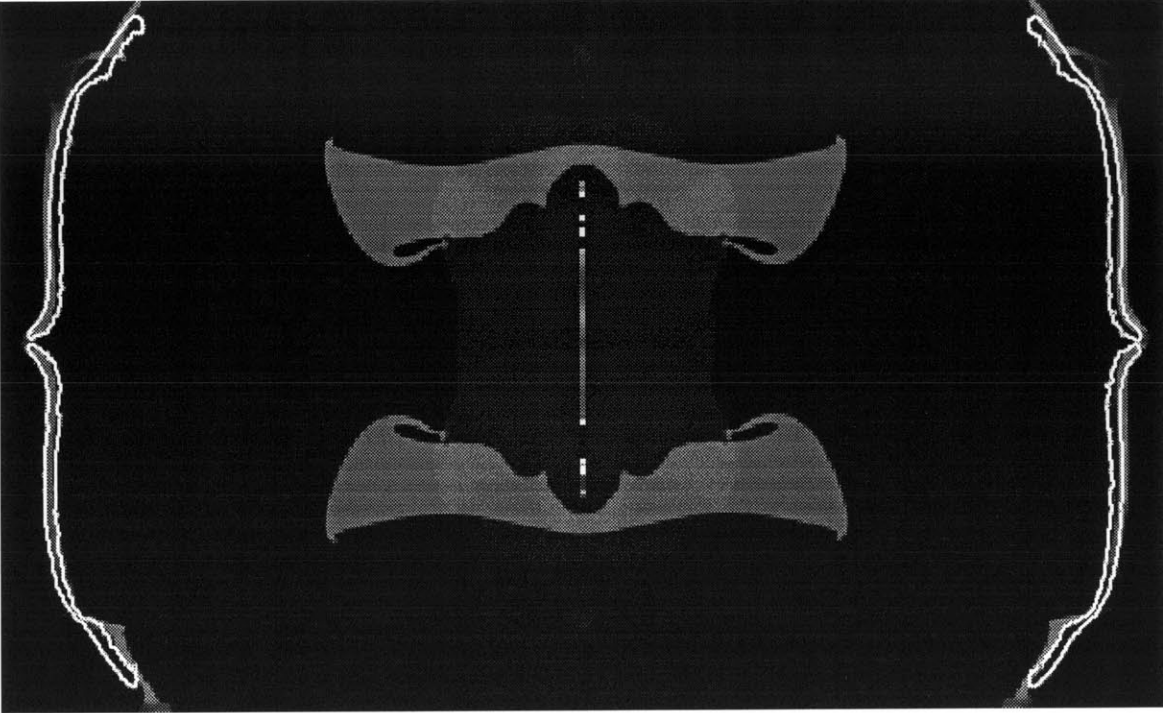


**Figure 4.5(d): Johnson-Cook Strength / Johnson Spall Fracture,
Divergent Overlays; White Outline = Experiment,
Shaded Region = MESA Calculation**

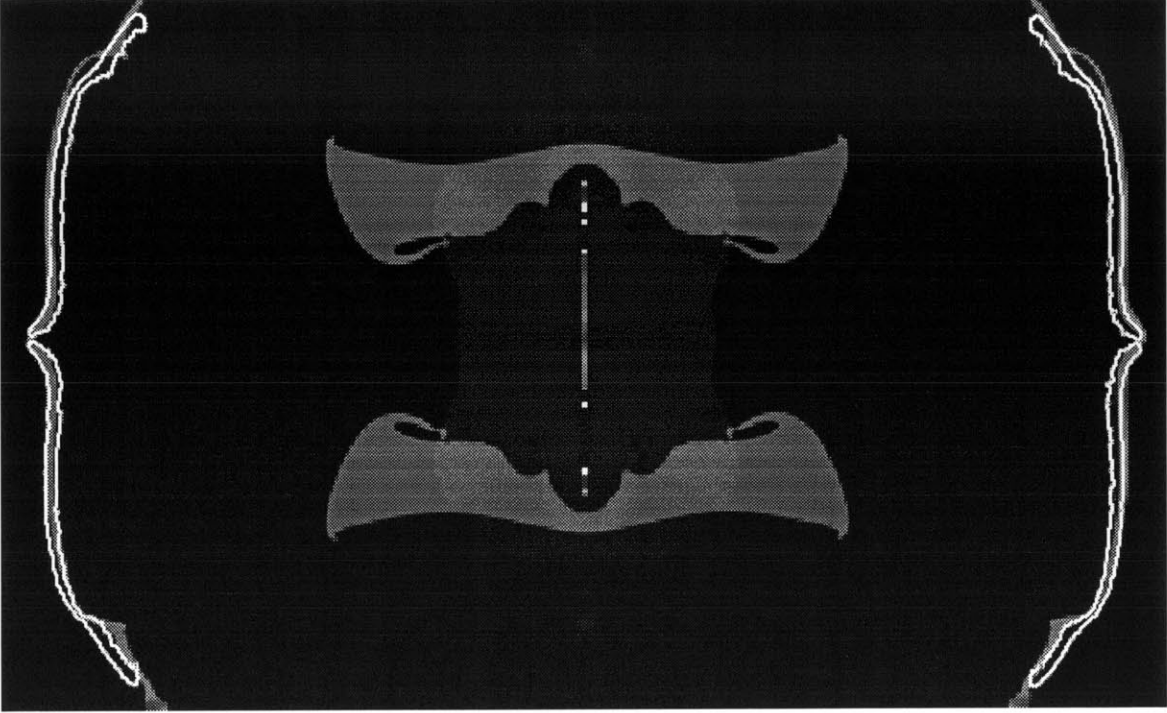


**Figure 4.5(e): Johnson-Cook Strength / Johnson-Cook Damage,
Divergent Overlays; White Outline = Experiment,
Shaded Region = MESA Calculation**

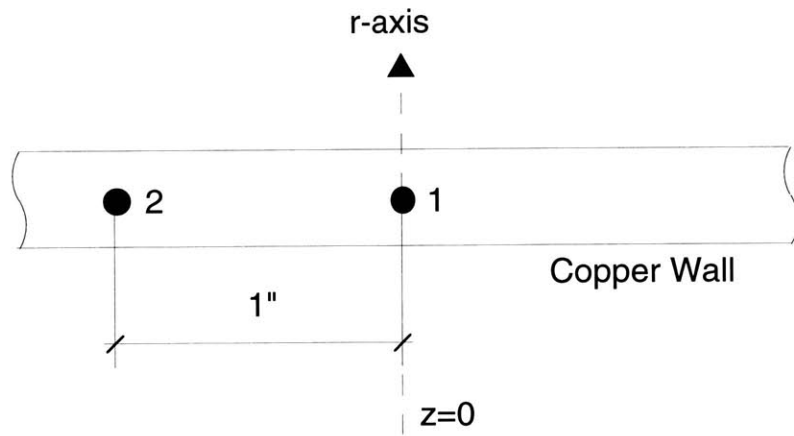
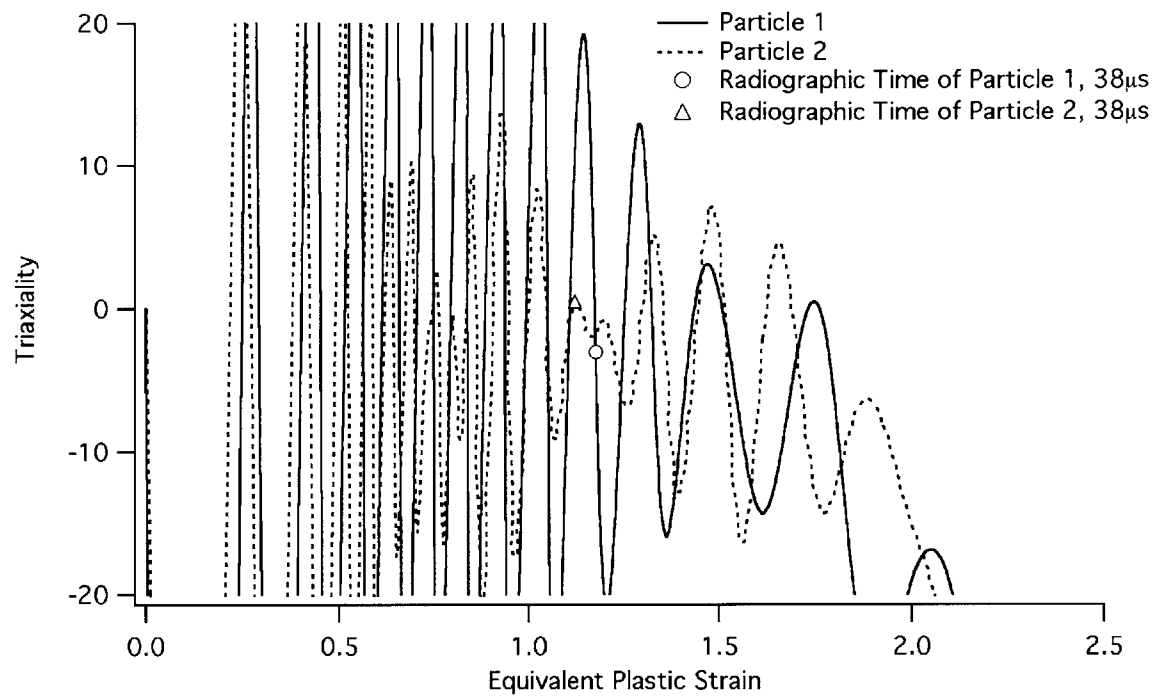


Figure 4.6: Placement of Massless Tracer Particles in Copper Tube Wall



**Figure 4.7(a): Elastic-Perfectly-Plastic, Convergent;
Triaxiality vs. Equivalent Plastic Strain Curves**

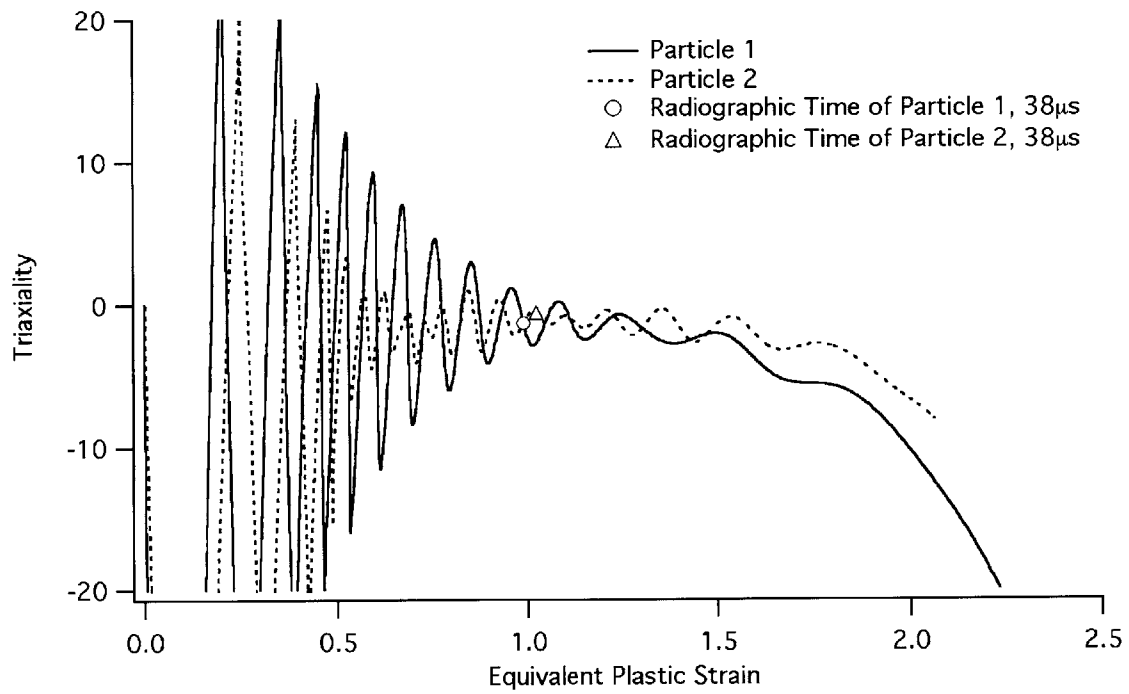


Figure 4.7(b): Johnson-Cook Strength, Convergent; Triaxiality vs. Equivalent Plastic Strain Curves

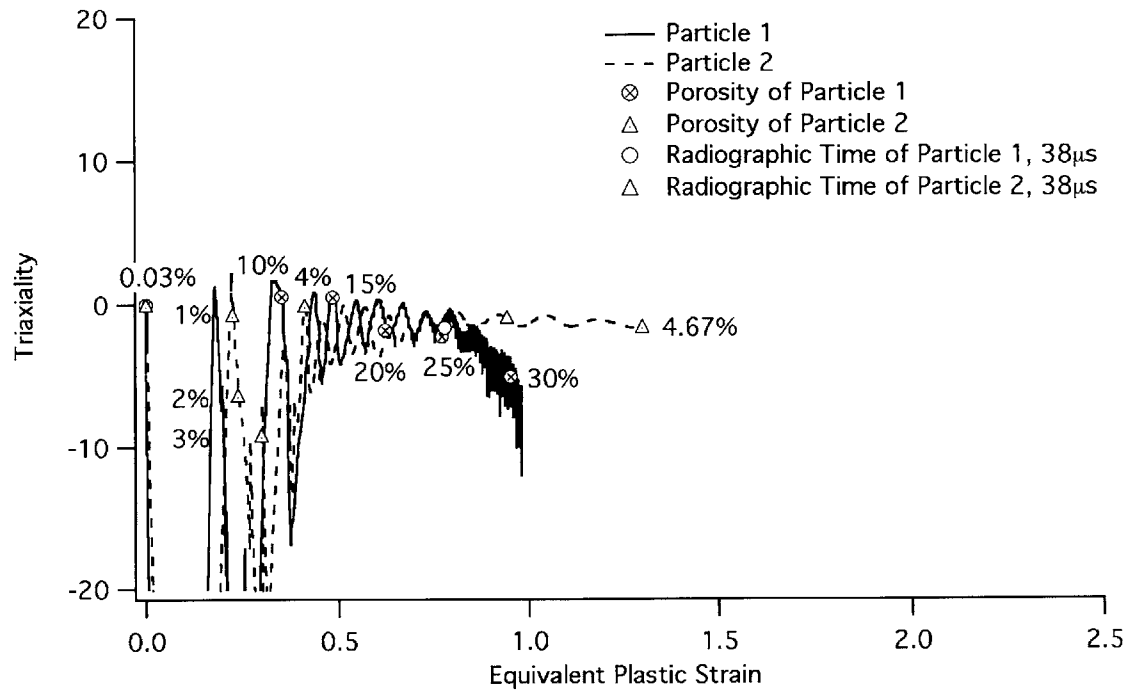


Figure 4.7(c): Johnson-Cook Strength / Johnson Spall Fracture, Convergent; Triaxiality vs. Equivalent Plastic Strain Curves

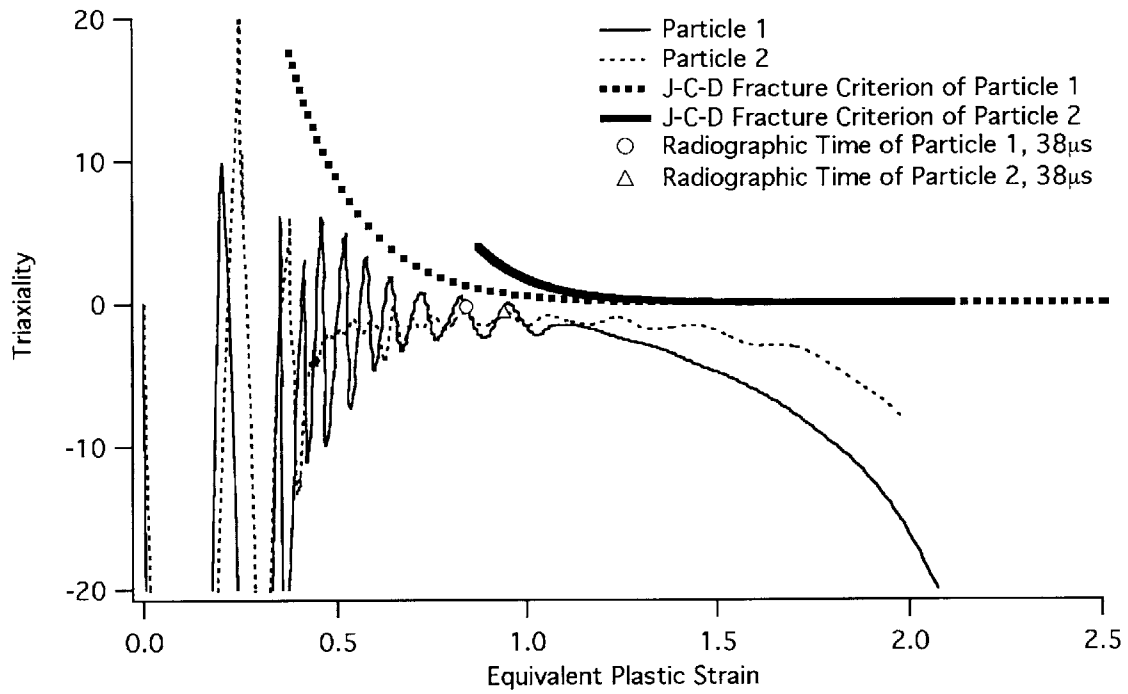


Figure 4.7(d): Johnson-Cook Strength / Johnson-Cook Damage, Convergent; Triaxiality vs. Equivalent Plastic Strain Curves

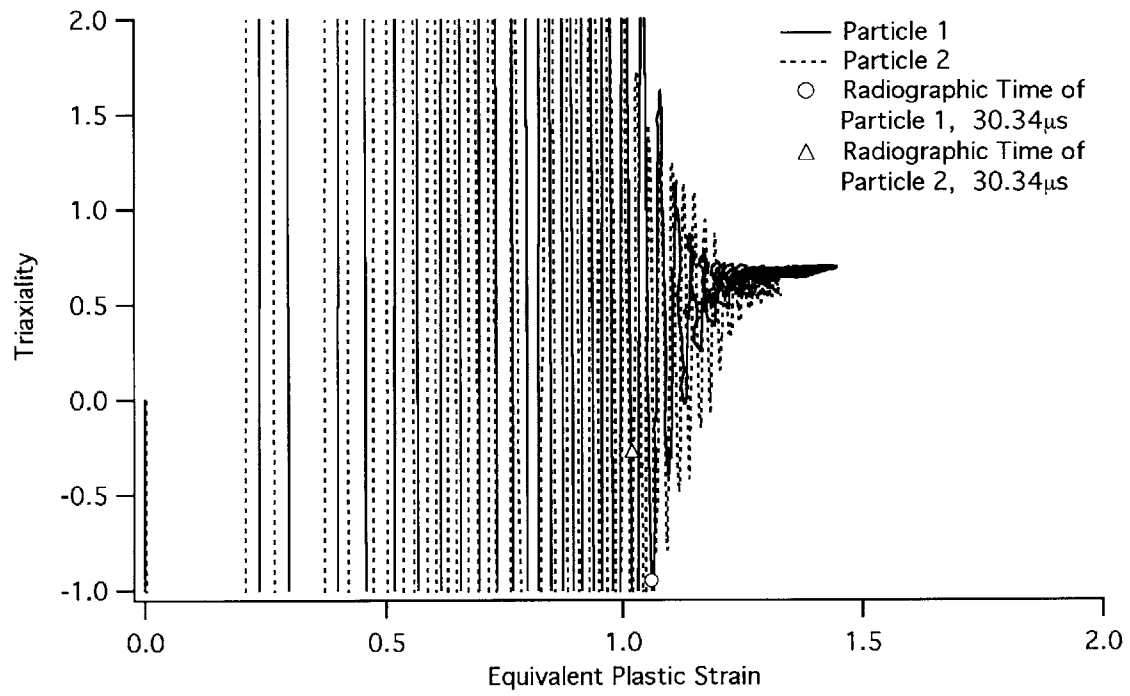


Figure 4.8(a): Elastic-Perfectly-Plastic, Divergent; Triaxiality vs. Equivalent Plastic Strain Curve

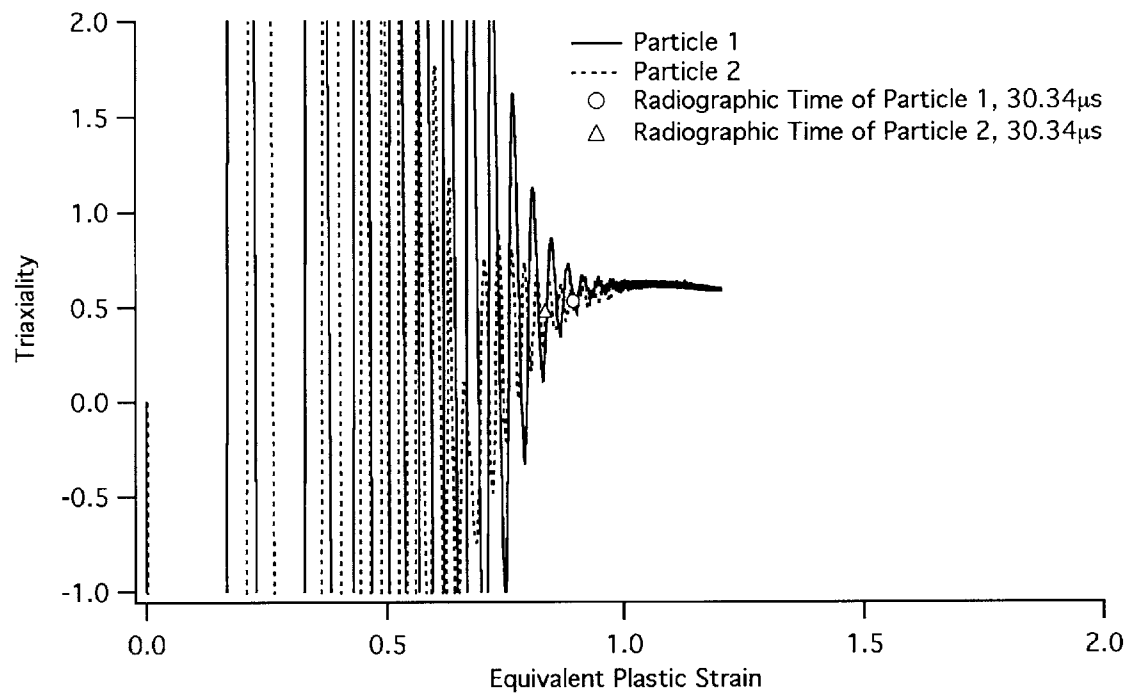


Figure 4.8(b): Johnson-Cook Strength, Divergent; Triaxiality vs. Equivalent Plastic Strain Curves

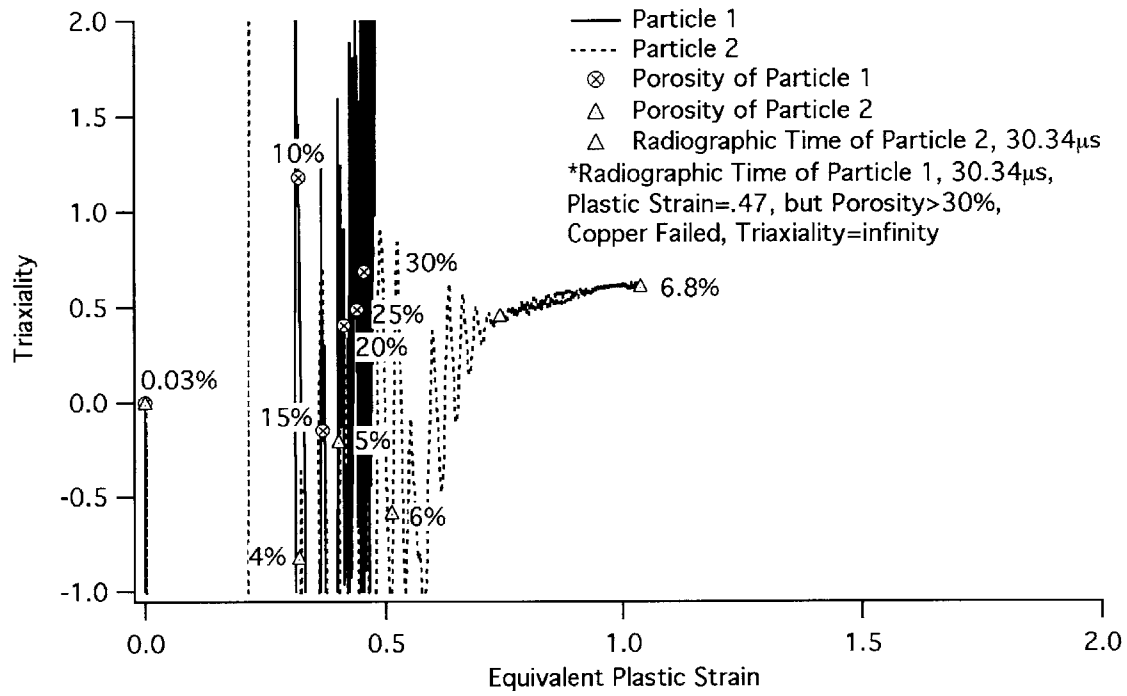


Figure 4.8(c): Johnson-Cook Strength / Johnson Spall Fracture, Divergent; Triaxiality vs. Equivalent Plastic Strain Curves

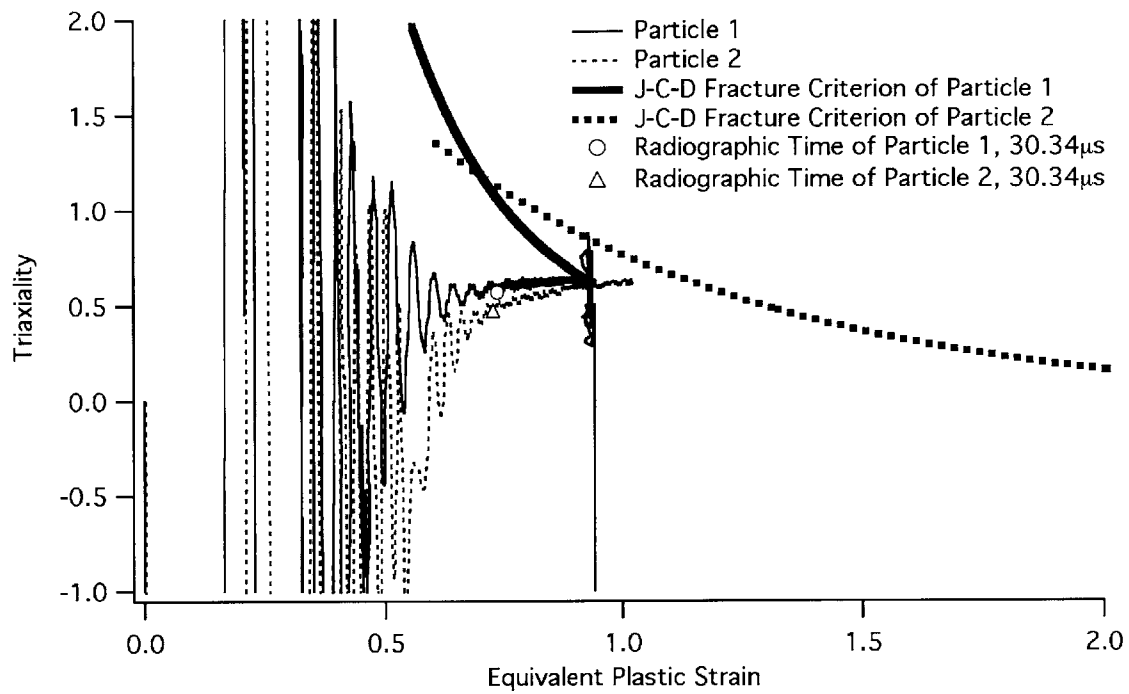


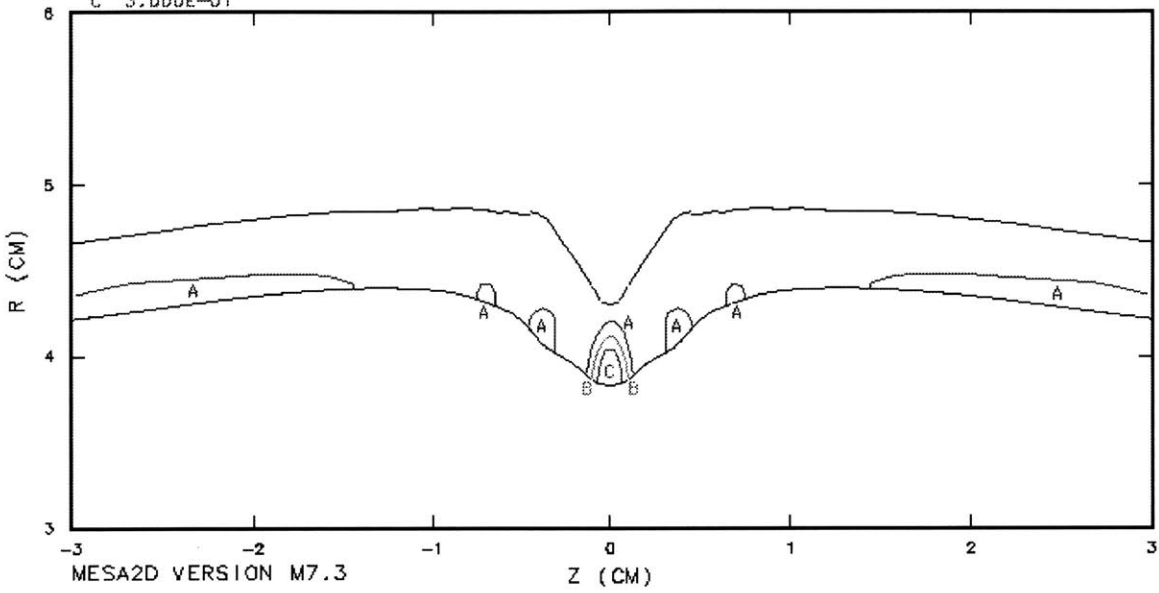
Figure 4.8(d): Johnson-Cook Strength / Johnson-Cook Damage, Divergent; Triaxiality vs. Equivalent Plastic Strain Curves

POROSITY

TIME 38.0141

CONVERGENT COPPER CYLINDER SYSTEM W/ EP-STRENGTH AND JS-FRAC

- A 1.000E-01
- B 2.000E-01
- C 3.000E-01



POROSITY

TIME 38.0135

CONVERGENT COPPER CYLINDER SYSTEM W/ JC-STRENGTH AND JS-FRAC

- A 1.000E-01
- B 2.000E-01
- C 3.000E-01

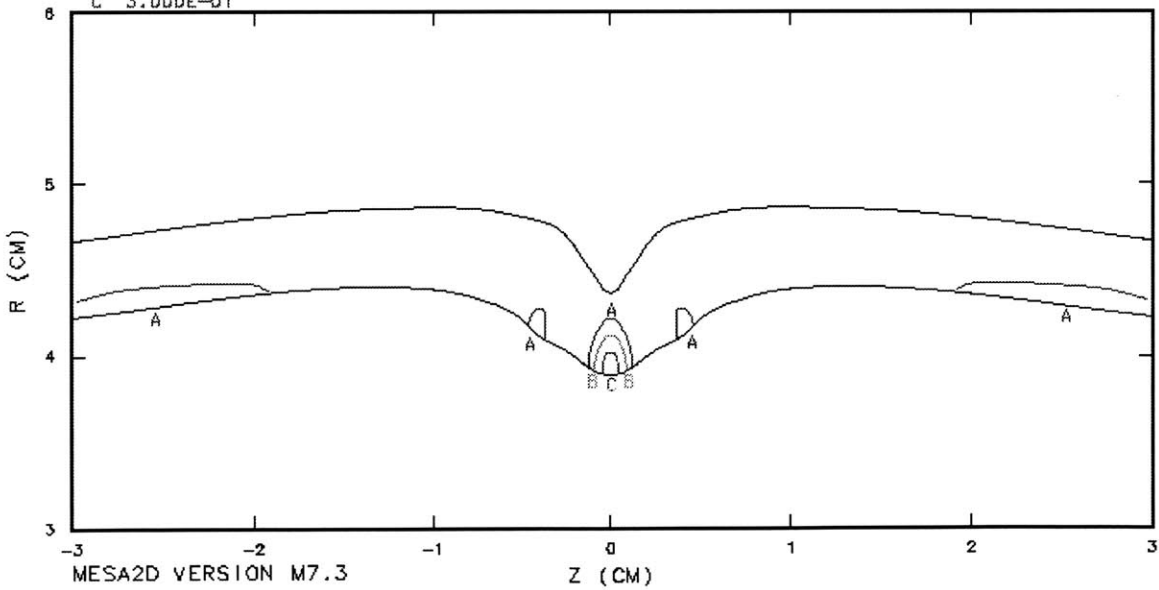


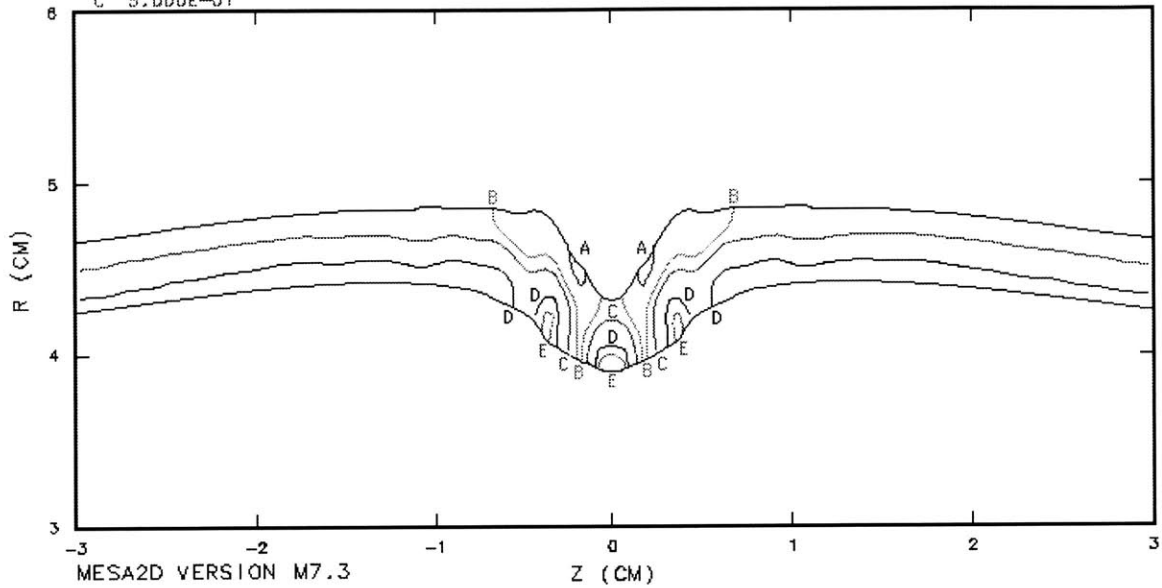
Figure 5.1: Convergent System MESA Calculations Comparing EPP to Johnson-Cook Strength with Johnson Spall Porosity Contours

DAMAGE

TIME 38.0082

CONVERGENT COPPER CYLINDER SYSTEM W/ EP-STRENGTH AND JC-FRAC

A 1.000E-01 D 9.000E-01
B 3.000E-01 E 1.000E+00
C 5.000E-01



DAMAGE

TIME 38.0139

CONVERGENT COPPER CYLINDER SYSTEM W/ JC-STRENGTH AND JC-FRAC

A 1.000E-01 D 9.000E-01
B 3.000E-01 E 1.000E+00
C 5.000E-01

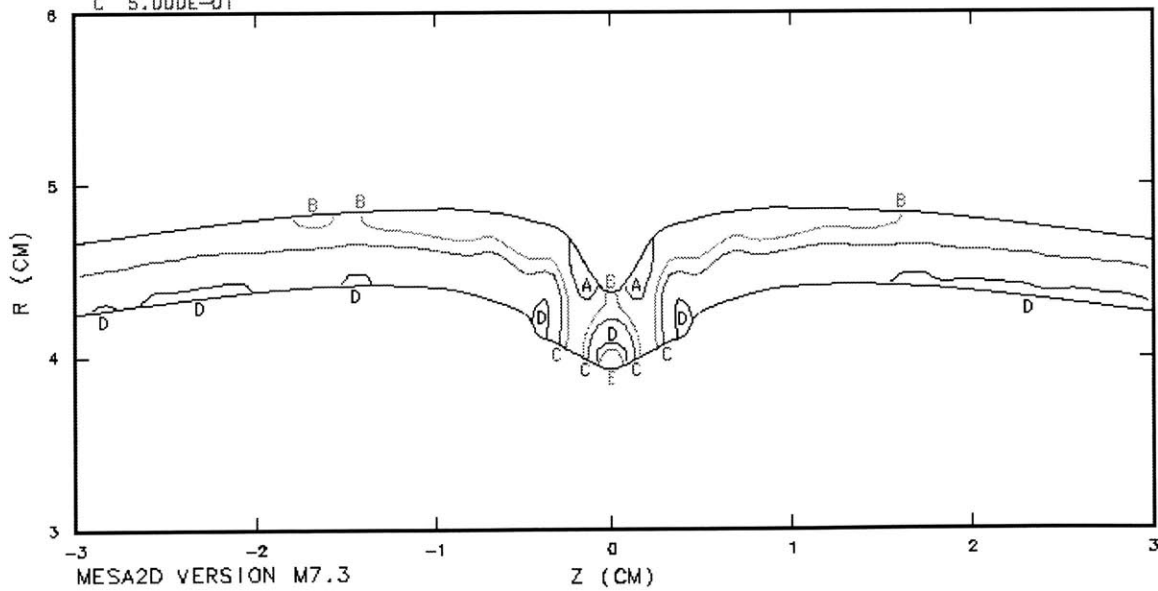


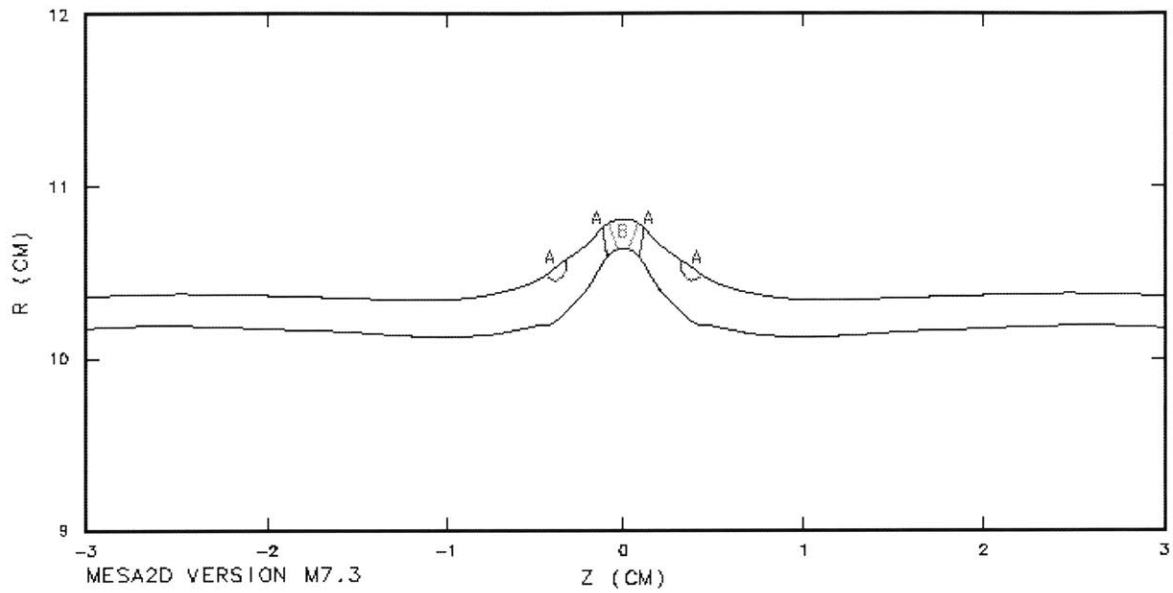
Figure 5.2: Convergent System MESA Calculations Comparing EPP to Johnson-Cook Strength with Johnson-Cook Damage Contours

POROSITY

TIME 30.3436

DIVERGENT COPPER CYLINDER SYSTEM W/ EP-STRENGTH AND JS-FRAC

A 1.000E-01
B 2.000E-01



POROSITY

TIME 30.3504

DIVERGENT COPPER CYLINDER SYSTEM W/ JC-STRENGTH AND JS-FRAC

A 1.000E-01
B 2.000E-01
C 3.000E-01

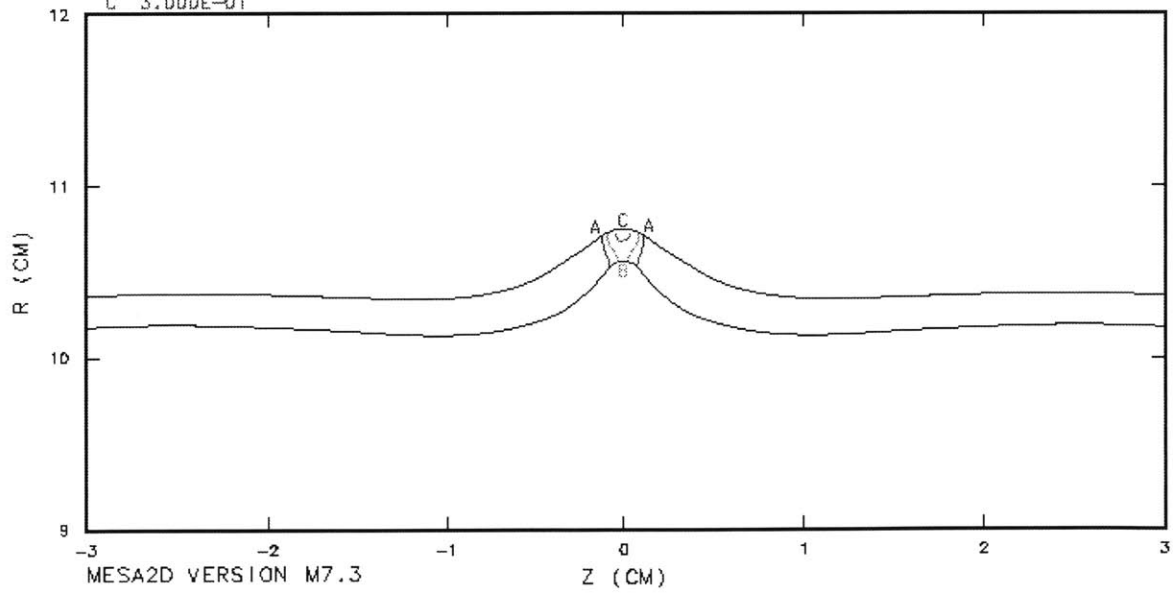


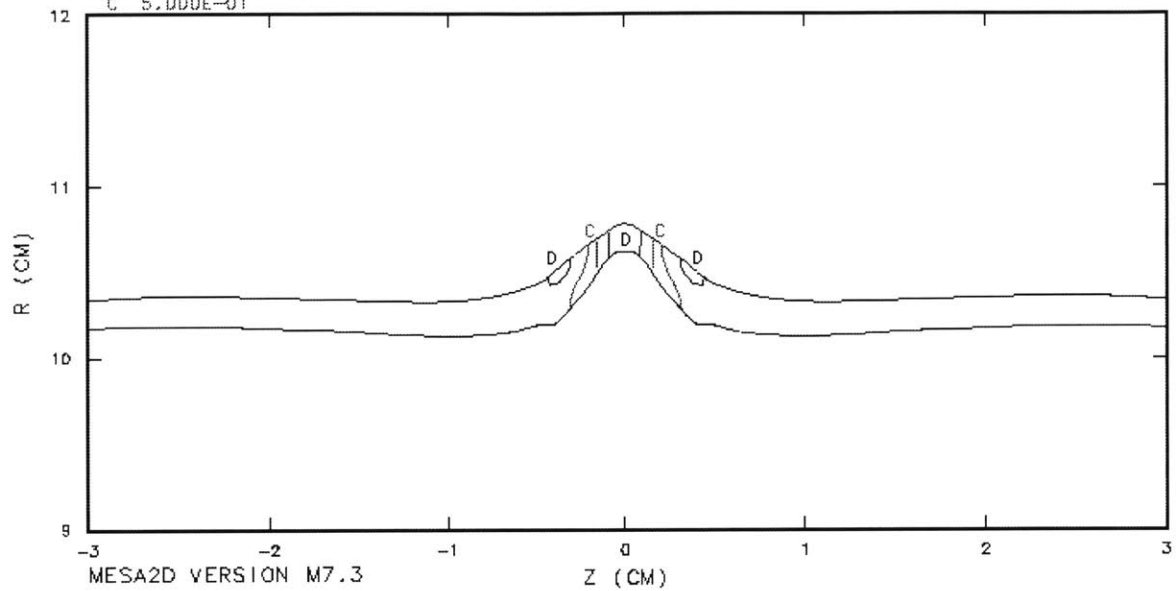
Figure 5.3: Divergent System MESA Calculations Comparing EPP to Johnson-Cook Strength with Johnson Spall Porosity Contours

DAMAGE

TIME 30.3552

DIVERGENT COPPER CYLINDER SYSTEM W/ EP-STRENGTH AND JC-FRAC

A 1.000E-01 D 9.000E-01
B 3.000E-01
C 5.000E-01



DAMAGE

TIME 30.3530

DIVERGENT COPPER CYLINDER SYSTEM W/ JC-STRENGTH AND JC-FRAC

A 1.000E-01 D 9.000E-01
B 3.000E-01
C 5.000E-01

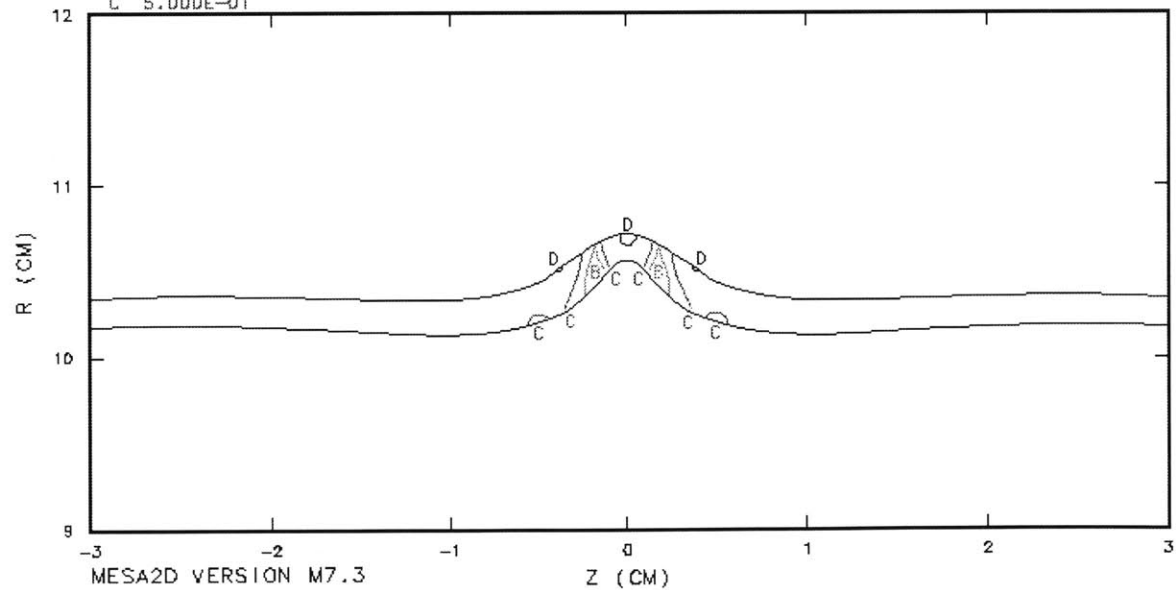


Figure 5.4: Divergent System MESA Calculations Comparing EPP to Johnson-Cook Strength with Johnson-Cook Damage Contours

POROSITY

TIME 30.3401

DIVERGENT COPPER CYLINDER SYSTEM W/ HIGH EP-STRENGTH AND JS-FRAC

A 1.000E-01

B 2.000E-01

C 3.000E-01

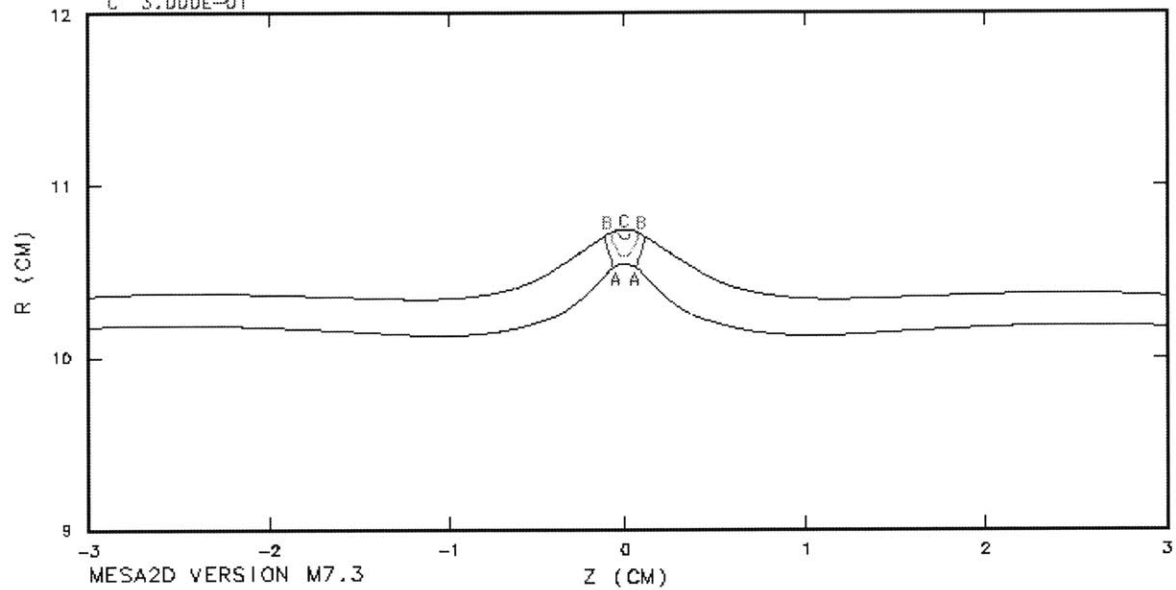


Figure 5.5: Divergent System MESA Calculations using EPP Strength with $Y_0=3.75$ kbars and Johnson Spall Porosity Contours

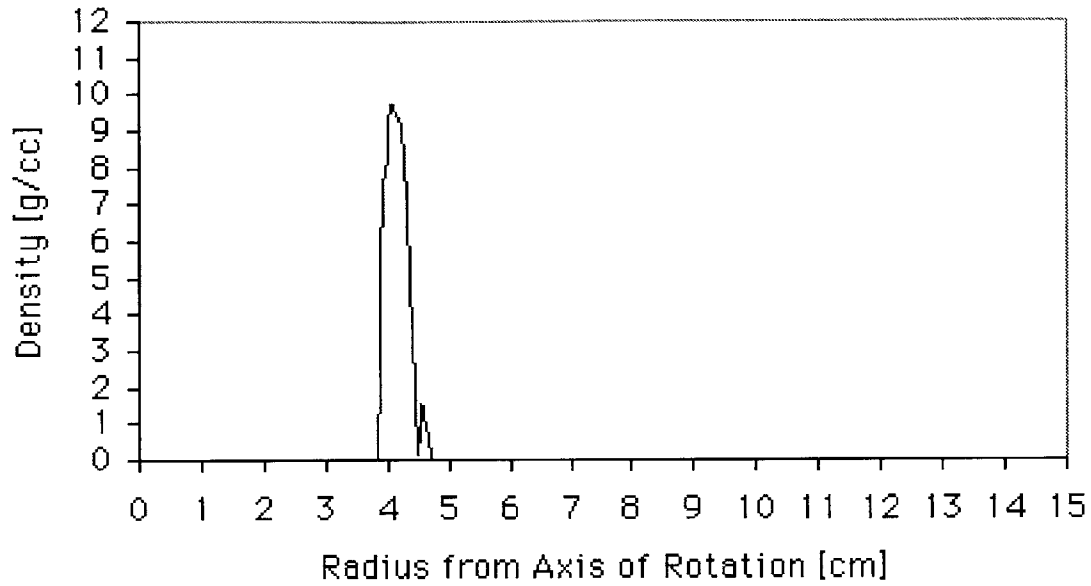


Figure 5.6: Density Profile of Wall on Cut Axis from Convergent Experiment Using Bayesian Reconstruction

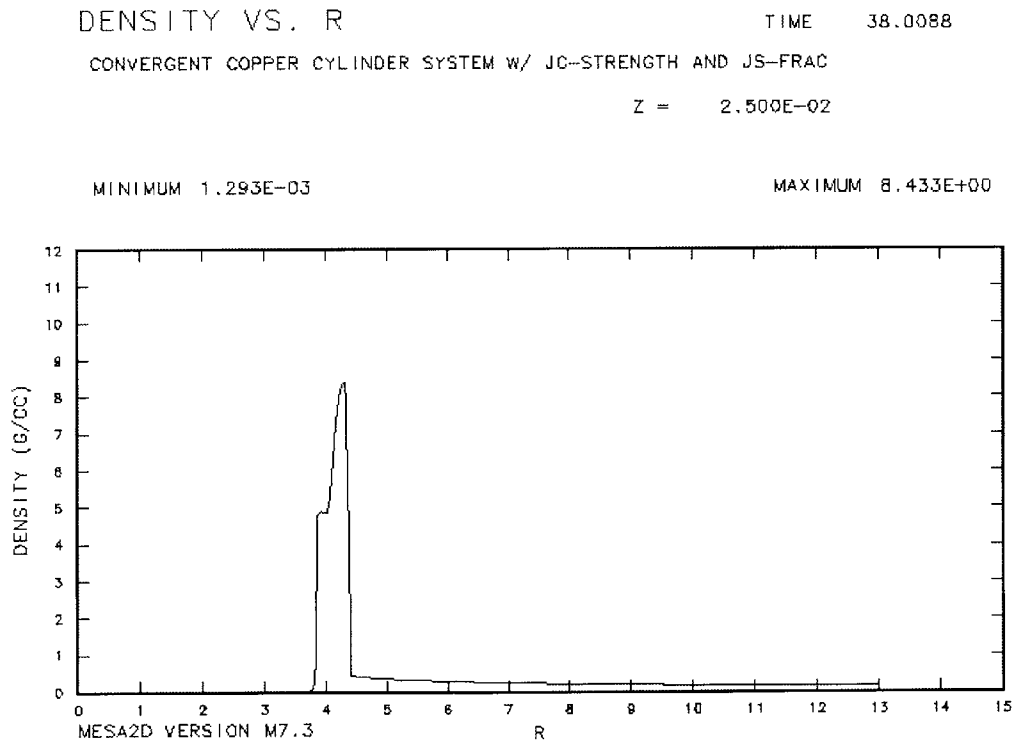
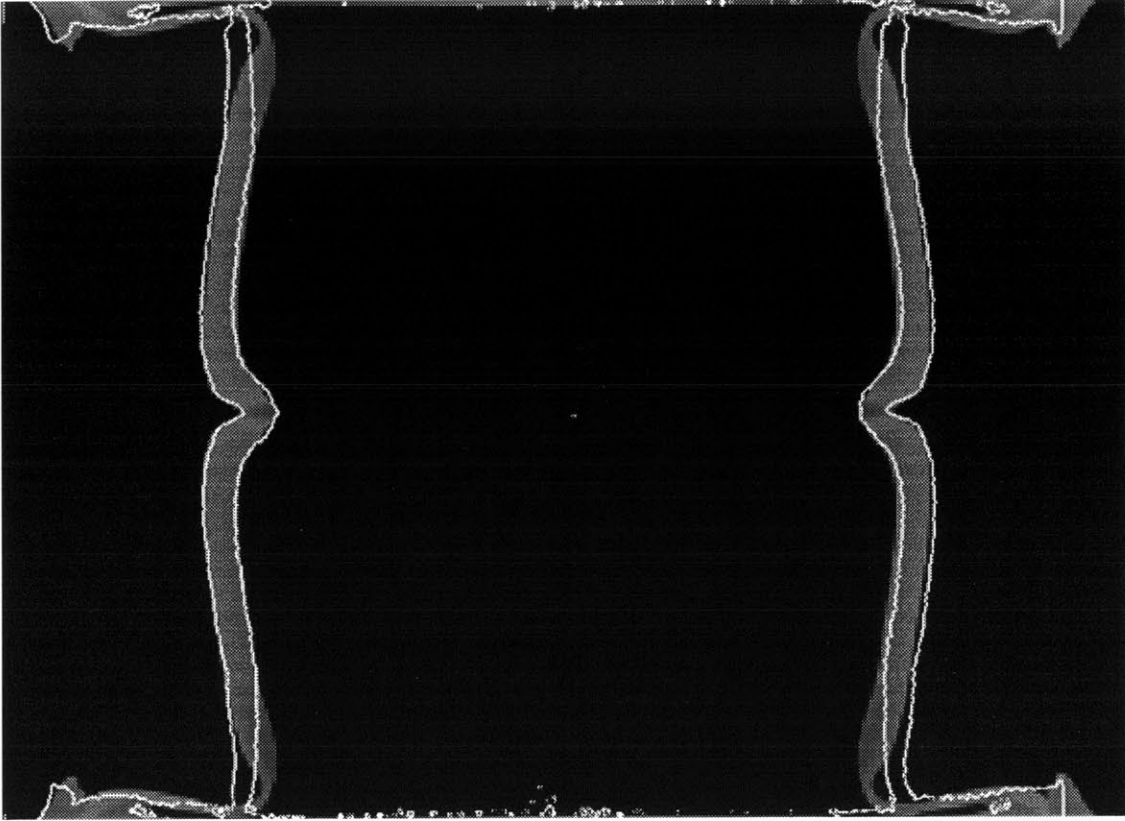


Figure 5.7: Density Profile of Wall on Cut Axis from Convergent Experiment from MESA Calculation



**Figure 5.8: Convergent System Overlay using Modified Johnson Spall Model
(no 30% failure criterion)**

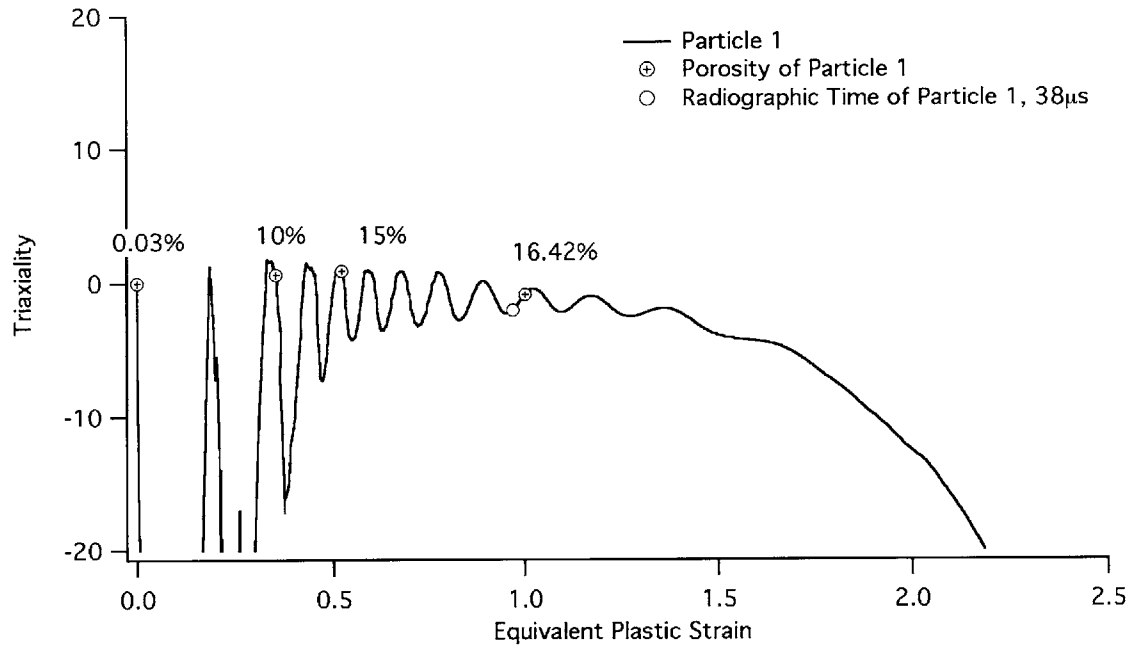


Figure 5.9(a): Convergent Triaxiality Plot

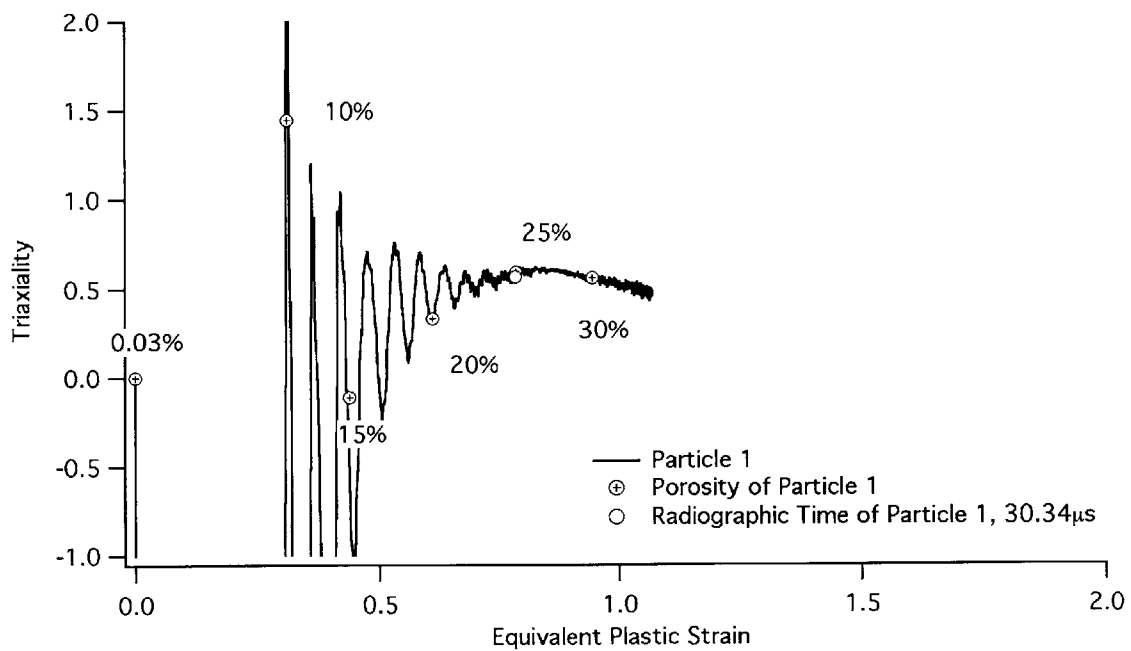


Figure 5.9(b): Divergent Triaxiality Plot

DENSITY VS. R

TIME 38.0135

CONVERGENT COPPER CYLINDER SYSTEM W/ JC-STRENGTH AND JS-FRAC

Z = 2.500E-02

MINIMUM 1.293E-03

MAXIMUM 8.405E+00

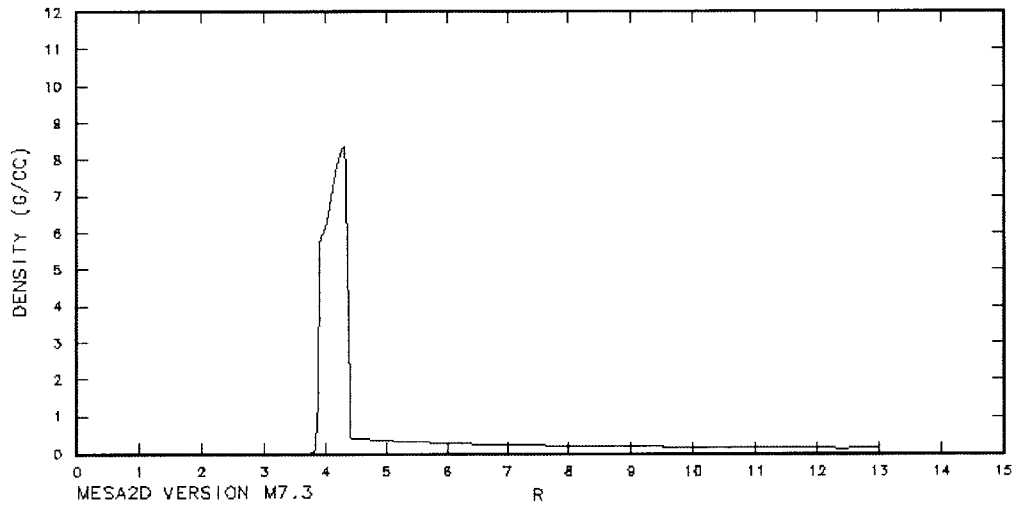


Figure 5.10: Density Profile of Wall on Cut Axis from Convergent Experiment from MESA Calculation using JS model w/out 30% Failure Criterion

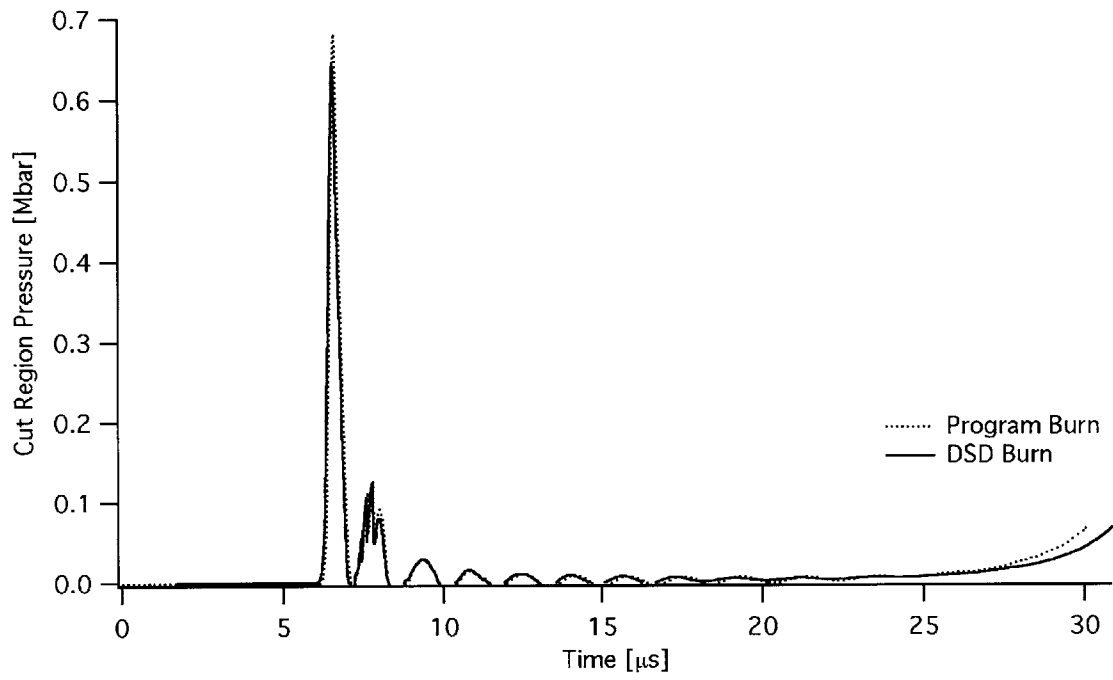


Figure 5.11(a): Simplified Convergent System Calculation Particle Plots Comparing DSD Burn to Program Burn in Cut Region Pressure

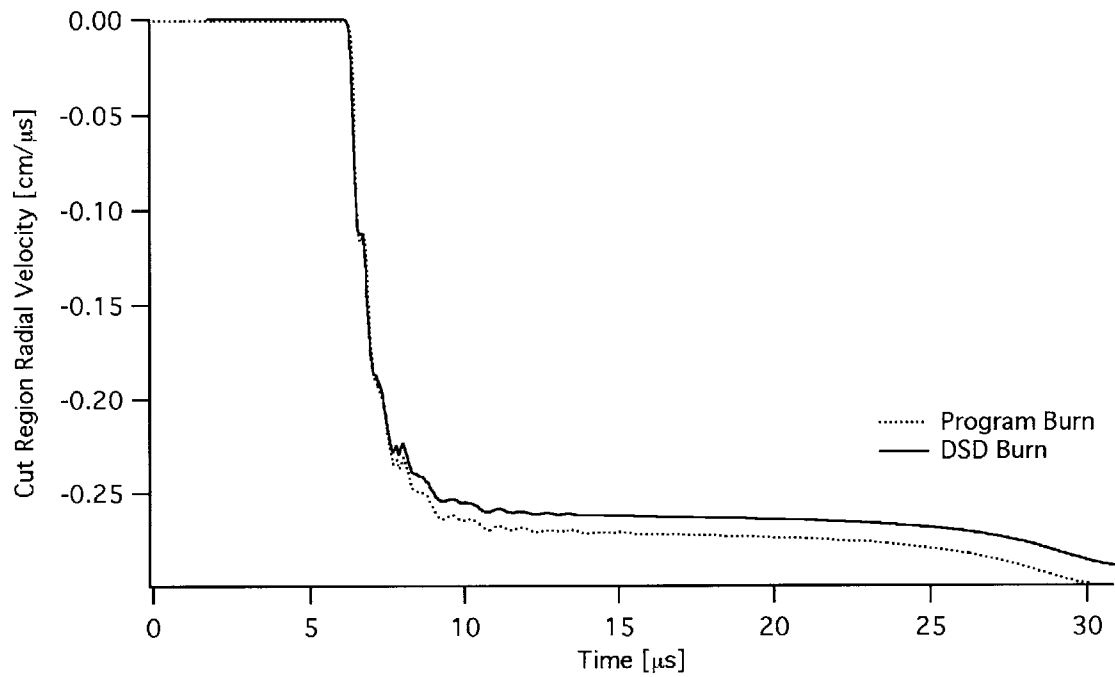


Figure 5.11(b): Simplified Convergent System Calculation Particle Plots Comparing DSD Burn to Program Burn in Cut Region Radial Velocity

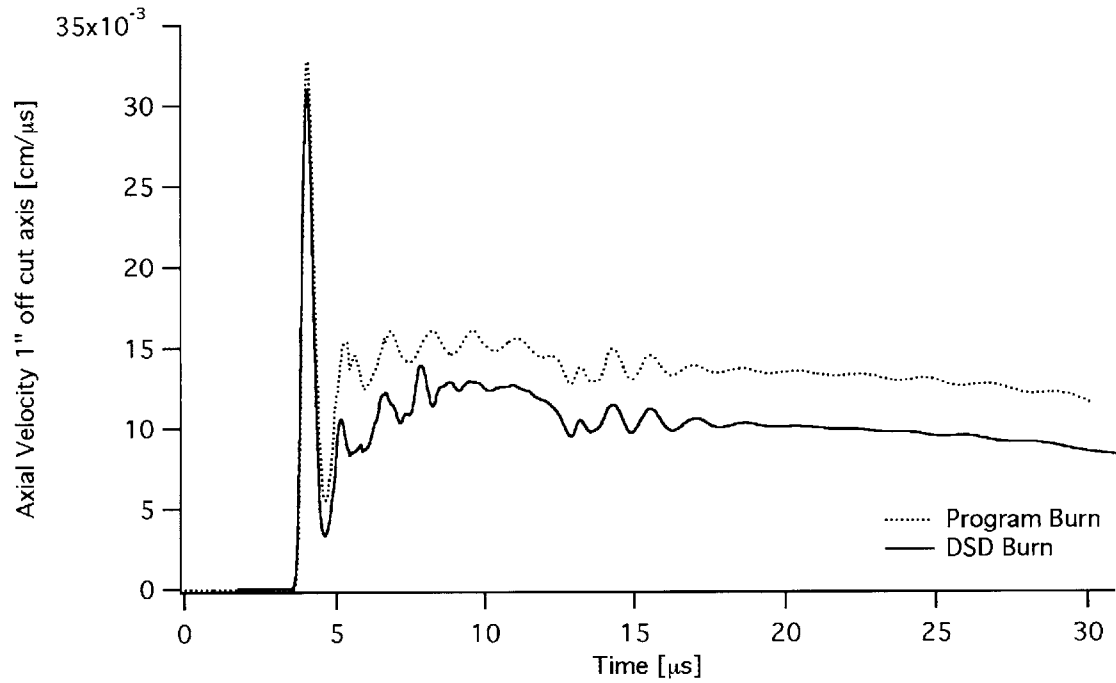


Figure 5.11(c): Simplified Convergent System Calculation Particle Plots Comparing DSD Burn to Program Burn in Axial Velocity 1" Off Cut Axis

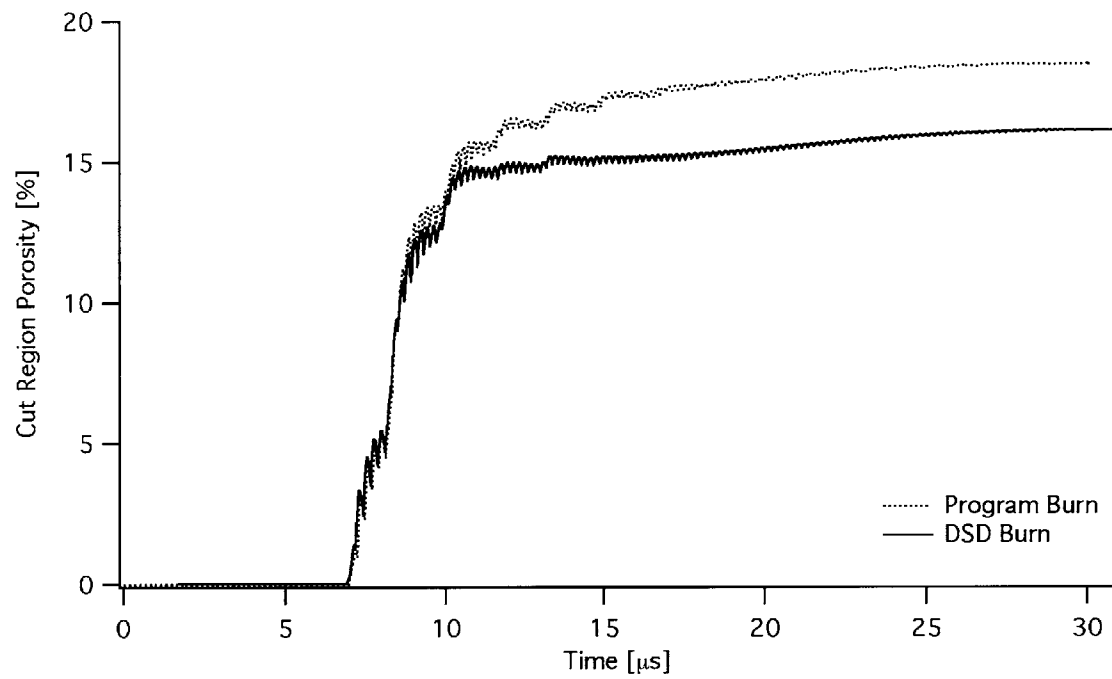


Figure 5.11(d): Simplified Convergent System Calculation Particle Plots Comparing DSD Burn to Program Burn in Cut Region Porosity

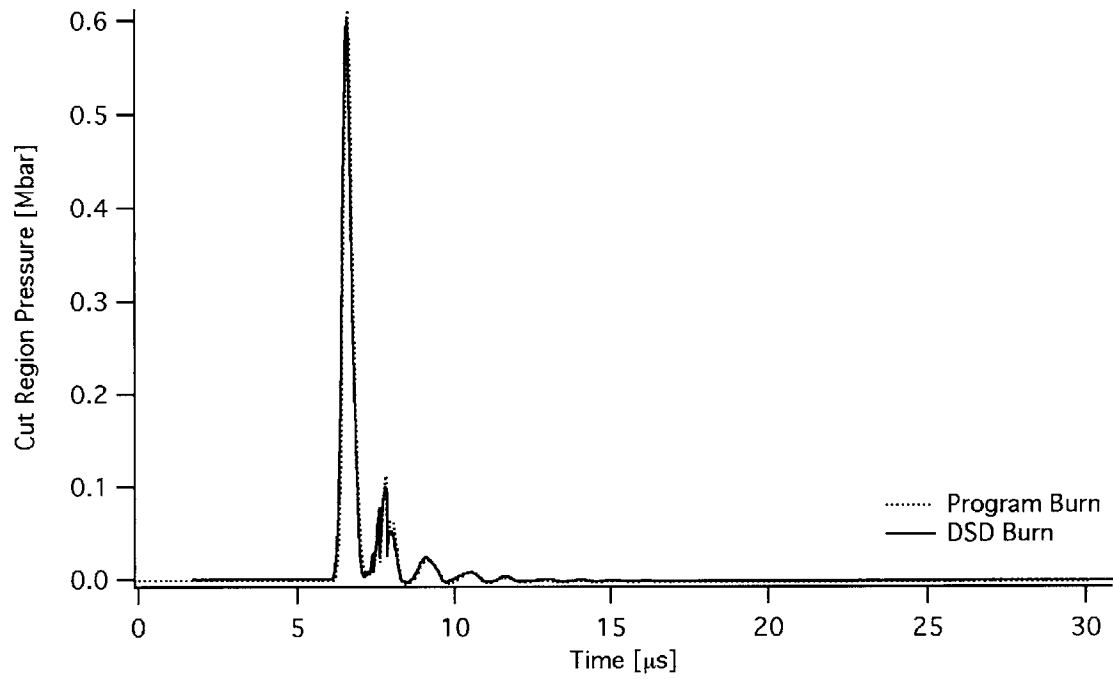


Figure 5.12(a): Simplified Divergent System Calculation Particle Plots Comparing DSD Burn to Program Burn in Cut Region Pressure

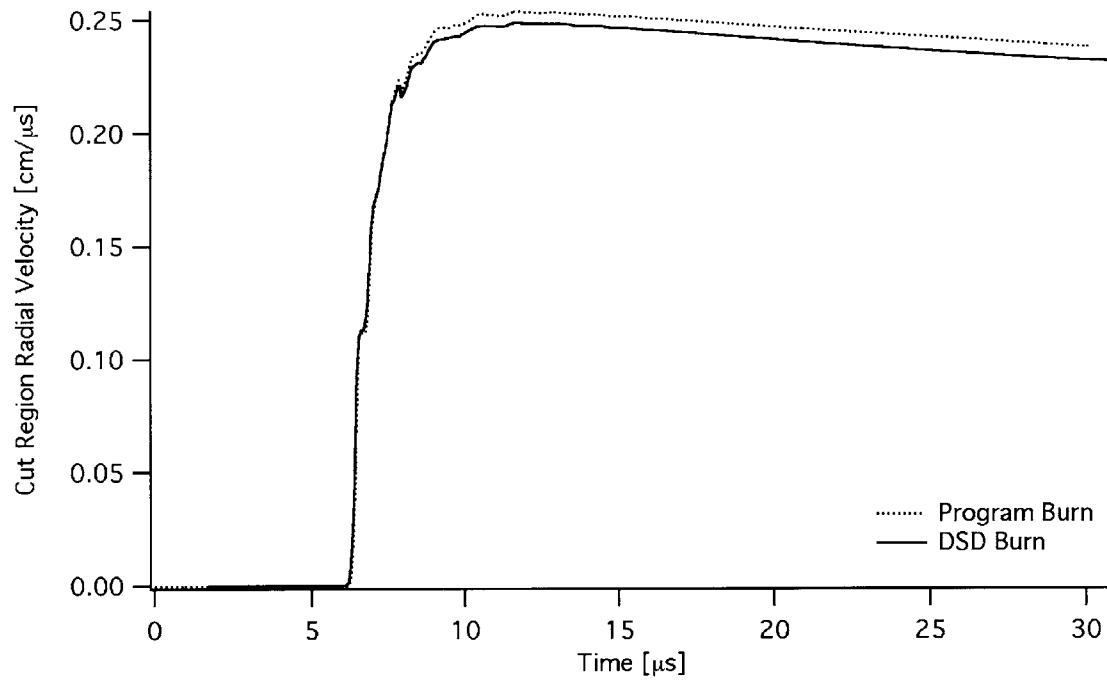


Figure 5.12(b): Simplified Divergent System Calculation Particle Plots Comparing DSD Burn to Program Burn in Cut Region Radial Velocity

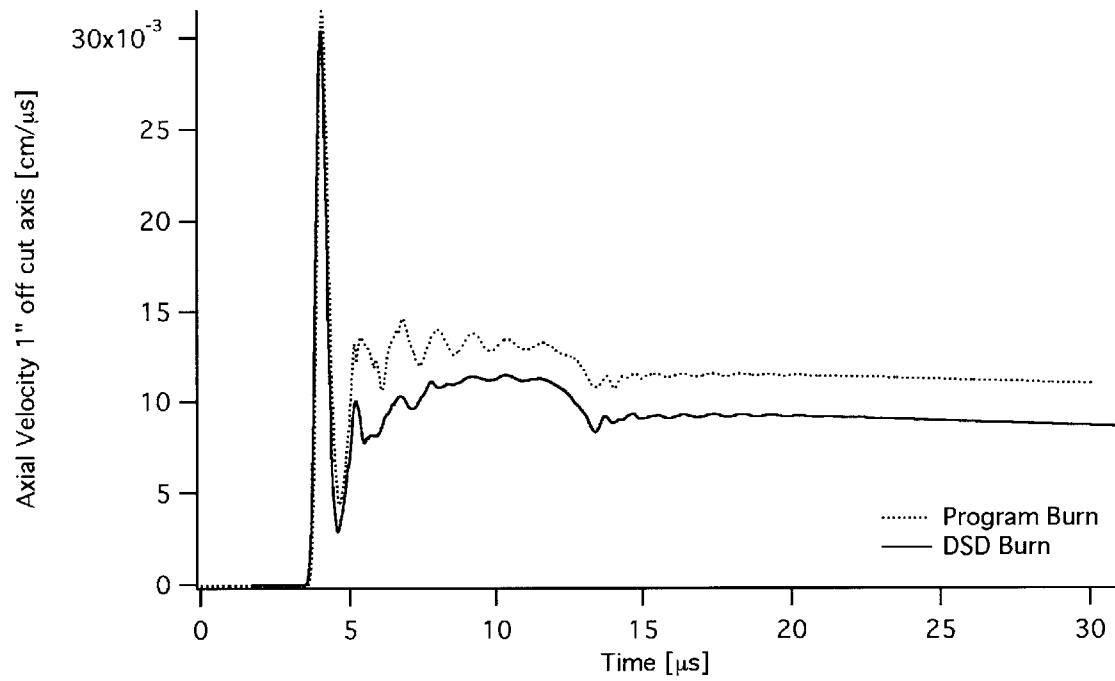


Figure 5.12(c): Simplified Divergent System Calculation Particle Plots Comparing DSD Burn to Program Burn in Axial Velocity 1'' Off Cut Axis

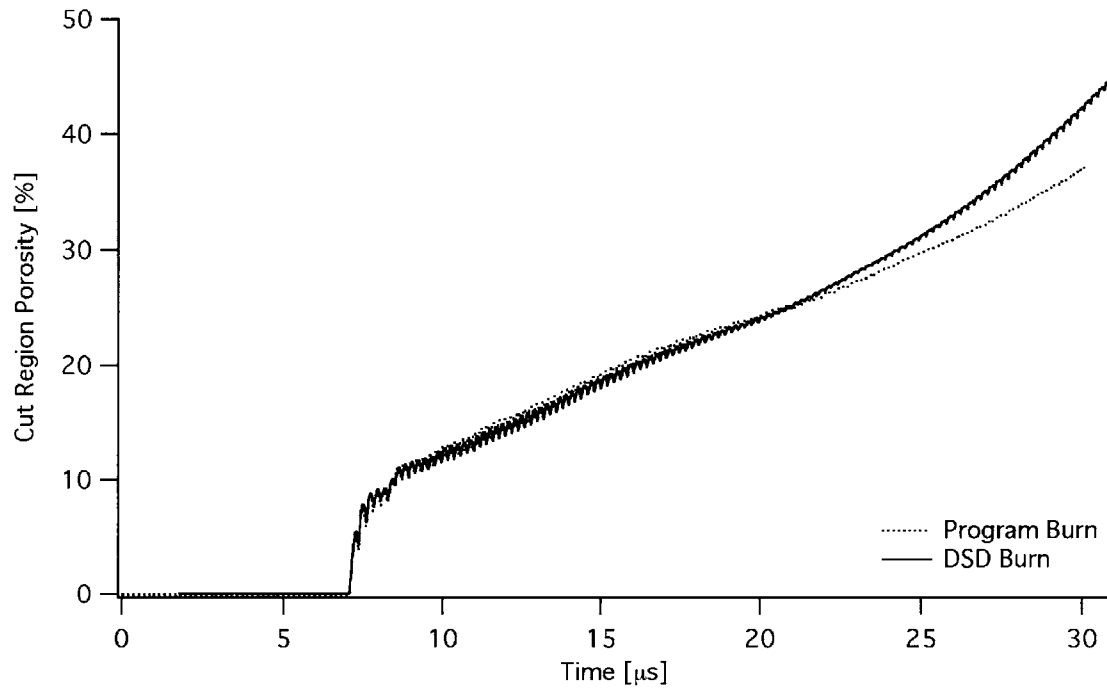


Figure 5.12(d): Simplified Divergent System Calculation Particle Plots Comparing DSD Burn to Program Burn in Cut Region Porosity

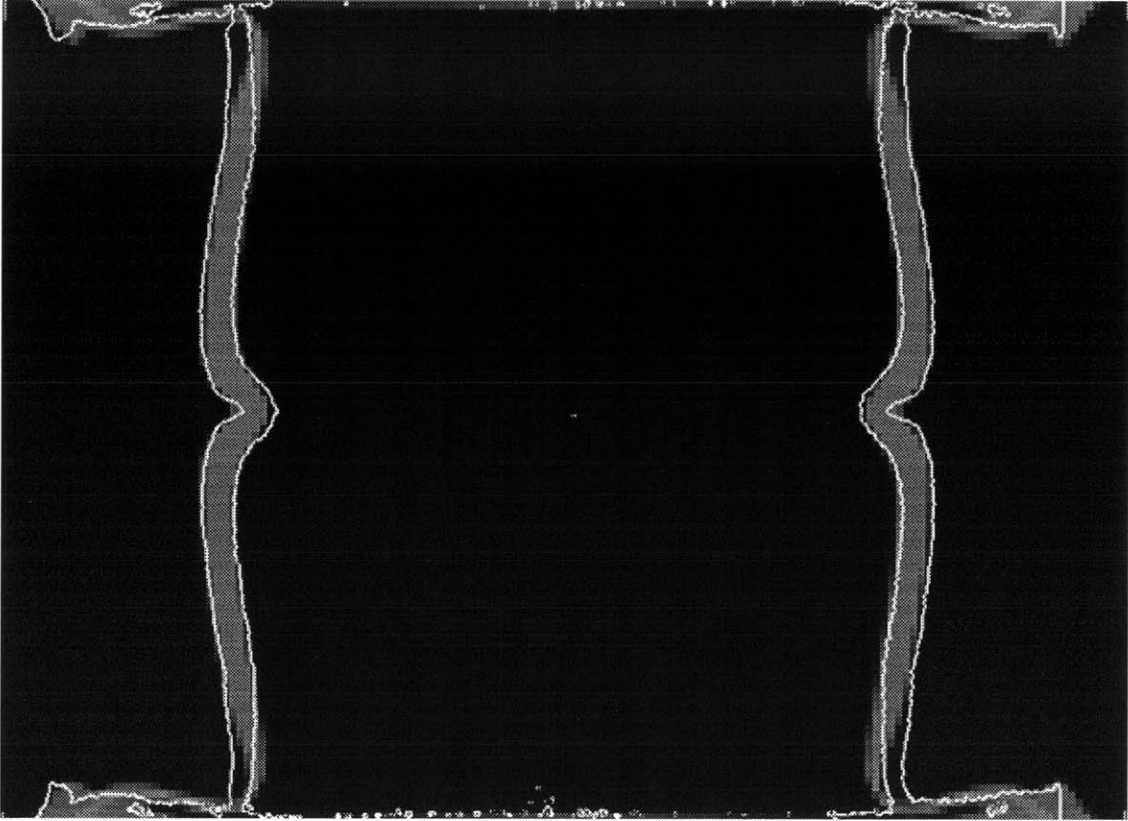


Figure 5.13(a): Calculation at Mesh Resolution = 0.1cm

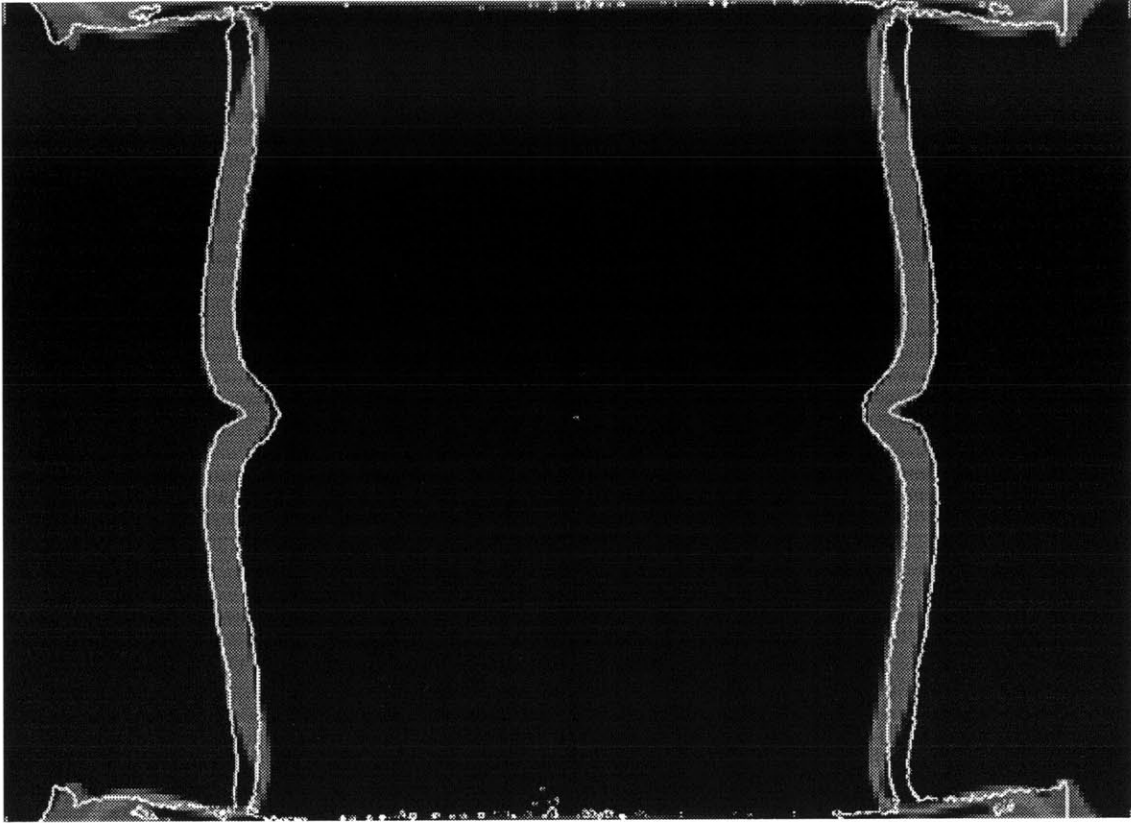


Figure 5.13(b): Calculation at Mesh Resolution = 0.075cm

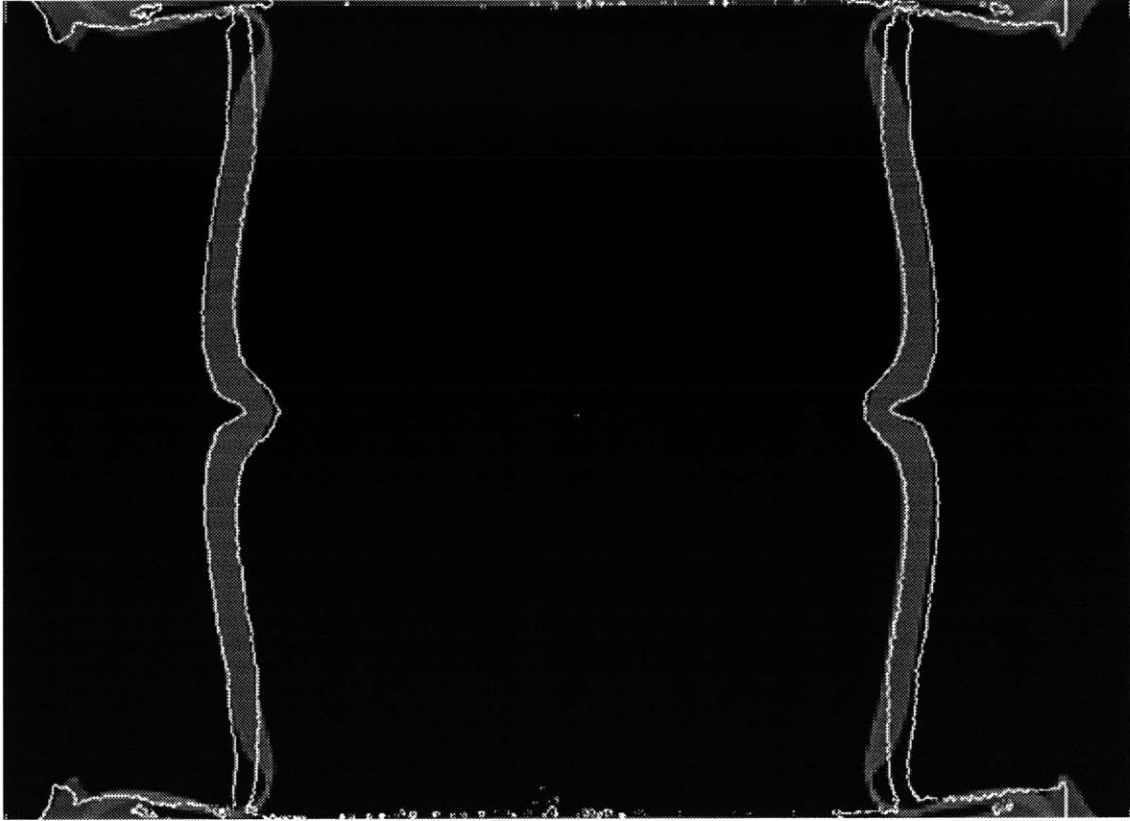


Figure 5.13(c): Calculation at Mesh Resolution = 0.05cm

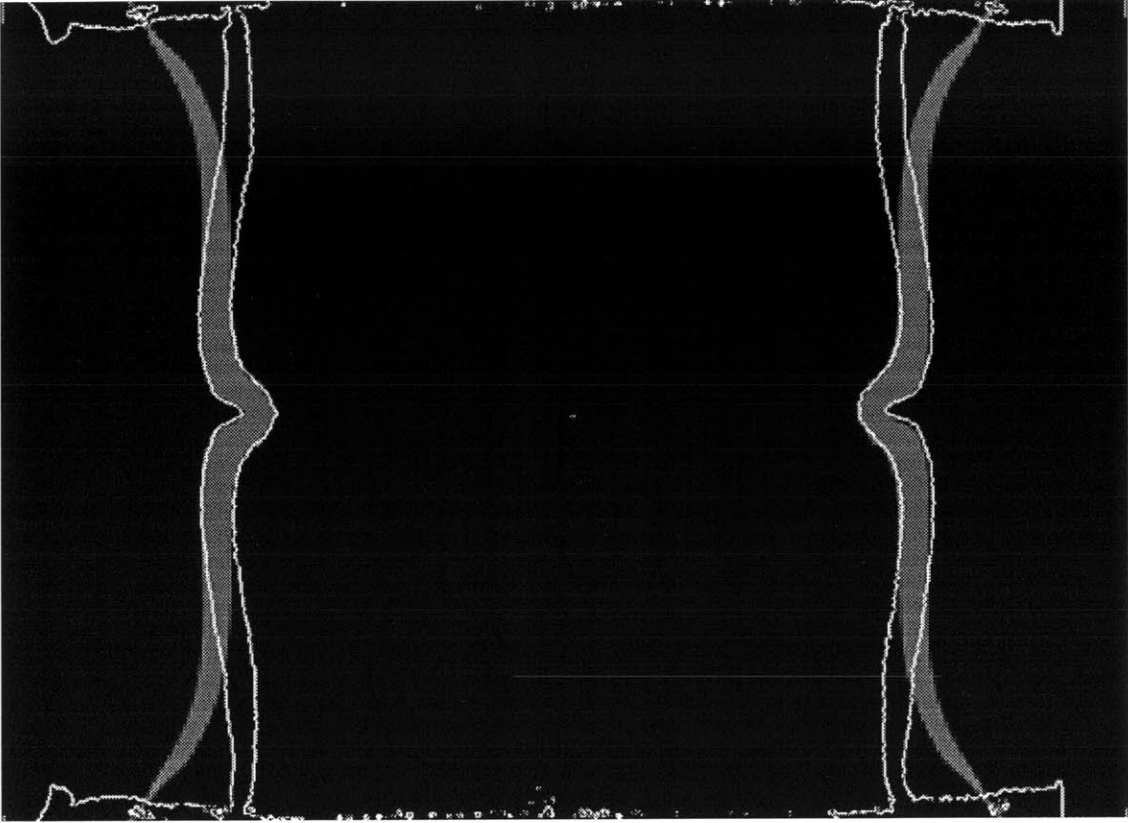


Figure 5.14: Simplified MESA Calculation Overlaid with Experimental Data

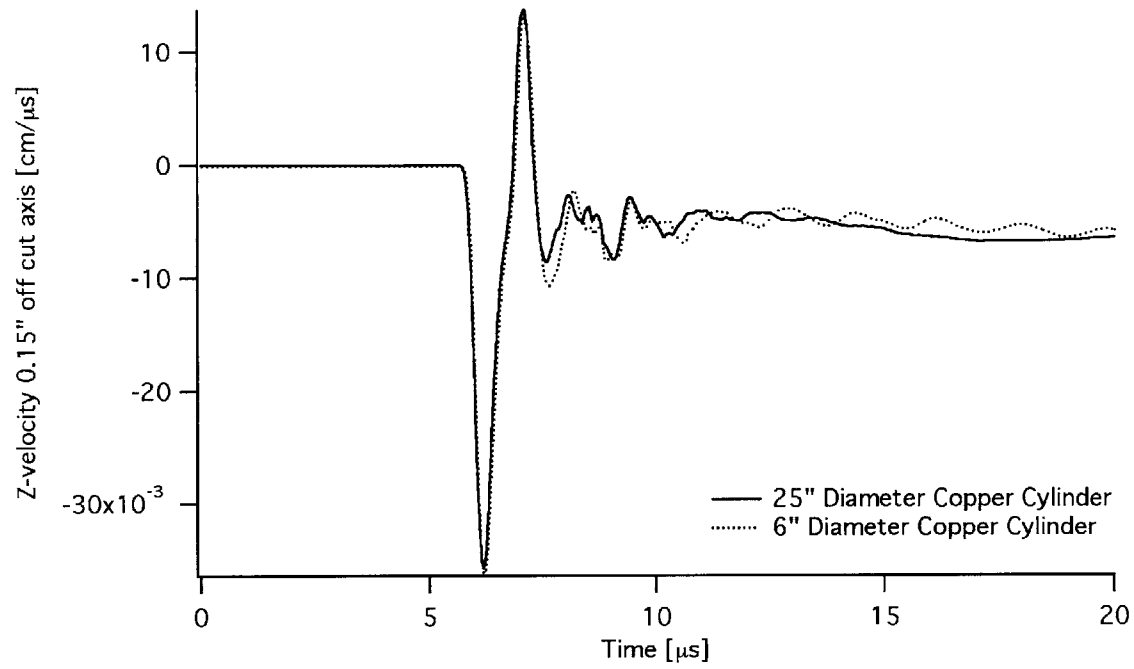


Figure 5.15: Axial Response of Copper 0.15" off Cut Axis for 6" and 25" OD Simulations

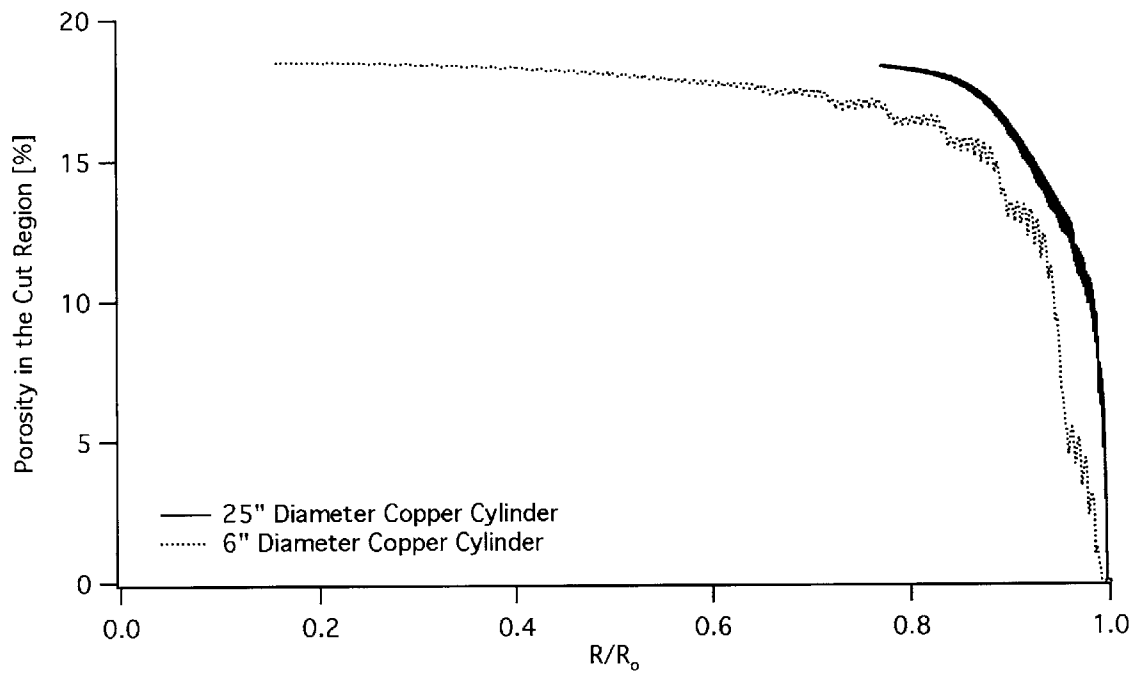


Figure 5.16: Cut Region Porosity versus Relative Radial Deformation for 6" and 25" OD Simulations

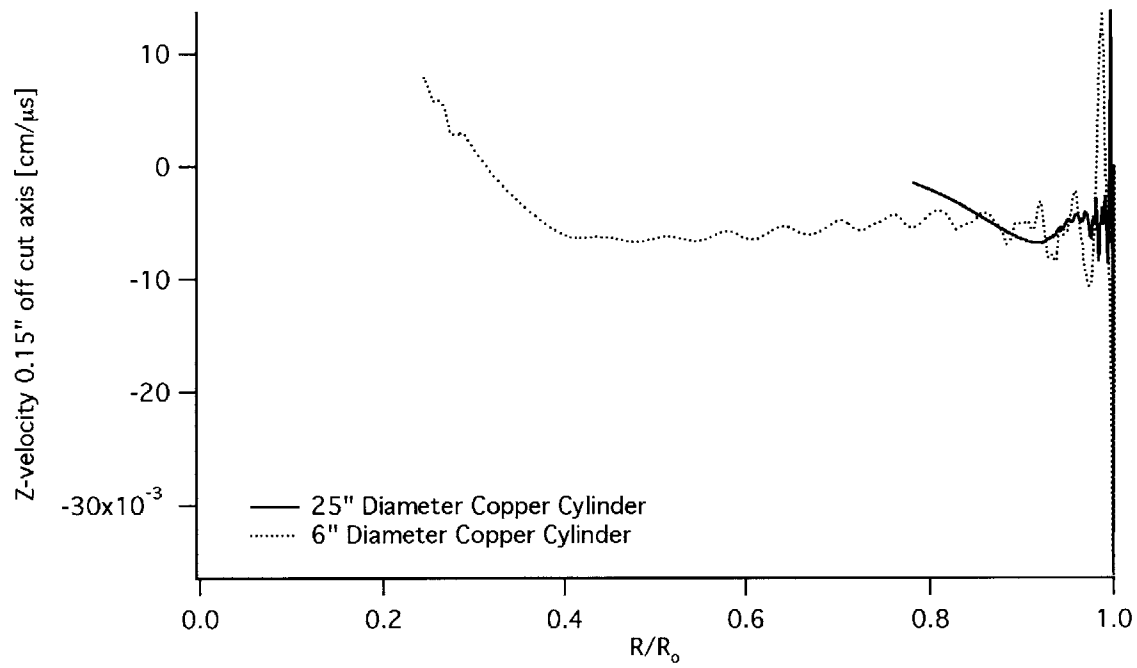


Figure 5.17: Axial Response of Copper 0.15" off Cut Axis versus Relative Radial Deformation for 6" and 25" OD Simulations

8.0 References

1. Hull, Lawrence; personal communication
2. MESA-2D (1995) *Reference Manuals*. Clancy, Sean P. and Bennion, S. Tom.
3. Johnson, G.R. and Holmquist, T.J. (1989) Test Data and Computational Strength and Fracture Model Constants for 23 Materials Subjected to Large Strains, High Strain Rates, and High Temperatures. *Report prepared by Honeywell Inc., Armament Systems Division., Brooklyn Park, MN for the Los Alamos National Laboratory*. Limited Access.
4. Johnson, G.R. and Cook, W.H. (1983) A Constitutive Model and Data for Metals Subjected to Large Strains, High Strain Rates and High Temperatures. *Proceedings of Seventh International Symposium on Ballistics, The Hague, The Netherlands*. April 1983, 541-548.
5. Johnson, G.R. and Holmquist, T.J. (1988) Evaluation of Cylinder Impact Test Data for Constitutive Model Constants. *Journal of Applied Physics* **64**, 3901-3910.
6. Johnson, J.N. (1981) Dynamic Fracture and Spallation in Ductile Solids. *Journal of Applied Physics* **52**, 2812-2825.
7. Meyers, Marc Andre (1994) *Dynamic Behavior of Materials*, pp.98-135. John Wiley & Sons, Inc., New York.
8. McQueen, R.G., Marsh, S.P., Taylor, J.W., Fritz, J.N., and Carter, W.J. (1970) The Equation of State of Solids From Shock Wave Studies. *High-Velocity Impact Phenomena*, edited by Kinslow, Ray. Academic Press, New York.
9. Follansbee, P.S. and Kock, U.F. (1988) A Constitutive Description of the Deformation of Copper Based on the Use of the Mechanical Threshold Stress as an Internal State Variable. *Acta Metall.* **36**, No. 1, 81-93.
10. Kothari M., Anand L. (1998) Elasto-Viscoplastic Constitutive Equations for Polycrystalline Metals: Application to Tantalum. *J. Mech. Phys. Solids* **46**, 51-83.
11. Watson, S.A. (1998) A Closed-Form, Fellget-Linfoot Radiographic Figure of Merit. *DARHT Technical Note No. 94*, Los Alamos National Laboratory.
12. Abel, N.H. (1826) Resolution d'un Probleme de Mecanique. *J. Reine u. Angew. Math.* **1**, 153-157.
13. Hanson, K.M. (1984) Tomographic Reconstruction of Axially Symmetric Objects from a Single Radiograph. *Proceedings of the 16th International Congress on High Speed Photography and Photonics, (Proc. SPIE, 491, 180-187)*, Strasbourg, France.

14. Steinburg, Daniel J. (1991) Equation of State and Strength Properties of Selected Materials. *Technical Paper #UCRL-MA-106439* Lawrence Livermore National Laboratory.
15. Chen, S.R. and Gray, G.T. (1996) Constitutive Behavior of Tantalum and Tantalum-Tungsten Alloys. *Metall. Mater. Trans. A* **27A**, 2994-3006.
16. Chen, S.R. personal communication.
17. Hanson, K. M. (1989) A Bayesian Approach to Nonlinear Inversion: Abel Inversion from X-ray Attenuation Data. Published in: Transport Theory, Invariant Imbedding, and Integral Equations. Nelson, Paul et al., ed., *Lecture Notes in Pure and Appl. Math* **115**, 363-378. Marcel-Decker, New York.
18. Stewart, D. Scott and Bdzil, John B. (1989) Examples of Detonation Shock Dynamics for Detonation Wave Spread Applications. *9th Symposium on Detonation, Portland, Oregon* **1**, 773-783.

9.0 Appendix

MESA Input Files (GEN & MESA) for Strength and Fracture Model Iteration Calculations

Hydrodynamic (No Strength, No Fracture):

GEN

mesa2d (g)

Convergent copper cylinder system w/ no strength and no frac
L=5", OD=6", t=0.1", mesh=0.05cm

\$probsize

heburn= .true. , strength= .false. , jcdfrac=.false.,
jsfrac= .false. , jhdfrc=.false.,
mcr= 260, mcz= 520,
mmats= 13 , mcomp= 13 , mmix= 25000,

\$end

\$options

ibcr1= 0 , ibcr2= 1 , ibcz1= 1 , ibcz2= 1 ,
idgeom= 2 ,
part=.true. ,
t=3.7,

\$end

\$mesh

ncellr= 200, 60,
coordr= 0.0, 10.0, 13.0,
rator= 1.0, 1.0,
ncellz= 120, 280, 120,
coordz= -13.0, -7.0, 7.0, 13.0,
ratioz= 1.0, 1.0, 1.0,

\$end

\$mats

matbak= 1 , pribak= 1,

matname(1)='air', eosform(1)='gas', strform(1)='none',
d0(1)=1.293e-03 , e0(1)=1.9335e-03 , pmin(1)=0.0,
eoscon(1)=1.4 ,

matname(2) = 'cu', eosform(2) = 'usup', strform(2) = 'none',
d0(2) = 8.93, e0(2) = 0.0, pmin(2) = -0.100, detvel(2) = 0.0,
eoscon(1,2) = 0.394, 1.489, 0.0, 2.02,
fracform(2) = 'none',

fracon(1,2) = 0.54, 4.89, -3.03, 0.014, 1.12,
0., 0.00407, 0.033, 0.024, 1.,
priority(2)=2,

matname(3) = '9501', eosform(3) = 'jwl', strform(3) = 'none',
d0(3) = 1.84, e0(3) = 0.05543, pmin(3) = 0.0, detvel(3) = 0.88,
eoscon(1,3) = 0.38, 8.524, 8.46, 0.1802, 2.39,
y0(3) = 0.0, ymax(3) = 0.0, g0(3) = 0.0, gmax(3) = 0.0,
strcon(1,3) = 0.0,
priority(3)=3,

matname(4) = 'polyethylene', eosform(4) = 'usup', strform(4) = 'none',
d0(4) = 0.916, e0(4) = 6.6567e-07, pmin(4) = -0.010, detvel(4) = 0.0,
eoscon(1,4) = 0.266, 1.55, 0.0, 1.64,
priority(4)=6,

matname(5) = 'polyethylene', eosform(5) = 'usup', strform(5) = 'none',
d0(5) = 0.916, e0(5) = 6.6567e-07, pmin(5) = -0.010, detvel(5) = 0.0,
eoscon(1,5) = 0.266, 1.55, 0.0, 1.64,
priority(5)=7,

matname(6) = 'stainless steel(304)', eosform(6) = 'usup', strform(6) = 'none',
d0(6) = 7.896, e0(6) = 0.0, pmin(6) = -0.10, detvel(6) = 0.0,
eoscon(1,6) = 0.457, 1.49, 0.0, 2.17,
y0(6) = 0.0034, ymax(6) = 0.025, g0(6) = 0.77, gmax(6) = 5.66,
strcon(1,6) = 43.0, 0.0, 0.35, 0.001, 0.00881, 2.26, 2.26,
fracform(6) = 'none', fracon(1,6)= 1.0003, fracon(2,6)= 0.0017,
fracon(3,6)= 0.00001, fracon(4,6)= 0.266
priority(6)=4,

matname(7) = 'stainless steel(304)', eosform(7) = 'usup', strform(7) = 'none',
d0(7) = 7.896, e0(7) = 0.0, pmin(7) = -0.10, detvel(7) = 0.0,
eoscon(1,7) = 0.457, 1.49, 0.0, 2.17,
y0(7) = 0.0034, ymax(7) = 0.025, g0(7) = 0.77, gmax(7) = 5.66,
strcon(1,7) = 43.0, 0.0, 0.35, 0.001, 0.00881, 2.26, 2.26,
fracform(7) = 'none', fracon(1,7)= 1.0003, fracon(2,7)= 0.0017,
fracon(3,7)= 0.00001, fracon(4,7)= 0.266
priority(7)=5,

matname(8) = '9501', eosform(8) = 'jwl', strform(8) = 'none',
d0(8) = 1.84, e0(8) = 0.05543, pmin(8) = 0.0, detvel(8) = 0.88,
eoscon(1,8) = 0.38, 8.524, 8.46, 0.1802, 2.39,
y0(8) = 0.0, ymax(8) = 0.0, g0(8) = 0.0, gmax(8) = 0.0,
strcon(1,8) = 0.0,
priority(8)=8,

matname(9) = '9501', eosform(9) = 'jwl', strform(9) = 'none',
d0(9) = 1.84, e0(9) = 0.05543, pmin(9) = 0.0, detvel(9) = 0.88,
eoscon(1,9) = 0.38, 8.524, 8.46, 0.1802, 2.39,
y0(9) = 0.0, ymax(9) = 0.0, g0(9) = 0.0, gmax(9) = 0.0,
strcon(1,9) = 0.0,
priority(9)=9,

matname(10) = '9407', eosform(10) = 'jwl', strform(10) = 'none',
d0(10) = 1.6, e0(10) = 0.0538, pmin(10) = 0.0, detvel(10) = 0.791,
eoscon(1,10) = 0.32, 5.7319, 7.4, 0.14639, 2.24,
y0(10) = 0.0, ymax(10) = 0.0, g0(10) = 0.0, gmax(10) = 0.0,
strcon(1,10) = 0.0,
priority(10)=10 ,

matname(11) = '9407', eosform(11) = 'jwl', strform(11) = 'none',
d0(11) = 1.6, e0(11) = 0.0538, pmin(11) = 0.0, detvel(11) = 0.791,
eoscon(1,11) = 0.32, 5.7319, 7.4, 0.14639, 2.24,
y0(11) = 0.0, ymax(11) = 0.0, g0(11) = 0.0, gmax(11) = 0.0,
strcon(1,11) = 0.0,
priority(11)=11 ,

matname(12) = 'polyethylene', eosform(12) = 'gas', strform(12) = 'none',
d0(12) = 0.916, e0(12) = 5.4585e-07, pmin(12) = -0.000, detvel(12) = 0.0,
eoscon(1,12) = 3.0,
priority(12)=12,

matname(13) = 'polyethylene', eosform(13) = 'gas', strform(13) = 'none',
d0(13) = 0.916, e0(13) = 5.4585e-07, pmin(13) = -0.000, detvel(13) = 0.0,
eoscon(1,13) = 3.0,
priority(13)=13,

\$end

\$points

rz=

1 , 0.000 , 12.065 ,
2 , 0.000 , 11.113 ,
3 , 0.000 , 9.843 ,
4 , 0.000 , 8.890 ,
5 , 0.000 , 7.620 ,
6 , 0.000 , 6.350 ,
7 , 0.000 , -6.350 ,
8 , 0.000 , -7.620 ,
9 , 0.000 , -8.890 ,


```
10 , 0.000 , -9.843 ,
11 , 0.000 , -11.113 ,
12 , 0.000 , -12.065 ,
13 , 0.635 , -11.113 ,
14 , 0.635 , -9.843 ,
15 , 0.635 , 9.843 ,
16 , 0.635 , 11.113 ,
17 , 7.366 , 6.350 ,
18 , 7.366 , -6.350 ,
19 , 7.620 , -6.350 ,
20 , 7.620 , -5.080 ,
21 , 7.620 , 5.080 ,
22 , 7.620 , 6.350 ,
23 , 7.938 , 7.620 ,
24 , 7.938 , 5.080 ,
25 , 7.938 , -5.080 ,
26 , 7.938 , -7.620 ,
27 , 8.090 , -8.890 ,
28 , 8.090 , 8.890 ,
29 , 9.201 , 5.080 ,
30 , 9.201 , -5.080 ,
31 , 9.525 , -5.080 ,
32 , 9.525 , 5.080 ,
33 , 9.843 , 9.843 ,
34 , 9.843 , 8.255 ,
35 , 9.843 , 5.080 ,
36 , 9.843 , -5.080 ,
37 , 9.843 , -8.255 ,
38 , 9.843 , -9.843 ,
39 , 10.478 , -12.065 ,
40 , 10.478 , -8.255 ,
41 , 10.478 , 8.255 ,
42 , 10.478 , 12.065 ,
```

\$end

```
$region
```

```
mat = 2,
```

```
points = 17, 18, 19, 20, 21, 22, 17,
```

\$end

```
$region
```

```
mat = 3,
```

```
points = 21, 20, 25, 30, 31, 32, 29, 24, 21,
```

\$end

```
$region
```

mat = 6,
points = 5, 6, 17, 22, 21, 24, 23, 5,
\$end

\$region
mat = 7,
points = 7, 8, 26, 25, 20, 19, 18, 7,
\$end

\$region
mat = 4,
points = 4, 5, 23, 24, 29, 28, 4,
\$end

\$region
mat = 5,
points = 8, 9, 27, 30, 25, 26, 8,
\$end

\$region
mat = 8,
points = 3, 4, 28, 29, 32, 35, 34, 33, 15, 3,
\$end

\$region
mat = 9,
points = 9, 10, 14, 38, 37, 36, 31, 30, 27, 9,
\$end

\$region
mat = 10,
points = 2, 3, 15, 16, 2,
\$end

\$region
mat = 11,
points = 10, 11, 13, 14, 10,
\$end

\$region
mat = 12,
points = 1, 2, 16, 15, 33, 34, 41, 42, 1,
\$end

\$region
mat = 13,

```
points = 14, 13, 11, 12, 39, 40, 37, 38, 14,  
$end
```

```
$dets
```

```
detr(1)=0.0, detz(1)= -11.112, dett(1)=3.7,  
detr(2)=0.0, detz(2)= 11.112, dett(2)=3.7,  
$end
```

```
$parts
```

```
partr(1) = 7.493, partz(1) = 0.000,  
partr(2) = 7.493, partz(2) = 0.381,  
partr(3) = 7.493, partz(3) = -2.540,
```

```
$end
```

```
MESA
```

```
mesa2d (m)  
0 , 0.0 , 0.0
```

```
$probsize
```

```
heburn= .true. , strength= .false. , jcdfrac=.false., jsfrac=.false. ,  
mcr= 260, mcz= 520 ,  
mmats= 13 , mcomp= 13, mmix=25000,  
$end
```

```
$options
```

```
mlagcyc=1 ,  
part=.true.,  
clean=.true.,  
cleandf(12)=0.6,  
cleandf(13)=0.6,  
cleandf(4)=0.2,  
cleandf(5)=0.2,  
dtmin=0.001,  
safdtc=0.25,  
safdtur=0.25,  
safdtuz=0.25,  
safdtdiv=0.25,  
safdyna=0.25,
```

```
$end
```

```
$mats
```

```
$end
```

```

$ops
  ropt = 3.7, 33.7, 37.7, 38.0, 51.0,
  ropdt = 0.01, 0.01, 0.01, 0.01,
  mrovsp= 500, 200, 10, 500,
  mroslp= 0, 0, 0, 0,
  mroslmp= 500, 200, 10, 500,
  mroslpout= 1, 1, 1, 1,
  mtps= 1, 1, 1, 1, 1, 1, 1, 0, 1, 1,
        1, 1, 1, 1, 1, 1, 1, 1, 0, 0,
        0, 0, 0,
$end

```

GEN

mesa2d (g)

Divergent copper cylinder system w/ no strength and no frac
 L=5", OD=6", t=0.1", mesh=0.05cm

\$probsize

```

  heburn= .true. , strength= .false. ,
  jsfrac= .false. , jcdfrac=.false.,
  mcr= 280, mcz= 360,
  mmats= 13 , mcomp= 13 , mmix= 20000,

```

\$end

\$options

```

  ibcr1= 0 , ibcr2= 1 , ibcz1= 1 , ibcz2= 1 ,
  idgeom= 2 ,
  part=.true. ,
  t=3.7,

```

\$end

\$mesh

```

  ncellr= 280,
  coordr= 0.0, 14.0,
  rator= 1.0,
  ncellz= 360,
  coordz= -9.0, 9.0,
  ratioz= 1.0,

```

\$end

\$mats

```

  matbak= 1 , pribak= 1,

```

```

  matname(1)='air', eosform(1)='gas', strform(1)='none',
  d0(1)=1.293e-03 , e0(1)=1.9335e-03 , pmin(1)=0.0,
  eoscon(1)=1.4 ,

```

matname(2) = 'cu', eosform(2) = 'usup', strform(2) = 'none',
d0(2) = 8.93, e0(2) = 0.0, pmin(2) = -0.100, detvel(2) = 0.0,
eoscon(1,2) = 0.394, 1.489, 0.0, 2.02,
fracform(2) = 'none',
fracon(1,2) = 0.54, 4.89, -3.03, 0.014, 1.12,
0., 0.00407, 0.033, 0.024, 1.0,
priority(2)=3,

matname(3) = '9501', eosform(3) = 'jwl', strform(3) = 'none',
d0(3) = 1.84, e0(3) = 0.05543, pmin(3) = 0.0, detvel(3) = 0.88,
eoscon(1,3) = 0.38, 8.524, 8.46, 0.1802, 2.39,
y0(3) = 0.0, ymax(3) = 0.0, g0(3) = 0.0, gmax(3) = 0.0,
strcon(1,3) = 0.0,
priority(3)=2,

matname(4) = 'polyethylene', eosform(4) = 'usup', strform(4) = 'none',
d0(4) = 0.916, e0(4) = 6.6567e-07, pmin(4) = -0.010, detvel(4) = 0.0,
eoscon(1,4) = 0.266, 1.55, 0.0, 1.64,
priority(4)=6,

matname(5) = 'polyethylene', eosform(5) = 'usup', strform(5) = 'none',
d0(5) = 0.916, e0(5) = 6.6567e-07, pmin(5) = -0.010, detvel(5) = 0.0,
eoscon(1,5) = 0.266, 1.55, 0.0, 1.64,
priority(5)=7,

matname(6) = 'stainless steel(304)', eosform(6) = 'usup', strform(6) = 'none',
d0(6) = 7.896, e0(6) = 0.0, pmin(6) = -0.10, detvel(6) = 0.0,
eoscon(1,6) = 0.457, 1.49, 0.0, 2.17,
y0(6) = 0.0034, ymax(6) = 0.025, g0(6) = 0.77, gmax(6) = 5.66,
strcon(1,6) = 43.0, 0.0, 0.35, 0.001, 0.00881, 2.26, 2.26,
fracform(6) = 'none', fracon(1,6)= 1.0003, fracon(2,6)= 0.0017,
fracon(3,6)= 0.00001, fracon(4,6)= 0.266
priority(6)=4,

matname(7) = 'stainless steel(304)', eosform(7) = 'usup', strform(7) = 'none',
d0(7) = 7.896, e0(7) = 0.0, pmin(7) = -0.10, detvel(7) = 0.0,
eoscon(1,7) = 0.457, 1.49, 0.0, 2.17,
y0(7) = 0.0034, ymax(7) = 0.025, g0(7) = 0.77, gmax(7) = 5.66,
strcon(1,7) = 43.0, 0.0, 0.35, 0.001, 0.00881, 2.26, 2.26,
fracform(7) = 'none', fracon(1,7)= 1.0003, fracon(2,7)= 0.0017,
fracon(3,7)= 0.00001, fracon(4,7)= 0.266
priority(7)=5,

matname(8) = '9501', eosform(8) = 'jwl', strform(8) = 'none',
d0(8) = 1.84, e0(8) = 0.05543, pmin(8) = 0.0, detvel(8) = 0.88,
eoscon(1,8) = 0.38, 8.524, 8.46, 0.1802, 2.39,
y0(8) = 0.0, ymax(8) = 0.0, g0(8) = 0.0, gmax(8) = 0.0,
strcon(1,8) = 0.0,
priority(8)=8,

matname(9) = '9501', eosform(9) = 'jwl', strform(9) = 'none',
d0(9) = 1.84, e0(9) = 0.05543, pmin(9) = 0.0, detvel(9) = 0.88,
eoscon(1,9) = 0.38, 8.524, 8.46, 0.1802, 2.39,
y0(9) = 0.0, ymax(9) = 0.0, g0(9) = 0.0, gmax(9) = 0.0,
strcon(1,9) = 0.0,
priority(9)=9,

matname(10) = '9407', eosform(10) = 'jwl', strform(10) = 'none',
d0(10) = 1.6, e0(10) = 0.0538, pmin(10) = 0.0, detvel(10) = 0.791,
eoscon(1,10) = 0.32, 5.7319, 7.4, 0.14639, 2.24,
y0(10) = 0.0, ymax(10) = 0.0, g0(10) = 0.0, gmax(10) = 0.0,
strcon(1,10) = 0.0,
priority(10)=10 ,

matname(11) = '9407', eosform(11) = 'jwl', strform(11) = 'none',
d0(11) = 1.6, e0(11) = 0.0538, pmin(11) = 0.0, detvel(11) = 0.791,
eoscon(1,11) = 0.32, 5.7319, 7.4, 0.14639, 2.24,
y0(11) = 0.0, ymax(11) = 0.0, g0(11) = 0.0, gmax(11) = 0.0,
strcon(1,11) = 0.0,
priority(11)=11 ,

matname(12) = 'polyethylene', eosform(12) = 'gas', strform(12) = 'none',
d0(12) = 0.916, e0(12) = 5.4585e-07, pmin(12) = -0.000, detvel(12) = 0.0,
eoscon(1,12) = 3.0,
priority(12)=12,

matname(13) = 'polyethylene', eosform(13) = 'gas', strform(13) = 'none',
d0(13) = 0.916, e0(13) = 5.4585e-07, pmin(13) = -0.000, detvel(13) = 0.0,
eoscon(1,13) = 3.0,
priority(13)=13,

\$end

\$points

rz=

1 , 0.000 , 7.938 ,
2 , 0.000 , 6.985 ,
3 , 0.000 , 5.715 ,
4 , 0.000 , 5.080 ,

5 , 0.000 , 3.810 ,
6 , 0.000 , 2.540 ,
7 , 0.000 , -2.540 ,
8 , 0.000 , -3.810 ,
9 , 0.000 , -5.080 ,
10 , 0.000 , -5.715 ,
11 , 0.000 , -6.985 ,
12 , 0.000 , -7.938 ,
13 , 0.635 , -6.985 ,
14 , 0.635 , -5.715 ,
15 , 0.635 , 5.715 ,
16 , 0.635 , 6.985 ,
17 , 5.461 , 5.080 ,
18 , 5.461 , 3.810 ,
19 , 5.461 , 2.540 ,
20 , 5.461 , -2.540 ,
21 , 5.461 , -3.810 ,
22 , 5.461 , -5.080 ,
23 , 5.779 , -5.715 ,
24 , 5.779 , -5.080 ,
25 , 5.779 , 5.080 ,
26 , 5.779 , 5.715 ,
27 , 7.366 , 7.938 ,
28 , 7.366 , 6.350 ,
29 , 7.366 , 5.080 ,
30 , 7.366 , -5.080 ,
31 , 7.366 , -6.350 ,
32 , 7.366 , -7.938 ,
33 , 7.620 , -6.350 ,
34 , 7.620 , 6.350 ,

\$end

\$region

mat = 2,

points = 28, 29, 30, 31, 33, 34, 28,

\$end

\$region

mat = 3,

points = 17, 18, 19, 20, 21, 22, 24, 30, 29, 25, 17,

\$end

\$region

mat = 6,

points = 5, 6, 19, 18, 5,

\$end

\$region
mat = 7,
points = 7, 8, 21, 20, 7,
\$end

\$region
mat = 4,
points = 4, 5, 18, 17, 4,
\$end

\$region
mat = 5,
points = 8, 9, 22, 21, 8,
\$end

\$region
mat = 8,
points = 3, 4, 17, 25, 26, 15, 3,
\$end

\$region
mat = 9,
points = 9, 10, 14, 23, 24, 22, 9,
\$end

\$region
mat = 10,
points = 2, 3, 15, 16, 2,
\$end

\$region
mat = 11,
points = 10, 11, 13, 14, 10,
\$end

\$region
mat = 12,
points = 1, 2, 16, 15, 26, 25, 29, 28, 27, 1,
\$end

\$region
mat = 13,
points = 14, 13, 11, 12, 32, 31, 30, 24, 23, 14,
\$end


```
$dets
detr(1)=0.0, detz(1)= -6.984, dett(1)=3.7,
detr(2)=0.0, detz(2)= 6.984, dett(2)=3.7,
$end
```

```
$parts
partr(1) = 7.493, partz(1) = 0.000,
partr(2) = 7.493, partz(2) = 0.381,
partr(3) = 7.493, partz(3) = -2.540,
```

```
$end
```

MESA

```
mesa2d (m)
0 , 0.0 , 0.0
```

```
$probsize
heburn= .true. , strength= .false. , jcdfrac=.false., jsfrac=.false. ,
mcr= 280, mcz= 360 ,
mmats= 13 , mcomp= 13 , mmix=20000,
$end
```

```
$options
mlagcyc=1 ,
part=.true.,
clean=.true.,
cleandf(12)=0.6,
cleandf(13)=0.6,
cleandf(4)=0.2,
cleandf(5)=0.2,
dtmin=0.001,
safdtc=0.25,
safdtur=0.25,
safdtuz=0.25,
safdtdiv=0.25,
safdyna=0.25,
$end
```

```
$mats
$end
```

```
$ops
ropt = 3.7, 28.7, 30.3, 30.34, 42.0,
ropdt = 0.01, 0.01, 0.01, 0.01,
```

```
mropsp=    500,   80,   2,   500,
mroplp=     0,    0,    0,    0,
mropdmp=   500,   80,   2,   500,
mroppout=   1,    1,    1,    1,
  mtps= 1, 1, 1, 1, 1, 1, 1, 0, 1, 1,
        1, 1, 1, 1, 1, 1, 1, 1, 0, 0,
        0, 0, 0,
Send
```

Elastic-Perfectly-Plastic Strength, No Fracture:

GEN

mesa2d (g)

Convergent copper cylinder system w/ ep-strength and no frac
L=5", OD=6", t=0.1", mesh=0.05cm

\$probsize

heburn= .true. , strength= .true. , jcdfrac=.false.,

jsfrac= .false. , jhdfrac=.false.,

mcr= 260, mcz= 520,

mmats= 13 , mcomp= 13 , mmix= 25000,

\$end

\$options

ibcr1= 0 , ibcr2= 1 , ibcz1= 1 , ibcz2= 1 ,

idgeom= 2 ,

part=.true. ,

t=3.7,

\$end

\$mesh

ncellr= 200, 60,

coordr= 0.0, 10.0, 13.0,

rator= 1.0, 1.0,

ncellz= 120, 280, 120,

coordz= -13.0, -7.0, 7.0, 13.0,

ratioz= 1.0, 1.0, 1.0,

\$end

\$mats

matbak= 1 , pribak= 1,

matname(1)='air', eosform(1)='gas', strform(1)='none',

d0(1)=1.293e-03 , e0(1)=1.9335e-03 , pmin(1)=0.0,

eoscon(1)=1.4 ,

matname(2) = 'cu', eosform(2) = 'usup', strform(2) = 'e-p',

d0(2) = 8.93, e0(2) = 0.0, pmin(2) = -0.100, detvel(2) = 0.0,

eoscon(1,2) = 0.394, 1.489, 0.0, 2.02,

y0(2) = 0.0012, ymax(2) = 0.0012, g0(2) = 0.477, gmax(2) = 0.477,

fracform(2) = 'none',

fracon(1,2) = 0.54, 4.89, -3.03, 0.014, 1.12,

0., 0.00407, 0.033, 0.024, 1.,

priority(2)=2,

matname(3) = '9501', eosform(3) = 'jwl', strform(3) = 'none',
d0(3) = 1.84, e0(3) = 0.05543, pmin(3) = 0.0, detvel(3) = 0.88,
eoscon(1,3) = 0.38, 8.524, 8.46, 0.1802, 2.39,
y0(3) = 0.0, ymax(3) = 0.0, g0(3) = 0.0, gmax(3) = 0.0,
strcon(1,3) = 0.0,
priority(3)=3,

matname(4) = 'polyethylene', eosform(4) = 'usup', strform(4) = 'none',
d0(4) = 0.916, e0(4) = 6.6567e-07, pmin(4) = -0.010, detvel(4) = 0.0,
eoscon(1,4) = 0.266, 1.55, 0.0, 1.64,
priority(4)=6,

matname(5) = 'polyethylene', eosform(5) = 'usup', strform(5) = 'none',
d0(5) = 0.916, e0(5) = 6.6567e-07, pmin(5) = -0.010, detvel(5) = 0.0,
eoscon(1,5) = 0.266, 1.55, 0.0, 1.64,
priority(5)=7,

matname(6) = 'stainless steel(304)', eosform(6) = 'usup', strform(6) = 's-g',
d0(6) = 7.896, e0(6) = 0.0, pmin(6) = -0.10, detvel(6) = 0.0,
eoscon(1,6) = 0.457, 1.49, 0.0, 2.17,
y0(6) = 0.0034, ymax(6) = 0.025, g0(6) = 0.77, gmax(6) = 5.66,
strcon(1,6) = 43.0, 0.0, 0.35, 0.001, 0.00881, 2.26, 2.26,
fracform(6) = 'none', fracon(1,6)= 1.0003, fracon(2,6)= 0.0017,
fraccon(3,6)= 0.00001, fracon(4,6)= 0.266
priority(6)=4,

matname(7) = 'stainless steel(304)', eosform(7) = 'usup', strform(7) = 's-g',
d0(7) = 7.896, e0(7) = 0.0, pmin(7) = -0.10, detvel(7) = 0.0,
eoscon(1,7) = 0.457, 1.49, 0.0, 2.17,
y0(7) = 0.0034, ymax(7) = 0.025, g0(7) = 0.77, gmax(7) = 5.66,
strcon(1,7) = 43.0, 0.0, 0.35, 0.001, 0.00881, 2.26, 2.26,
fracform(7) = 'none', fracon(1,7)= 1.0003, fracon(2,7)= 0.0017,
fraccon(3,7)= 0.00001, fracon(4,7)= 0.266
priority(7)=5,

matname(8) = '9501', eosform(8) = 'jwl', strform(8) = 'none',
d0(8) = 1.84, e0(8) = 0.05543, pmin(8) = 0.0, detvel(8) = 0.88,
eoscon(1,8) = 0.38, 8.524, 8.46, 0.1802, 2.39,
y0(8) = 0.0, ymax(8) = 0.0, g0(8) = 0.0, gmax(8) = 0.0,
strcon(1,8) = 0.0,
priority(8)=8,

matname(9) = '9501', eosform(9) = 'jwl', strform(9) = 'none',
d0(9) = 1.84, e0(9) = 0.05543, pmin(9) = 0.0, detvel(9) = 0.88,
eoscon(1,9) = 0.38, 8.524, 8.46, 0.1802, 2.39,

y0(9) = 0.0, ymax(9) = 0.0, g0(9) = 0.0, gmax(9) = 0.0,
strcon(1,9) = 0.0,
priority(9)=9,

matname(10) = '9407', eosform(10) = 'jwl', strform(10) = 'none',
d0(10) = 1.6, e0(10) = 0.0538, pmin(10) = 0.0, detvel(10) = 0.791,
eoscon(1,10) = 0.32, 5.7319, 7.4, 0.14639, 2.24,
y0(10) = 0.0, ymax(10) = 0.0, g0(10) = 0.0, gmax(10) = 0.0,
strcon(1,10) = 0.0,
priority(10)=10 ,

matname(11) = '9407', eosform(11) = 'jwl', strform(11) = 'none',
d0(11) = 1.6, e0(11) = 0.0538, pmin(11) = 0.0, detvel(11) = 0.791,
eoscon(1,11) = 0.32, 5.7319, 7.4, 0.14639, 2.24,
y0(11) = 0.0, ymax(11) = 0.0, g0(11) = 0.0, gmax(11) = 0.0,
strcon(1,11) = 0.0,
priority(11)=11 ,

matname(12) = 'polyethylene', eosform(12) = 'gas', strform(12) = 'none',
d0(12) = 0.916, e0(12) = 5.4585e-07, pmin(12) = -0.000, detvel(12) = 0.0,
eoscon(1,12) = 3.0,
priority(12)=12,

matname(13) = 'polyethylene', eosform(13) = 'gas', strform(13) = 'none',
d0(13) = 0.916, e0(13) = 5.4585e-07, pmin(13) = -0.000, detvel(13) = 0.0,
eoscon(1,13) = 3.0,
priority(13)=13,

\$end

\$points

rz=

1 , 0.000 , 12.065 ,
2 , 0.000 , 11.113 ,
3 , 0.000 , 9.843 ,
4 , 0.000 , 8.890 ,
5 , 0.000 , 7.620 ,
6 , 0.000 , 6.350 ,
7 , 0.000 , -6.350 ,
8 , 0.000 , -7.620 ,
9 , 0.000 , -8.890 ,
10 , 0.000 , -9.843 ,
11 , 0.000 , -11.113 ,
12 , 0.000 , -12.065 ,
13 , 0.635 , -11.113 ,

```
14 , 0.635 , -9.843 ,  
15 , 0.635 , 9.843 ,  
16 , 0.635 , 11.113 ,  
17 , 7.366 , 6.350 ,  
18 , 7.366 , -6.350 ,  
19 , 7.620 , -6.350 ,  
20 , 7.620 , -5.080 ,  
21 , 7.620 , 5.080 ,  
22 , 7.620 , 6.350 ,  
23 , 7.938 , 7.620 ,  
24 , 7.938 , 5.080 ,  
25 , 7.938 , -5.080 ,  
26 , 7.938 , -7.620 ,  
27 , 8.090 , -8.890 ,  
28 , 8.090 , 8.890 ,  
29 , 9.201 , 5.080 ,  
30 , 9.201 , -5.080 ,  
31 , 9.525 , -5.080 ,  
32 , 9.525 , 5.080 ,  
33 , 9.843 , 9.843 ,  
34 , 9.843 , 8.255 ,  
35 , 9.843 , 5.080 ,  
36 , 9.843 , -5.080 ,  
37 , 9.843 , -8.255 ,  
38 , 9.843 , -9.843 ,  
39 , 10.478 , -12.065 ,  
40 , 10.478 , -8.255 ,  
41 , 10.478 , 8.255 ,  
42 , 10.478 , 12.065 ,  
Send
```

```
$region  
mat = 2,  
points = 17, 18, 19, 20, 21, 22, 17,  
Send
```

```
$region  
mat = 3,  
points = 21, 20, 25, 30, 31, 32, 29, 24, 21,  
Send
```

```
$region  
mat = 6,  
points = 5, 6, 17, 22, 21, 24, 23, 5,  
Send
```

\$region
mat = 7,
points = 7, 8, 26, 25, 20, 19, 18, 7,
\$end

\$region
mat = 4,
points = 4, 5, 23, 24, 29, 28, 4,
\$end

\$region
mat = 5,
points = 8, 9, 27, 30, 25, 26, 8,
\$end

\$region
mat = 8,
points = 3, 4, 28, 29, 32, 35, 34, 33, 15, 3,
\$end

\$region
mat = 9,
points = 9, 10, 14, 38, 37, 36, 31, 30, 27, 9,
\$end

\$region
mat = 10,
points = 2, 3, 15, 16, 2,
\$end

\$region
mat = 11,
points = 10, 11, 13, 14, 10,
\$end

\$region
mat = 12,
points = 1, 2, 16, 15, 33, 34, 41, 42, 1,
\$end

\$region
mat = 13,
points = 14, 13, 11, 12, 39, 40, 37, 38, 14,
\$end

\$dets

```
detr(1)=0.0, detz(1)= -11.112, dett(1)=3.7,  
detr(2)=0.0, detz(2)= 11.112, dett(2)=3.7,  
$end
```

```
$parts  
partr(1) = 7.493, partz(1) = 0.000,  
partr(2) = 7.493, partz(2) = 0.381,  
partr(3) = 7.493, partz(3) = -2.540,
```

```
$end
```

MESA

```
mesa2d (m)  
0 , 0.0 , 0.0
```

```
$probsize  
heburn= .true. , strength= .true. , jcdfrac=.false., jsfrac=.false. ,  
mcr= 260, mcz= 520 ,  
mmats= 13 , mcomp= 13, mmix=25000,  
$end
```

```
$options  
mlagcyc=1 ,  
part=.true.,  
clean=.true.,  
cleandf(12)=0.6,  
cleandf(13)=0.6,  
cleandf(4)=0.2,  
cleandf(5)=0.2,  
dtmin=0.001,  
safdtc=0.25,  
safdtur=0.25,  
safdtuz=0.25,  
safdtdiv=0.25,  
safdyna=0.25,  
$end
```

```
$mats  
$end
```

```
$ops  
ropt = 3.7, 33.7, 37.7, 38.0, 51.0,  
ropdt = 0.01, 0.01, 0.01, 0.01,
```



```
mrovsp= 500, 200, 10, 500,  
mroplp= 0, 0, 0, 0,  
mropdmp= 500, 200, 10, 500,  
mroppout= 1, 1, 1, 1,  
mtps= 1, 1, 1, 1, 1, 1, 1, 0, 1, 1,  
1, 1, 1, 1, 1, 1, 1, 1, 0, 0,  
0, 0, 0,
```

\$end

GEN

mesa2d (g)

Divergent copper cylinder system w/ ep-strength and no frac
L=5", OD=6", t=0.1", mesh=0.05cm

\$probsize

```
heburn= .true. , strength= .true. ,  
jsfrac= .false. , jcdfrac=.false.,  
mcr= 280, mcz= 360,  
mmats= 13 , mcomp= 13 , mmix= 20000,
```

\$end

\$options

```
ibcr1= 0 , ibcr2= 1 , ibcz1= 1 , ibcz2= 1 ,  
idgeom= 2 ,  
part=.true. ,  
t=3.7,
```

\$end

\$mesh

```
ncellr= 280,  
coordr= 0.0, 14.0,  
rator= 1.0,  
ncellz= 360,  
coordz= -9.0, 9.0,  
ratioz= 1.0,
```

\$end

\$mats

```
matbak= 1 , pribak= 1,
```

```
matname(1)='air', eosform(1)='gas', strform(1)='none',  
d0(1)=1.293e-03 , e0(1)=1.9335e-03 , pmin(1)=0.0,  
eoscon(1)=1.4 ,
```

```
matname(2) = 'cu', eosform(2) = 'usup', strform(2) = 'e-p',  
d0(2) = 8.93, e0(2) = 0.0, pmin(2) = -0.100, detvel(2) = 0.0,
```

eoscon(1,2) = 0.394, 1.489, 0.0, 2.02,
y0(2) = 0.0012, ymax(2) = 0.0012, g0(2) = 0.477, gmax(2) = 0.477,
fracform(2) = 'none',
fracon(1,2) = 0.54, 4.89, -3.03, 0.014, 1.12,
0., 0.00407, 0.033, 0.024, 1.0,
priority(2)=3,

matname(3) = '9501', eosform(3) = 'jwl', strform(3) = 'none',
d0(3) = 1.84, e0(3) = 0.05543, pmin(3) = 0.0, detvel(3) = 0.88,
eoscon(1,3) = 0.38, 8.524, 8.46, 0.1802, 2.39,
y0(3) = 0.0, ymax(3) = 0.0, g0(3) = 0.0, gmax(3) = 0.0,
strcon(1,3) = 0.0,
priority(3)=2,

matname(4) = 'polyethylene', eosform(4) = 'usup', strform(4) = 'none',
d0(4) = 0.916, e0(4) = 6.6567e-07, pmin(4) = -0.010, detvel(4) = 0.0,
eoscon(1,4) = 0.266, 1.55, 0.0, 1.64,
priority(4)=6,

matname(5) = 'polyethylene', eosform(5) = 'usup', strform(5) = 'none',
d0(5) = 0.916, e0(5) = 6.6567e-07, pmin(5) = -0.010, detvel(5) = 0.0,
eoscon(1,5) = 0.266, 1.55, 0.0, 1.64,
priority(5)=7,

matname(6) = 'stainless steel(304)', eosform(6) = 'usup', strform(6) = 's-g',
d0(6) = 7.896, e0(6) = 0.0, pmin(6) = -0.10, detvel(6) = 0.0,
eoscon(1,6) = 0.457, 1.49, 0.0, 2.17,
y0(6) = 0.0034, ymax(6) = 0.025, g0(6) = 0.77, gmax(6) = 5.66,
strcon(1,6) = 43.0, 0.0, 0.35, 0.001, 0.00881, 2.26, 2.26,
fracform(6) = 'none', fracon(1,6)= 1.0003, fracon(2,6)= 0.0017,
fracon(3,6)= 0.00001, fracon(4,6)= 0.266
priority(6)=4,

matname(7) = 'stainless steel(304)', eosform(7) = 'usup', strform(7) = 's-g',
d0(7) = 7.896, e0(7) = 0.0, pmin(7) = -0.10, detvel(7) = 0.0,
eoscon(1,7) = 0.457, 1.49, 0.0, 2.17,
y0(7) = 0.0034, ymax(7) = 0.025, g0(7) = 0.77, gmax(7) = 5.66,
strcon(1,7) = 43.0, 0.0, 0.35, 0.001, 0.00881, 2.26, 2.26,
fracform(7) = 'none', fracon(1,7)= 1.0003, fracon(2,7)= 0.0017,
fracon(3,7)= 0.00001, fracon(4,7)= 0.266
priority(7)=5,

matname(8) = '9501', eosform(8) = 'jwl', strform(8) = 'none',
d0(8) = 1.84, e0(8) = 0.05543, pmin(8) = 0.0, detvel(8) = 0.88,
eoscon(1,8) = 0.38, 8.524, 8.46, 0.1802, 2.39,

y0(8) = 0.0, ymax(8) = 0.0, g0(8) = 0.0, gmax(8) = 0.0,
strcon(1,8) = 0.0,
priority(8)=8,

matname(9) = '9501', eosform(9) = 'jwl', strform(9) = 'none',
d0(9) = 1.84, e0(9) = 0.05543, pmin(9) = 0.0, detvel(9) = 0.88,
eoscon(1,9) = 0.38, 8.524, 8.46, 0.1802, 2.39,
y0(9) = 0.0, ymax(9) = 0.0, g0(9) = 0.0, gmax(9) = 0.0,
strcon(1,9) = 0.0,
priority(9)=9,

matname(10) = '9407', eosform(10) = 'jwl', strform(10) = 'none',
d0(10) = 1.6, e0(10) = 0.0538, pmin(10) = 0.0, detvel(10) = 0.791,
eoscon(1,10) = 0.32, 5.7319, 7.4, 0.14639, 2.24,
y0(10) = 0.0, ymax(10) = 0.0, g0(10) = 0.0, gmax(10) = 0.0,
strcon(1,10) = 0.0,
priority(10)=10 ,

matname(11) = '9407', eosform(11) = 'jwl', strform(11) = 'none',
d0(11) = 1.6, e0(11) = 0.0538, pmin(11) = 0.0, detvel(11) = 0.791,
eoscon(1,11) = 0.32, 5.7319, 7.4, 0.14639, 2.24,
y0(11) = 0.0, ymax(11) = 0.0, g0(11) = 0.0, gmax(11) = 0.0,
strcon(1,11) = 0.0,
priority(11)=11 ,

matname(12) = 'polyethylene', eosform(12) = 'gas', strform(12) = 'none',
d0(12) = 0.916, e0(12) = 5.4585e-07, pmin(12) = -0.000, detvel(12) = 0.0,
eoscon(1,12) = 3.0,
priority(12)=12,

matname(13) = 'polyethylene', eosform(13) = 'gas', strform(13) = 'none',
d0(13) = 0.916, e0(13) = 5.4585e-07, pmin(13) = -0.000, detvel(13) = 0.0,
eoscon(1,13) = 3.0,
priority(13)=13,

\$end

\$points

rz=

1 , 0.000 , 7.938 ,
2 , 0.000 , 6.985 ,
3 , 0.000 , 5.715 ,
4 , 0.000 , 5.080 ,
5 , 0.000 , 3.810 ,
6 , 0.000 , 2.540 ,
7 , 0.000 , -2.540 ,

8 , 0.000 , -3.810 ,
9 , 0.000 , -5.080 ,
10 , 0.000 , -5.715 ,
11 , 0.000 , -6.985 ,
12 , 0.000 , -7.938 ,
13 , 0.635 , -6.985 ,
14 , 0.635 , -5.715 ,
15 , 0.635 , 5.715 ,
16 , 0.635 , 6.985 ,
17 , 5.461 , 5.080 ,
18 , 5.461 , 3.810 ,
19 , 5.461 , 2.540 ,
20 , 5.461 , -2.540 ,
21 , 5.461 , -3.810 ,
22 , 5.461 , -5.080 ,
23 , 5.779 , -5.715 ,
24 , 5.779 , -5.080 ,
25 , 5.779 , 5.080 ,
26 , 5.779 , 5.715 ,
27 , 7.366 , 7.938 ,
28 , 7.366 , 6.350 ,
29 , 7.366 , 5.080 ,
30 , 7.366 , -5.080 ,
31 , 7.366 , -6.350 ,
32 , 7.366 , -7.938 ,
33 , 7.620 , -6.350 ,
34 , 7.620 , 6.350 ,

\$end

\$region

mat = 2,
points = 28, 29, 30, 31, 33, 34, 28,
\$end

\$region

mat = 3,
points = 17, 18, 19, 20, 21, 22, 24, 30, 29, 25, 17,
\$end

\$region

mat = 6,
points = 5, 6, 19, 18, 5,
\$end

\$region

mat = 7,
points = 7, 8, 21, 20, 7,
\$end

\$region
mat = 4,
points = 4, 5, 18, 17, 4,
\$end

\$region
mat = 5,
points = 8, 9, 22, 21, 8,
\$end

\$region
mat = 8,
points = 3, 4, 17, 25, 26, 15, 3,
\$end

\$region
mat = 9,
points = 9, 10, 14, 23, 24, 22, 9,
\$end

\$region
mat = 10,
points = 2, 3, 15, 16, 2,
\$end

\$region
mat = 11,
points = 10, 11, 13, 14, 10,
\$end

\$region
mat = 12,
points = 1, 2, 16, 15, 26, 25, 29, 28, 27, 1,
\$end

\$region
mat = 13,
points = 14, 13, 11, 12, 32, 31, 30, 24, 23, 14,
\$end

\$dets
detr(1)=0.0, detz(1)= -6.984, dett(1)=3.7,

```
detr(2)=0.0, detz(2)= 6.984, dett(2)=3.7,  
$end
```

```
$parts  
partr(1) = 7.493, partz(1) = 0.000,  
partr(2) = 7.493, partz(2) = 0.381,  
partr(3) = 7.493, partz(3) = -2.540,
```

```
$end
```

MESA

```
mesa2d (m)  
0 , 0.0 , 0.0
```

```
$probsize  
heburn= .true. , strength= .true. , jcdfrac=.false., jsfrac=.false. ,  
mcr= 280, mcz= 360 ,  
mmats= 13 , mcomp= 13 , mmix=20000,  
$end
```

```
$options  
mlagcyc=1 ,  
part=.true.,  
clean=.true.,  
cleandf(12)=0.6,  
cleandf(13)=0.6,  
cleandf(4)=0.2,  
cleandf(5)=0.2,  
dtmin=0.001,  
safdtc=0.25,  
safdtur=0.25,  
safdtuz=0.25,  
safdtdiv=0.25,  
safdyna=0.25,  
$end
```

```
$mats  
$end
```

```
$ops  
ropt = 3.7, 28.7, 30.3, 30.34, 42.0,  
ropdt = 0.01, 0.01, 0.01, 0.01,  
mropsp= 500, 80, 2, 500,  
mroplp= 0, 0, 0, 0,
```

```
mropdmp=    500,   80,   2,   500,  
mroppout=   1,    1,   1,    1,  
  mtps= 1, 1, 1, 1, 1, 1, 1, 0, 1, 1,  
        1, 1, 1, 1, 1, 1, 1, 1, 0, 0,  
        0, 0, 0,  
$end
```

Johnson-Cook Strength, No Fracture:

GEN

mesa2d (g)

Convergent copper cylinder system w/ jc-strength and no frac
L=5", OD=6", t=0.1", mesh=0.05cm

\$probsize

heburn= .true. , strength= .true. , jcdfrac=.false.,

jsfrac= .false. , jhdfac=.false.,

mcr= 260, mcz= 520,

mmats= 13 , mcomp= 13 , mmix= 25000,

\$end

\$options

ibcr1= 0 , ibcr2= 1 , ibcz1= 1 , ibcz2= 1 ,

idgeom= 2 ,

part=.true. ,

t=3.7,

\$end

\$mesh

ncellr= 200, 60,

coordr= 0.0, 10.0, 13.0,

rator= 1.0, 1.0,

ncellz= 120, 280, 120,

coordz= -13.0, -7.0, 7.0, 13.0,

ratioz= 1.0, 1.0, 1.0,

\$end

\$mats

matbak= 1 , pribak= 1,

matname(1)='air', eosform(1)='gas', strform(1)='none',

d0(1)=1.293e-03 , e0(1)=1.9335e-03 , pmin(1)=0.0,

eoscon(1)=1.4 ,

matname(2) = 'cu', eosform(2) = 'usup', strform(2) = 'j-c',

d0(2) = 8.93, e0(2) = 0.0, pmin(2) = -0.100, detvel(2) = 0.0,

eoscon(1,2) = 0.394, 1.489, 0.0, 2.02,

y0(2) = 0.00035, ymax(2) = 0.0064, g0(2) = 0.477, gmax(2) = 2.54,

strcon(1,2) = .00375, 0.0175, 0.30, 1.2, 0.00407, 0., 0.,

fracform(2) = 'none',

fracon(1,2) = 0.54, 4.89, -3.03, 0.014, 1.12,

0., 0.00407, 0.033, 0.024, 1.,

priority(2)=2,

matname(3) = '9501', eosform(3) = 'jwl', strform(3) = 'none',
d0(3) = 1.84, e0(3) = 0.05543, pmin(3) = 0.0, detvel(3) = 0.88,
eoscon(1,3) = 0.38, 8.524, 8.46, 0.1802, 2.39,
y0(3) = 0.0, ymax(3) = 0.0, g0(3) = 0.0, gmax(3) = 0.0,
strcon(1,3) = 0.0,
priority(3)=3,

matname(4) = 'polyethylene', eosform(4) = 'usup', strform(4) = 'none',
d0(4) = 0.916, e0(4) = 6.6567e-07, pmin(4) = -0.010, detvel(4) = 0.0,
eoscon(1,4) = 0.266, 1.55, 0.0, 1.64,
priority(4)=6,

matname(5) = 'polyethylene', eosform(5) = 'usup', strform(5) = 'none',
d0(5) = 0.916, e0(5) = 6.6567e-07, pmin(5) = -0.010, detvel(5) = 0.0,
eoscon(1,5) = 0.266, 1.55, 0.0, 1.64,
priority(5)=7,

matname(6) = 'stainless steel(304)', eosform(6) = 'usup', strform(6) = 's-g',
d0(6) = 7.896, e0(6) = 0.0, pmin(6) = -0.10, detvel(6) = 0.0,
eoscon(1,6) = 0.457, 1.49, 0.0, 2.17,
y0(6) = 0.0034, ymax(6) = 0.025, g0(6) = 0.77, gmax(6) = 5.66,
strcon(1,6) = 43.0, 0.0, 0.35, 0.001, 0.00881, 2.26, 2.26,
fracform(6) = 'none', fracon(1,6)= 1.0003, fracon(2,6)= 0.0017,
fraccon(3,6)= 0.00001, fracon(4,6)= 0.266
priority(6)=4,

matname(7) = 'stainless steel(304)', eosform(7) = 'usup', strform(7) = 's-g',
d0(7) = 7.896, e0(7) = 0.0, pmin(7) = -0.10, detvel(7) = 0.0,
eoscon(1,7) = 0.457, 1.49, 0.0, 2.17,
y0(7) = 0.0034, ymax(7) = 0.025, g0(7) = 0.77, gmax(7) = 5.66,
strcon(1,7) = 43.0, 0.0, 0.35, 0.001, 0.00881, 2.26, 2.26,
fracform(7) = 'none', fracon(1,7)= 1.0003, fracon(2,7)= 0.0017,
fraccon(3,7)= 0.00001, fracon(4,7)= 0.266
priority(7)=5,

matname(8) = '9501', eosform(8) = 'jwl', strform(8) = 'none',
d0(8) = 1.84, e0(8) = 0.05543, pmin(8) = 0.0, detvel(8) = 0.88,
eoscon(1,8) = 0.38, 8.524, 8.46, 0.1802, 2.39,
y0(8) = 0.0, ymax(8) = 0.0, g0(8) = 0.0, gmax(8) = 0.0,
strcon(1,8) = 0.0,
priority(8)=8,

matname(9) = '9501', eosform(9) = 'jwl', strform(9) = 'none',
d0(9) = 1.84, e0(9) = 0.05543, pmin(9) = 0.0, detvel(9) = 0.88,

eoscon(1,9) = 0.38, 8.524, 8.46, 0.1802, 2.39,
y0(9) = 0.0, ymax(9) = 0.0, g0(9) = 0.0, gmax(9) = 0.0,
strcon(1,9) = 0.0,
priority(9)=9,

matname(10) = '9407', eosform(10) = 'jwl', strform(10) = 'none',
d0(10) = 1.6, e0(10) = 0.0538, pmin(10) = 0.0, detvel(10) = 0.791,
eoscon(1,10) = 0.32, 5.7319, 7.4, 0.14639, 2.24,
y0(10) = 0.0, ymax(10) = 0.0, g0(10) = 0.0, gmax(10) = 0.0,
strcon(1,10) = 0.0,
priority(10)=10 ,

matname(11) = '9407', eosform(11) = 'jwl', strform(11) = 'none',
d0(11) = 1.6, e0(11) = 0.0538, pmin(11) = 0.0, detvel(11) = 0.791,
eoscon(1,11) = 0.32, 5.7319, 7.4, 0.14639, 2.24,
y0(11) = 0.0, ymax(11) = 0.0, g0(11) = 0.0, gmax(11) = 0.0,
strcon(1,11) = 0.0,
priority(11)=11 ,

matname(12) = 'polyethylene', eosform(12) = 'gas', strform(12) = 'none',
d0(12) = 0.916, e0(12) = 5.4585e-07, pmin(12) = -0.000, detvel(12) = 0.0,
eoscon(1,12) = 3.0,
priority(12)=12,

matname(13) = 'polyethylene', eosform(13) = 'gas', strform(13) = 'none',
d0(13) = 0.916, e0(13) = 5.4585e-07, pmin(13) = -0.000, detvel(13) = 0.0,
eoscon(1,13) = 3.0,
priority(13)=13,

Send

\$points

rz=

1 , 0.000 , 12.065 ,
2 , 0.000 , 11.113 ,
3 , 0.000 , 9.843 ,
4 , 0.000 , 8.890 ,
5 , 0.000 , 7.620 ,
6 , 0.000 , 6.350 ,
7 , 0.000 , -6.350 ,
8 , 0.000 , -7.620 ,
9 , 0.000 , -8.890 ,
10 , 0.000 , -9.843 ,
11 , 0.000 , -11.113 ,
12 , 0.000 , -12.065 ,

```

13 , 0.635 , -11.113 ,
14 , 0.635 , -9.843 ,
15 , 0.635 , 9.843 ,
16 , 0.635 , 11.113 ,
17 , 7.366 , 6.350 ,
18 , 7.366 , -6.350 ,
19 , 7.620 , -6.350 ,
20 , 7.620 , -5.080 ,
21 , 7.620 , 5.080 ,
22 , 7.620 , 6.350 ,
23 , 7.938 , 7.620 ,
24 , 7.938 , 5.080 ,
25 , 7.938 , -5.080 ,
26 , 7.938 , -7.620 ,
27 , 8.090 , -8.890 ,
28 , 8.090 , 8.890 ,
29 , 9.201 , 5.080 ,
30 , 9.201 , -5.080 ,
31 , 9.525 , -5.080 ,
32 , 9.525 , 5.080 ,
33 , 9.843 , 9.843 ,
34 , 9.843 , 8.255 ,
35 , 9.843 , 5.080 ,
36 , 9.843 , -5.080 ,
37 , 9.843 , -8.255 ,
38 , 9.843 , -9.843 ,
39 , 10.478 , -12.065 ,
40 , 10.478 , -8.255 ,
41 , 10.478 , 8.255 ,
42 , 10.478 , 12.065 ,
$end

$region
mat = 2,
points = 17, 18, 19, 20, 21, 22, 17,
$end

$region
mat = 3,
points = 21, 20, 25, 30, 31, 32, 29, 24, 21,
$end

$region
mat = 6,
points = 5, 6, 17, 22, 21, 24, 23, 5,
$end

```

\$region
mat = 7,
points = 7, 8, 26, 25, 20, 19, 18, 7,
\$end

\$region
mat = 4,
points = 4, 5, 23, 24, 29, 28, 4,
\$end

\$region
mat = 5,
points = 8, 9, 27, 30, 25, 26, 8,
\$end

\$region
mat = 8,
points = 3, 4, 28, 29, 32, 35, 34, 33, 15, 3,
\$end

\$region
mat = 9,
points = 9, 10, 14, 38, 37, 36, 31, 30, 27, 9,
\$end

\$region
mat = 10,
points = 2, 3, 15, 16, 2,
\$end

\$region
mat = 11,
points = 10, 11, 13, 14, 10,
\$end

\$region
mat = 12,
points = 1, 2, 16, 15, 33, 34, 41, 42, 1,
\$end

\$region
mat = 13,
points = 14, 13, 11, 12, 39, 40, 37, 38, 14,
\$end

\$dets

detr(1)=0.0, detz(1)= -11.112, dett(1)=3.7,
detr(2)=0.0, detz(2)= 11.112, dett(2)=3.7,
\$end

\$parts

partr(1) = 7.493, partz(1) = 0.000,
partr(2) = 7.493, partz(2) = 0.381,
partr(3) = 7.493, partz(3) = -2.540,

\$end

MESA

mesa2d (m)
0 , 0.0 , 0.0

\$probsize

heburn= .true. , strength= .true. , jcdfrac=.false., jsfrac=.false. ,
mcr= 260, mcz= 520 ,
mmats= 13 , mcomp= 13, mmix=25000,
\$end

\$options

mlagcyc=1 ,
part=.true.,
clean=.true.,
cleandf(12)=0.6,
cleandf(13)=0.6,
cleandf(4)=0.2,
cleandf(5)=0.2,
dtmin=0.001,
safdtc=0.25,
safdtur=0.25,
safdtuz=0.25,
safdtdiv=0.25,
safdyna=0.25,

\$end

\$mats

\$end

\$ops

ropt = 3.7, 33.7, 37.7, 38.0, 51.0,

```

ropdt = 0.01, 0.01, 0.01, 0.01,
mropsp= 500, 200, 10, 500,
mroplp= 0, 0, 0, 0,
mropdmp= 500, 200, 10, 500,
mroppout= 1, 1, 1, 1,
mtps= 1, 1, 1, 1, 1, 1, 1, 0, 1, 1,
      1, 1, 1, 1, 1, 1, 1, 1, 0, 0,
      0, 0, 0,

```

\$end

GEN

mesa2d (g)

Divergent copper cylinder system w/ jc-strength and no frac
L=5", OD=6", t=0.1", mesh=0.05cm

\$probsize

```

heburn= .true. , strength= .true. ,
jsfrac= .false. , jcdfrac=.false.,
mcr= 280, mcz= 360,
mmats= 13 , mcomp= 13 , mmix= 20000,

```

\$end

\$options

```

ibcr1= 0 , ibcr2= 1 , ibcz1= 1 , ibcz2= 1 ,
idgeom= 2 ,
part=.true. ,
t=3.7,

```

\$end

\$mesh

```

ncellr= 280,
coordr= 0.0, 14.0,
rator= 1.0,
ncellz= 360,
coordz= -9.0, 9.0,
ratioz= 1.0,

```

\$end

\$mats

```

matbak= 1 , pribak= 1,

```

```

matname(1)='air', eosform(1)='gas', strform(1)='none',
d0(1)=1.293e-03 , e0(1)=1.9335e-03 , pmin(1)=0.0,
eoscon(1)=1.4 ,

```

```

matname(2) = 'cu', eosform(2) = 'usup', strform(2) = 'j-c',

```

d0(2) = 8.93, e0(2) = 0.0, pmin(2) = -0.100, detvel(2) = 0.0,
eoscon(1,2) = 0.394, 1.489, 0.0, 2.02,
y0(2) = 0.00035, ymax(2) = 0.0064, g0(2) = 0.477, gmax(2) = 2.54,
strcon(1,2) = .00375, 0.0175, 0.30, 1.2, 0.00407, 0., 0.,
fracform(2) = 'none',
fracon(1,2) = 0.54, 4.89, -3.03, 0.014, 1.12,
0., 0.00407, 0.033, 0.024, 1.0,
priority(2)=3,

matname(3) = '9501', eosform(3) = 'jwl', strform(3) = 'none',
d0(3) = 1.84, e0(3) = 0.05543, pmin(3) = 0.0, detvel(3) = 0.88,
eoscon(1,3) = 0.38, 8.524, 8.46, 0.1802, 2.39,
y0(3) = 0.0, ymax(3) = 0.0, g0(3) = 0.0, gmax(3) = 0.0,
strcon(1,3) = 0.0,
priority(3)=2,

matname(4) = 'polyethylene', eosform(4) = 'usup', strform(4) = 'none',
d0(4) = 0.916, e0(4) = 6.6567e-07, pmin(4) = -0.010, detvel(4) = 0.0,
eoscon(1,4) = 0.266, 1.55, 0.0, 1.64,
priority(4)=6,

matname(5) = 'polyethylene', eosform(5) = 'usup', strform(5) = 'none',
d0(5) = 0.916, e0(5) = 6.6567e-07, pmin(5) = -0.010, detvel(5) = 0.0,
eoscon(1,5) = 0.266, 1.55, 0.0, 1.64,
priority(5)=7,

matname(6) = 'stainless steel(304)', eosform(6) = 'usup', strform(6) = 's-g',
d0(6) = 7.896, e0(6) = 0.0, pmin(6) = -0.10, detvel(6) = 0.0,
eoscon(1,6) = 0.457, 1.49, 0.0, 2.17,
y0(6) = 0.0034, ymax(6) = 0.025, g0(6) = 0.77, gmax(6) = 5.66,
strcon(1,6) = 43.0, 0.0, 0.35, 0.001, 0.00881, 2.26, 2.26,
fracform(6) = 'none', fracon(1,6)= 1.0003, fracon(2,6)= 0.0017,
fracon(3,6)= 0.00001, fracon(4,6)= 0.266
priority(6)=4,

matname(7) = 'stainless steel(304)', eosform(7) = 'usup', strform(7) = 's-g',
d0(7) = 7.896, e0(7) = 0.0, pmin(7) = -0.10, detvel(7) = 0.0,
eoscon(1,7) = 0.457, 1.49, 0.0, 2.17,
y0(7) = 0.0034, ymax(7) = 0.025, g0(7) = 0.77, gmax(7) = 5.66,
strcon(1,7) = 43.0, 0.0, 0.35, 0.001, 0.00881, 2.26, 2.26,
fracform(7) = 'none', fracon(1,7)= 1.0003, fracon(2,7)= 0.0017,
fracon(3,7)= 0.00001, fracon(4,7)= 0.266
priority(7)=5,

matname(8) = '9501', eosform(8) = 'jwl', strform(8) = 'none',

d0(8) = 1.84, e0(8) = 0.05543, pmin(8) = 0.0, detvel(8) = 0.88,
eoscon(1,8) = 0.38, 8.524, 8.46, 0.1802, 2.39,
y0(8) = 0.0, ymax(8) = 0.0, g0(8) = 0.0, gmax(8) = 0.0,
strcon(1,8) = 0.0,
priority(8)=8,

matname(9) = '9501', eosform(9) = 'jwl', strform(9) = 'none',
d0(9) = 1.84, e0(9) = 0.05543, pmin(9) = 0.0, detvel(9) = 0.88,
eoscon(1,9) = 0.38, 8.524, 8.46, 0.1802, 2.39,
y0(9) = 0.0, ymax(9) = 0.0, g0(9) = 0.0, gmax(9) = 0.0,
strcon(1,9) = 0.0,
priority(9)=9,

matname(10) = '9407', eosform(10) = 'jwl', strform(10) = 'none',
d0(10) = 1.6, e0(10) = 0.0538, pmin(10) = 0.0, detvel(10) = 0.791,
eoscon(1,10) = 0.32, 5.7319, 7.4, 0.14639, 2.24,
y0(10) = 0.0, ymax(10) = 0.0, g0(10) = 0.0, gmax(10) = 0.0,
strcon(1,10) = 0.0,
priority(10)=10 ,

matname(11) = '9407', eosform(11) = 'jwl', strform(11) = 'none',
d0(11) = 1.6, e0(11) = 0.0538, pmin(11) = 0.0, detvel(11) = 0.791,
eoscon(1,11) = 0.32, 5.7319, 7.4, 0.14639, 2.24,
y0(11) = 0.0, ymax(11) = 0.0, g0(11) = 0.0, gmax(11) = 0.0,
strcon(1,11) = 0.0,
priority(11)=11 ,

matname(12) = 'polyethylene', eosform(12) = 'gas', strform(12) = 'none',
d0(12) = 0.916, e0(12) = 5.4585e-07, pmin(12) = -0.000, detvel(12) = 0.0,
eoscon(1,12) = 3.0,
priority(12)=12,

matname(13) = 'polyethylene', eosform(13) = 'gas', strform(13) = 'none',
d0(13) = 0.916, e0(13) = 5.4585e-07, pmin(13) = -0.000, detvel(13) = 0.0,
eoscon(1,13) = 3.0,
priority(13)=13,

\$end

\$points

rz=

1 , 0.000 , 7.938 ,
2 , 0.000 , 6.985 ,
3 , 0.000 , 5.715 ,
4 , 0.000 , 5.080 ,
5 , 0.000 , 3.810 ,

6 , 0.000 , 2.540 ,
7 , 0.000 , -2.540 ,
8 , 0.000 , -3.810 ,
9 , 0.000 , -5.080 ,
10 , 0.000 , -5.715 ,
11 , 0.000 , -6.985 ,
12 , 0.000 , -7.938 ,
13 , 0.635 , -6.985 ,
14 , 0.635 , -5.715 ,
15 , 0.635 , 5.715 ,
16 , 0.635 , 6.985 ,
17 , 5.461 , 5.080 ,
18 , 5.461 , 3.810 ,
19 , 5.461 , 2.540 ,
20 , 5.461 , -2.540 ,
21 , 5.461 , -3.810 ,
22 , 5.461 , -5.080 ,
23 , 5.779 , -5.715 ,
24 , 5.779 , -5.080 ,
25 , 5.779 , 5.080 ,
26 , 5.779 , 5.715 ,
27 , 7.366 , 7.938 ,
28 , 7.366 , 6.350 ,
29 , 7.366 , 5.080 ,
30 , 7.366 , -5.080 ,
31 , 7.366 , -6.350 ,
32 , 7.366 , -7.938 ,
33 , 7.620 , -6.350 ,
34 , 7.620 , 6.350 ,

\$end

\$region

mat = 2,

points = 28, 29, 30, 31, 33, 34, 28,

\$end

\$region

mat = 3,

points = 17, 18, 19, 20, 21, 22, 24, 30, 29, 25, 17,

\$end

\$region

mat = 6,

points = 5, 6, 19, 18, 5,

\$end

```
$region  
mat = 7,  
points = 7, 8, 21, 20, 7,  
$end
```

```
$region  
mat = 4,  
points = 4, 5, 18, 17, 4,  
$end
```

```
$region  
mat = 5,  
points = 8, 9, 22, 21, 8,  
$end
```

```
$region  
mat = 8,  
points = 3, 4, 17, 25, 26, 15, 3,  
$end
```

```
$region  
mat = 9,  
points = 9, 10, 14, 23, 24, 22, 9,  
$end
```

```
$region  
mat = 10,  
points = 2, 3, 15, 16, 2,  
$end
```

```
$region  
mat = 11,  
points = 10, 11, 13, 14, 10,  
$end
```

```
$region  
mat = 12,  
points = 1, 2, 16, 15, 26, 25, 29, 28, 27, 1,  
$end
```

```
$region  
mat = 13,  
points = 14, 13, 11, 12, 32, 31, 30, 24, 23, 14,  
$end
```

```
$dets
detr(1)=0.0, detz(1)= -6.984, dett(1)=3.7,
detr(2)=0.0, detz(2)= 6.984, dett(2)=3.7,
$end
```

```
$parts
partr(1) = 7.493, partz(1) = 0.000,
partr(2) = 7.493, partz(2) = 0.381,
partr(3) = 7.493, partz(3) = -2.540,
```

```
$end
```

MESA

```
mesa2d (m)
0 , 0.0 , 0.0
```

```
$probsize
heburn= .true. , strength= .true. , jcdfrac=.false., jsfrac=.false. ,
mcr= 280, mcz= 360 ,
mmats= 13 , mcomp= 13 , mmix=20000,
$end
```

```
$options
mlagcyc=1 ,
part=.true.,
clean=.true.,
cleandf(12)=0.6,
cleandf(13)=0.6,
cleandf(4)=0.2,
cleandf(5)=0.2,
dtmin=0.001,
safdtc=0.25,
safdtur=0.25,
safdtuz=0.25,
safdtdiv=0.25,
safdyna=0.25,
```

```
$end
```

```
$mats
```

```
$end
```

```
$ops
ropt = 3.7, 28.7, 30.3, 30.34, 42.0,
ropdt = 0.01, 0.01, 0.01, 0.01,
```

```
mropsp=    500,   80,   2,   500,
mroplp=     0,    0,    0,    0,
mropdmp=   500,   80,   2,   500,
mroppout=   1,    1,    1,    1,
  mtps= 1, 1, 1, 1, 1, 1, 1, 0, 1, 1,
        1, 1, 1, 1, 1, 1, 1, 1, 0, 0,
        0, 0, 0,
$end
```

Johnson-Cook Strength, Johnson-Spall Fracture:

GEN

mesa2d (g)

Convergent copper cylinder system w/ jc-strength and js-frac
L=5", OD=6", t=0.1", mesh=0.05cm

\$probsize

heburn= .true. , strength= .true. , jcdfrac=.false.,

jsfrac= .true. , jhdfrac=.false.,

mcr= 260, mcz= 520,

mmats= 13 , mcomp= 13 , mmix= 25000,

\$end

\$options

ibcr1= 0 , ibcr2= 1 , ibcz1= 1 , ibcz2= 1 ,

idgeom= 2 ,

part=.true. ,

t=3.7,

\$end

\$mesh

ncellr= 200, 60,

coordr= 0.0, 10.0, 13.0,

rator= 1.0, 1.0,

ncellz= 120, 280, 120,

coordz= -13.0, -7.0, 7.0, 13.0,

ratioz= 1.0, 1.0, 1.0,

\$end

\$mats

matbak= 1 , pribak= 1,

matname(1)='air', eosform(1)='gas', strform(1)='none',

d0(1)=1.293e-03 , e0(1)=1.9335e-03 , pmin(1)=0.0,

eoscon(1)=1.4 ,

matname(2) = 'cu', eosform(2) = 'usup', strform(2) = 'j-c',

d0(2) = 8.93, e0(2) = 0.0, pmin(2) = -0.100, detvel(2) = 0.0,

eoscon(1,2) = 0.394, 1.489, 0.0, 2.02,

y0(2) = 0.00035, ymax(2) = 0.0064, g0(2) = 0.477, gmax(2) = 2.54,

strcon(1,2) = .00375, 0.0175, 0.30, 1.2, 0.00407, 0., 0.,

fracform(2) = 'js',

fracon(1,2)= 1.0003, fracon(2,2)= 0.0017,

fracon(3,2)= 0.00001, fracon(4,2)= 0.345,

priority(2)=2,

matname(3) = '9501', eosform(3) = 'jwl', strform(3) = 'none',
d0(3) = 1.84, e0(3) = 0.05543, pmin(3) = 0.0, detvel(3) = 0.88,
eoscon(1,3) = 0.38, 8.524, 8.46, 0.1802, 2.39,
y0(3) = 0.0, ymax(3) = 0.0, g0(3) = 0.0, gmax(3) = 0.0,
strcon(1,3) = 0.0,
priority(3)=3,

matname(4) = 'polyethylene', eosform(4) = 'usup', strform(4) = 'none',
d0(4) = 0.916, e0(4) = 6.6567e-07, pmin(4) = -0.010, detvel(4) = 0.0,
eoscon(1,4) = 0.266, 1.55, 0.0, 1.64,
priority(4)=6,

matname(5) = 'polyethylene', eosform(5) = 'usup', strform(5) = 'none',
d0(5) = 0.916, e0(5) = 6.6567e-07, pmin(5) = -0.010, detvel(5) = 0.0,
eoscon(1,5) = 0.266, 1.55, 0.0, 1.64,
priority(5)=7,

matname(6) = 'stainless steel(304)', eosform(6) = 'usup', strform(6) = 's-g',
d0(6) = 7.896, e0(6) = 0.0, pmin(6) = -0.10, detvel(6) = 0.0,
eoscon(1,6) = 0.457, 1.49, 0.0, 2.17,
y0(6) = 0.0034, ymax(6) = 0.025, g0(6) = 0.77, gmax(6) = 5.66,
strcon(1,6) = 43.0, 0.0, 0.35, 0.001, 0.00881, 2.26, 2.26,
fracform(6) = 'none', fracon(1,6)= 1.0003, fracon(2,6)= 0.0017,
fraccon(3,6)= 0.00001, fracon(4,6)= 0.266
priority(6)=4,

matname(7) = 'stainless steel(304)', eosform(7) = 'usup', strform(7) = 's-g',
d0(7) = 7.896, e0(7) = 0.0, pmin(7) = -0.10, detvel(7) = 0.0,
eoscon(1,7) = 0.457, 1.49, 0.0, 2.17,
y0(7) = 0.0034, ymax(7) = 0.025, g0(7) = 0.77, gmax(7) = 5.66,
strcon(1,7) = 43.0, 0.0, 0.35, 0.001, 0.00881, 2.26, 2.26,
fracform(7) = 'none', fracon(1,7)= 1.0003, fracon(2,7)= 0.0017,
fraccon(3,7)= 0.00001, fracon(4,7)= 0.266
priority(7)=5,

matname(8) = '9501', eosform(8) = 'jwl', strform(8) = 'none',
d0(8) = 1.84, e0(8) = 0.05543, pmin(8) = 0.0, detvel(8) = 0.88,
eoscon(1,8) = 0.38, 8.524, 8.46, 0.1802, 2.39,
y0(8) = 0.0, ymax(8) = 0.0, g0(8) = 0.0, gmax(8) = 0.0,
strcon(1,8) = 0.0,
priority(8)=8,

matname(9) = '9501', eosform(9) = 'jwl', strform(9) = 'none',
d0(9) = 1.84, e0(9) = 0.05543, pmin(9) = 0.0, detvel(9) = 0.88,

eoscon(1,9) = 0.38, 8.524, 8.46, 0.1802, 2.39,
y0(9) = 0.0, ymax(9) = 0.0, g0(9) = 0.0, gmax(9) = 0.0,
strcon(1,9) = 0.0,
priority(9)=9,

matname(10) = '9407', eosform(10) = 'jwl', strform(10) = 'none',
d0(10) = 1.6, e0(10) = 0.0538, pmin(10) = 0.0, detvel(10) = 0.791,
eoscon(1,10) = 0.32, 5.7319, 7.4, 0.14639, 2.24,
y0(10) = 0.0, ymax(10) = 0.0, g0(10) = 0.0, gmax(10) = 0.0,
strcon(1,10) = 0.0,
priority(10)=10 ,

matname(11) = '9407', eosform(11) = 'jwl', strform(11) = 'none',
d0(11) = 1.6, e0(11) = 0.0538, pmin(11) = 0.0, detvel(11) = 0.791,
eoscon(1,11) = 0.32, 5.7319, 7.4, 0.14639, 2.24,
y0(11) = 0.0, ymax(11) = 0.0, g0(11) = 0.0, gmax(11) = 0.0,
strcon(1,11) = 0.0,
priority(11)=11 ,

matname(12) = 'polyethylene', eosform(12) = 'gas', strform(12) = 'none',
d0(12) = 0.916, e0(12) = 5.4585e-07, pmin(12) = -0.000, detvel(12) = 0.0,
eoscon(1,12) = 3.0,
priority(12)=12,

matname(13) = 'polyethylene', eosform(13) = 'gas', strform(13) = 'none',
d0(13) = 0.916, e0(13) = 5.4585e-07, pmin(13) = -0.000, detvel(13) = 0.0,
eoscon(1,13) = 3.0,
priority(13)=13,

\$end

\$points

rz=

1 , 0.000 , 12.065 ,
2 , 0.000 , 11.113 ,
3 , 0.000 , 9.843 ,
4 , 0.000 , 8.890 ,
5 , 0.000 , 7.620 ,
6 , 0.000 , 6.350 ,
7 , 0.000 , -6.350 ,
8 , 0.000 , -7.620 ,
9 , 0.000 , -8.890 ,
10 , 0.000 , -9.843 ,
11 , 0.000 , -11.113 ,
12 , 0.000 , -12.065 ,

13 , 0.635 , -11.113 ,
14 , 0.635 , -9.843 ,
15 , 0.635 , 9.843 ,
16 , 0.635 , 11.113 ,
17 , 7.366 , 6.350 ,
18 , 7.366 , -6.350 ,
19 , 7.620 , -6.350 ,
20 , 7.620 , -5.080 ,
21 , 7.620 , 5.080 ,
22 , 7.620 , 6.350 ,
23 , 7.938 , 7.620 ,
24 , 7.938 , 5.080 ,
25 , 7.938 , -5.080 ,
26 , 7.938 , -7.620 ,
27 , 8.090 , -8.890 ,
28 , 8.090 , 8.890 ,
29 , 9.201 , 5.080 ,
30 , 9.201 , -5.080 ,
31 , 9.525 , -5.080 ,
32 , 9.525 , 5.080 ,
33 , 9.843 , 9.843 ,
34 , 9.843 , 8.255 ,
35 , 9.843 , 5.080 ,
36 , 9.843 , -5.080 ,
37 , 9.843 , -8.255 ,
38 , 9.843 , -9.843 ,
39 , 10.478 , -12.065 ,
40 , 10.478 , -8.255 ,
41 , 10.478 , 8.255 ,
42 , 10.478 , 12.065 ,

\$end

\$region

mat = 2,

points = 17, 18, 19, 20, 21, 22, 17,

\$end

\$region

mat = 3,

points = 21, 20, 25, 30, 31, 32, 29, 24, 21,

\$end

\$region

mat = 6,

points = 5, 6, 17, 22, 21, 24, 23, 5,

\$end

\$region
mat = 7,
points = 7, 8, 26, 25, 20, 19, 18, 7,
\$end

\$region
mat = 4,
points = 4, 5, 23, 24, 29, 28, 4,
\$end

\$region
mat = 5,
points = 8, 9, 27, 30, 25, 26, 8,
\$end

\$region
mat = 8,
points = 3, 4, 28, 29, 32, 35, 34, 33, 15, 3,
\$end

\$region
mat = 9,
points = 9, 10, 14, 38, 37, 36, 31, 30, 27, 9,
\$end

\$region
mat = 10,
points = 2, 3, 15, 16, 2,
\$end

\$region
mat = 11,
points = 10, 11, 13, 14, 10,
\$end

\$region
mat = 12,
points = 1, 2, 16, 15, 33, 34, 41, 42, 1,
\$end

\$region
mat = 13,
points = 14, 13, 11, 12, 39, 40, 37, 38, 14,
\$end

\$dets

```
detr(1)=0.0, detz(1)= -11.112, dett(1)=3.7,  
detr(2)=0.0, detz(2)= 11.112, dett(2)=3.7,  
$end
```

\$parts

```
partr(1) = 7.493, partz(1) = 0.000,  
partr(2) = 7.493, partz(2) = 0.381,  
partr(3) = 7.493, partz(3) = -2.540,
```

\$end

MESA

```
mesa2d (m)  
0 , 0.0 , 0.0
```

\$probsize

```
heburn= .true. , strength= .true. , jcdfrac=.false., jsfrac=.true. ,  
mcr= 260, mcz= 520 ,  
mmats= 13 , mcomp= 13, mmix=25000,  
$end
```

\$options

```
mflagcyc=1 ,  
part=.true.,  
clean=.true.,  
cleandf(12)=0.6,  
cleandf(13)=0.6,  
cleandf(4)=0.2,  
cleandf(5)=0.2,  
dtmin=0.001,  
safdtc=0.25,  
safdtur=0.25,  
safdtuz=0.25,  
safdtdiv=0.25,  
safdyna=0.25,  
$end
```

\$mats

\$end

\$ops

```
ropt = 3.7, 33.7, 37.7, 38.0, 51.0,
```

```

ropdt = 0.01, 0.01, 0.01, 0.01,
mropsp= 500, 200, 10, 500,
mroplp= 0, 0, 0, 0,
mropdmp= 500, 200, 10, 500,
mroppout= 1, 1, 1, 1,
mtps= 1, 1, 1, 1, 1, 1, 1, 0, 1, 1,
      1, 1, 1, 1, 1, 1, 1, 1, 1, 0,
      0, 0, 0,

```

\$end

GEN

mesa2d (g)

Divergent copper cylinder system w/ jc-strength and js-frac
L=5", OD=6", t=0.1", mesh=0.05cm

\$probsize

```

heburn= .true. , strength= .true. ,
jsfrac= .true. , jcdfrac=.false.,
mcr= 280, mcz= 360,
mmats= 13 , mcomp= 13 , mmix= 20000,

```

\$end

\$options

```

ibcr1= 0 , ibcr2= 1 , ibcz1= 1 , ibcz2= 1 ,
idgeom= 2 ,
part=.true. ,
t=3.7,

```

\$end

\$mesh

```

ncellr= 280,
coordr= 0.0, 14.0,
rator= 1.0,
ncellz= 360,
coordz= -9.0, 9.0,
ratioz= 1.0,

```

\$end

\$mats

```

matbak= 1 , pribak= 1,

```

```

matname(1)='air', eosform(1)='gas', strform(1)='none',
d0(1)=1.293e-03 , e0(1)=1.9335e-03 , pmin(1)=0.0,
eoscon(1)=1.4 ,

```

```

matname(2) = 'cu', eosform(2) = 'usup', strform(2) = 'j-c',

```

d0(2) = 8.93, e0(2) = 0.0, pmin(2) = -0.100, detvel(2) = 0.0,
eoscon(1,2) = 0.394, 1.489, 0.0, 2.02,
y0(2) = 0.00035, ymax(2) = 0.0064, g0(2) = 0.477, gmax(2) = 2.54,
strcon(1,2) = .00375, 0.0175, 0.30, 1.2, 0.00407, 0., 0.,
fracform(2) = 'js',
fracon(1,2)= 1.0003, fracon(2,2)= 0.0017,
fracon(3,2)= 0.00001, fracon(4,2)= 0.345,
priority(2)=3,

matname(3) = '9501', eosform(3) = 'jwl', strform(3) = 'none',
d0(3) = 1.84, e0(3) = 0.05543, pmin(3) = 0.0, detvel(3) = 0.88,
eoscon(1,3) = 0.38, 8.524, 8.46, 0.1802, 2.39,
y0(3) = 0.0, ymax(3) = 0.0, g0(3) = 0.0, gmax(3) = 0.0,
strcon(1,3) = 0.0,
priority(3)=2,

matname(4) = 'polyethylene', eosform(4) = 'usup', strform(4) = 'none',
d0(4) = 0.916, e0(4) = 6.6567e-07, pmin(4) = -0.010, detvel(4) = 0.0,
eoscon(1,4) = 0.266, 1.55, 0.0, 1.64,
priority(4)=6,

matname(5) = 'polyethylene', eosform(5) = 'usup', strform(5) = 'none',
d0(5) = 0.916, e0(5) = 6.6567e-07, pmin(5) = -0.010, detvel(5) = 0.0,
eoscon(1,5) = 0.266, 1.55, 0.0, 1.64,
priority(5)=7,

matname(6) = 'stainless steel(304)', eosform(6) = 'usup', strform(6) = 's-g',
d0(6) = 7.896, e0(6) = 0.0, pmin(6) = -0.10, detvel(6) = 0.0,
eoscon(1,6) = 0.457, 1.49, 0.0, 2.17,
y0(6) = 0.0034, ymax(6) = 0.025, g0(6) = 0.77, gmax(6) = 5.66,
strcon(1,6) = 43.0, 0.0, 0.35, 0.001, 0.00881, 2.26, 2.26,
fracform(6) = 'none', fracon(1,6)= 1.0003, fracon(2,6)= 0.0017,
fracon(3,6)= 0.00001, fracon(4,6)= 0.266
priority(6)=4,

matname(7) = 'stainless steel(304)', eosform(7) = 'usup', strform(7) = 's-g',
d0(7) = 7.896, e0(7) = 0.0, pmin(7) = -0.10, detvel(7) = 0.0,
eoscon(1,7) = 0.457, 1.49, 0.0, 2.17,
y0(7) = 0.0034, ymax(7) = 0.025, g0(7) = 0.77, gmax(7) = 5.66,
strcon(1,7) = 43.0, 0.0, 0.35, 0.001, 0.00881, 2.26, 2.26,
fracform(7) = 'none', fracon(1,7)= 1.0003, fracon(2,7)= 0.0017,
fracon(3,7)= 0.00001, fracon(4,7)= 0.266
priority(7)=5,

matname(8) = '9501', eosform(8) = 'jwl', strform(8) = 'none',

d0(8) = 1.84, e0(8) = 0.05543, pmin(8) = 0.0, detvel(8) = 0.88,
eoscon(1,8) = 0.38, 8.524, 8.46, 0.1802, 2.39,
y0(8) = 0.0, ymax(8) = 0.0, g0(8) = 0.0, gmax(8) = 0.0,
strcon(1,8) = 0.0,
priority(8)=8,

matname(9) = '9501', eosform(9) = 'jwl', strform(9) = 'none',
d0(9) = 1.84, e0(9) = 0.05543, pmin(9) = 0.0, detvel(9) = 0.88,
eoscon(1,9) = 0.38, 8.524, 8.46, 0.1802, 2.39,
y0(9) = 0.0, ymax(9) = 0.0, g0(9) = 0.0, gmax(9) = 0.0,
strcon(1,9) = 0.0,
priority(9)=9,

matname(10) = '9407', eosform(10) = 'jwl', strform(10) = 'none',
d0(10) = 1.6, e0(10) = 0.0538, pmin(10) = 0.0, detvel(10) = 0.791,
eoscon(1,10) = 0.32, 5.7319, 7.4, 0.14639, 2.24,
y0(10) = 0.0, ymax(10) = 0.0, g0(10) = 0.0, gmax(10) = 0.0,
strcon(1,10) = 0.0,
priority(10)=10 ,

matname(11) = '9407', eosform(11) = 'jwl', strform(11) = 'none',
d0(11) = 1.6, e0(11) = 0.0538, pmin(11) = 0.0, detvel(11) = 0.791,
eoscon(1,11) = 0.32, 5.7319, 7.4, 0.14639, 2.24,
y0(11) = 0.0, ymax(11) = 0.0, g0(11) = 0.0, gmax(11) = 0.0,
strcon(1,11) = 0.0,
priority(11)=11 ,

matname(12) = 'polyethylene', eosform(12) = 'gas', strform(12) = 'none',
d0(12) = 0.916, e0(12) = 5.4585e-07, pmin(12) = -0.000, detvel(12) = 0.0,
eoscon(1,12) = 3.0,
priority(12)=12,

matname(13) = 'polyethylene', eosform(13) = 'gas', strform(13) = 'none',
d0(13) = 0.916, e0(13) = 5.4585e-07, pmin(13) = -0.000, detvel(13) = 0.0,
eoscon(1,13) = 3.0,
priority(13)=13,

\$end

\$points

rz=

1 , 0.000 , 7.938 ,
2 , 0.000 , 6.985 ,
3 , 0.000 , 5.715 ,
4 , 0.000 , 5.080 ,
5 , 0.000 , 3.810 ,

6 , 0.000 , 2.540 ,
7 , 0.000 , -2.540 ,
8 , 0.000 , -3.810 ,
9 , 0.000 , -5.080 ,
10 , 0.000 , -5.715 ,
11 , 0.000 , -6.985 ,
12 , 0.000 , -7.938 ,
13 , 0.635 , -6.985 ,
14 , 0.635 , -5.715 ,
15 , 0.635 , 5.715 ,
16 , 0.635 , 6.985 ,
17 , 5.461 , 5.080 ,
18 , 5.461 , 3.810 ,
19 , 5.461 , 2.540 ,
20 , 5.461 , -2.540 ,
21 , 5.461 , -3.810 ,
22 , 5.461 , -5.080 ,
23 , 5.779 , -5.715 ,
24 , 5.779 , -5.080 ,
25 , 5.779 , 5.080 ,
26 , 5.779 , 5.715 ,
27 , 7.366 , 7.938 ,
28 , 7.366 , 6.350 ,
29 , 7.366 , 5.080 ,
30 , 7.366 , -5.080 ,
31 , 7.366 , -6.350 ,
32 , 7.366 , -7.938 ,
33 , 7.620 , -6.350 ,
34 , 7.620 , 6.350 ,

\$end

\$region

mat = 2,

points = 28, 29, 30, 31, 33, 34, 28,

\$end

\$region

mat = 3,

points = 17, 18, 19, 20, 21, 22, 24, 30, 29, 25, 17,

\$end

\$region

mat = 6,

points = 5, 6, 19, 18, 5,

\$end

```
$region
mat = 7,
points = 7, 8, 21, 20, 7,
$end
```

```
$region
mat = 4,
points = 4, 5, 18, 17, 4,
$end
```

```
$region
mat = 5,
points = 8, 9, 22, 21, 8,
$end
```

```
$region
mat = 8,
points = 3, 4, 17, 25, 26, 15, 3,
$end
```

```
$region
mat = 9,
points = 9, 10, 14, 23, 24, 22, 9,
$end
```

```
$region
mat = 10,
points = 2, 3, 15, 16, 2,
$end
```

```
$region
mat = 11,
points = 10, 11, 13, 14, 10,
$end
```

```
$region
mat = 12,
points = 1, 2, 16, 15, 26, 25, 29, 28, 27, 1,
$end
```

```
$region
mat = 13,
points = 14, 13, 11, 12, 32, 31, 30, 24, 23, 14,
$end
```

```
$dets
detr(1)=0.0, detz(1)= -6.984, dett(1)=3.7,
detr(2)=0.0, detz(2)= 6.984, dett(2)=3.7,
$end
```

```
$parts
partr(1) = 7.493, partz(1) = 0.000,
partr(2) = 7.493, partz(2) = 0.381,
partr(3) = 7.493, partz(3) = -2.540,
```

```
$end
```

MESA

```
mesa2d (m)
0 , 0.0 , 0.0
```

```
$probsize
heburn= .true. , strength= .true. , jcdffrac=.false., jsfrac=.true. ,
mcr= 280, mcz= 360 ,
mmats= 13 , mcomp= 13 , mmix=20000,
$end
```

```
$options
mlagcyc=1 ,
part=.true.,
clean=.true.,
cleandf(12)=0.6,
cleandf(13)=0.6,
cleandf(4)=0.2,
cleandf(5)=0.2,
dtmin=0.001,
safdtc=0.25,
safdtur=0.25,
safdtuz=0.25,
safdtdiv=0.25,
safdyna=0.25,
$end
```

```
$mats
$end
```

```
$ops
ropt = 3.7, 28.7, 30.3, 30.34, 42.0,
ropdt = 0.01, 0.01, 0.01, 0.01,
```



```
mropsp=    500,   80,   2,   500,  
mroplp=     0,    0,    0,    0,  
mropdmp=   500,   80,   2,   500,  
mroppout=    1,    1,    1,    1,  
  mtps= 1, 1, 1, 1, 1, 1, 1, 0, 1, 1,  
        1, 1, 1, 1, 1, 1, 1, 1, 1, 0,  
        0, 0, 0,
```

\$end

Johnson-Cook Strength, Johnson-Cook Damage:

GEN

mesa2d (g)

Convergent copper cylinder system w/ jc-strength and jc-frac
L=5", OD=6", t=0.1", mesh=0.05cm

\$probsize

heburn= .true. , strength= .true. , jcdfrac=.true.,

jsfrac= .false. , jhdfrac=.false.,

mcr= 260, mcz= 520,

mmats= 13 , mcomp= 13 , mmix= 25000,

\$end

\$options

ibcr1= 0 , ibcr2= 1 , ibcz1= 1 , ibcz2= 1 ,

idgeom= 2 ,

part=.true. ,

t=3.7,

\$end

\$mesh

ncellr= 200, 60,

coordr= 0.0, 10.0, 13.0,

rator= 1.0, 1.0,

ncellz= 120, 280, 120,

coordz= -13.0, -7.0, 7.0, 13.0,

ratioz= 1.0, 1.0, 1.0,

\$end

\$mats

matbak= 1 , pribak= 1,

matname(1)='air', eosform(1)='gas', strform(1)='none',

d0(1)=1.293e-03 , e0(1)=1.9335e-03 , pmin(1)=0.0,

eoscon(1)=1.4 ,

matname(2) = 'cu', eosform(2) = 'usup', strform(2) = 'j-c',

d0(2) = 8.93, e0(2) = 0.0, pmin(2) = -0.100, detvel(2) = 0.0,

eoscon(1,2) = 0.394, 1.489, 0.0, 2.02,

y0(2) = 0.00035, ymax(2) = 0.0064, g0(2) = 0.477, gmax(2) = 2.54,

strcon(1,2) = .00375, 0.0175, 0.30, 1.2, 0.00407, 0., 0.,

fracform(2) = 'j-c-d',

fraccon(1,2) = 0.54, 4.89, -3.03, 0.014, 1.12,

0., 0.00407, 0.033, 0.024, 1.,

priority(2)=2,

matname(3) = '9501', eosform(3) = 'jwl', strform(3) = 'none',
d0(3) = 1.84, e0(3) = 0.05543, pmin(3) = 0.0, detvel(3) = 0.88,
eoscon(1,3) = 0.38, 8.524, 8.46, 0.1802, 2.39,
y0(3) = 0.0, ymax(3) = 0.0, g0(3) = 0.0, gmax(3) = 0.0,
strcon(1,3) = 0.0,
priority(3)=3,

matname(4) = 'polyethylene', eosform(4) = 'usup', strform(4) = 'none',
d0(4) = 0.916, e0(4) = 6.6567e-07, pmin(4) = -0.010, detvel(4) = 0.0,
eoscon(1,4) = 0.266, 1.55, 0.0, 1.64,
priority(4)=6,

matname(5) = 'polyethylene', eosform(5) = 'usup', strform(5) = 'none',
d0(5) = 0.916, e0(5) = 6.6567e-07, pmin(5) = -0.010, detvel(5) = 0.0,
eoscon(1,5) = 0.266, 1.55, 0.0, 1.64,
priority(5)=7,

matname(6) = 'stainless steel(304)', eosform(6) = 'usup', strform(6) = 's-g',
d0(6) = 7.896, e0(6) = 0.0, pmin(6) = -0.10, detvel(6) = 0.0,
eoscon(1,6) = 0.457, 1.49, 0.0, 2.17,
y0(6) = 0.0034, ymax(6) = 0.025, g0(6) = 0.77, gmax(6) = 5.66,
strcon(1,6) = 43.0, 0.0, 0.35, 0.001, 0.00881, 2.26, 2.26,
fracform(6) = 'none', fracon(1,6)= 1.0003, fracon(2,6)= 0.0017,
fraccon(3,6)= 0.00001, fracon(4,6)= 0.266
priority(6)=4,

matname(7) = 'stainless steel(304)', eosform(7) = 'usup', strform(7) = 's-g',
d0(7) = 7.896, e0(7) = 0.0, pmin(7) = -0.10, detvel(7) = 0.0,
eoscon(1,7) = 0.457, 1.49, 0.0, 2.17,
y0(7) = 0.0034, ymax(7) = 0.025, g0(7) = 0.77, gmax(7) = 5.66,
strcon(1,7) = 43.0, 0.0, 0.35, 0.001, 0.00881, 2.26, 2.26,
fracform(7) = 'none', fracon(1,7)= 1.0003, fracon(2,7)= 0.0017,
fraccon(3,7)= 0.00001, fracon(4,7)= 0.266
priority(7)=5,

matname(8) = '9501', eosform(8) = 'jwl', strform(8) = 'none',
d0(8) = 1.84, e0(8) = 0.05543, pmin(8) = 0.0, detvel(8) = 0.88,
eoscon(1,8) = 0.38, 8.524, 8.46, 0.1802, 2.39,
y0(8) = 0.0, ymax(8) = 0.0, g0(8) = 0.0, gmax(8) = 0.0,
strcon(1,8) = 0.0,
priority(8)=8,

matname(9) = '9501', eosform(9) = 'jwl', strform(9) = 'none',
d0(9) = 1.84, e0(9) = 0.05543, pmin(9) = 0.0, detvel(9) = 0.88,

eoscon(1,9) = 0.38, 8.524, 8.46, 0.1802, 2.39,
y0(9) = 0.0, ymax(9) = 0.0, g0(9) = 0.0, gmax(9) = 0.0,
strcon(1,9) = 0.0,
priority(9)=9,

matname(10) = '9407', eosform(10) = 'jwl', strform(10) = 'none',
d0(10) = 1.6, e0(10) = 0.0538, pmin(10) = 0.0, detvel(10) = 0.791,
eoscon(1,10) = 0.32, 5.7319, 7.4, 0.14639, 2.24,
y0(10) = 0.0, ymax(10) = 0.0, g0(10) = 0.0, gmax(10) = 0.0,
strcon(1,10) = 0.0,
priority(10)=10 ,

matname(11) = '9407', eosform(11) = 'jwl', strform(11) = 'none',
d0(11) = 1.6, e0(11) = 0.0538, pmin(11) = 0.0, detvel(11) = 0.791,
eoscon(1,11) = 0.32, 5.7319, 7.4, 0.14639, 2.24,
y0(11) = 0.0, ymax(11) = 0.0, g0(11) = 0.0, gmax(11) = 0.0,
strcon(1,11) = 0.0,
priority(11)=11 ,

matname(12) = 'polyethylene', eosform(12) = 'gas', strform(12) = 'none',
d0(12) = 0.916, e0(12) = 5.4585e-07, pmin(12) = -0.000, detvel(12) = 0.0,
eoscon(1,12) = 3.0,
priority(12)=12,

matname(13) = 'polyethylene', eosform(13) = 'gas', strform(13) = 'none',
d0(13) = 0.916, e0(13) = 5.4585e-07, pmin(13) = -0.000, detvel(13) = 0.0,
eoscon(1,13) = 3.0,
priority(13)=13,

\$end

\$points

rz=

1 , 0.000 , 12.065 ,
2 , 0.000 , 11.113 ,
3 , 0.000 , 9.843 ,
4 , 0.000 , 8.890 ,
5 , 0.000 , 7.620 ,
6 , 0.000 , 6.350 ,
7 , 0.000 , -6.350 ,
8 , 0.000 , -7.620 ,
9 , 0.000 , -8.890 ,
10 , 0.000 , -9.843 ,
11 , 0.000 , -11.113 ,
12 , 0.000 , -12.065 ,

13 , 0.635 , -11.113 ,
14 , 0.635 , -9.843 ,
15 , 0.635 , 9.843 ,
16 , 0.635 , 11.113 ,
17 , 7.366 , 6.350 ,
18 , 7.366 , -6.350 ,
19 , 7.620 , -6.350 ,
20 , 7.620 , -5.080 ,
21 , 7.620 , 5.080 ,
22 , 7.620 , 6.350 ,
23 , 7.938 , 7.620 ,
24 , 7.938 , 5.080 ,
25 , 7.938 , -5.080 ,
26 , 7.938 , -7.620 ,
27 , 8.090 , -8.890 ,
28 , 8.090 , 8.890 ,
29 , 9.201 , 5.080 ,
30 , 9.201 , -5.080 ,
31 , 9.525 , -5.080 ,
32 , 9.525 , 5.080 ,
33 , 9.843 , 9.843 ,
34 , 9.843 , 8.255 ,
35 , 9.843 , 5.080 ,
36 , 9.843 , -5.080 ,
37 , 9.843 , -8.255 ,
38 , 9.843 , -9.843 ,
39 , 10.478 , -12.065 ,
40 , 10.478 , -8.255 ,
41 , 10.478 , 8.255 ,
42 , 10.478 , 12.065 ,

\$end

\$region

mat = 2,

points = 17, 18, 19, 20, 21, 22, 17,

\$end

\$region

mat = 3,

points = 21, 20, 25, 30, 31, 32, 29, 24, 21,

\$end

\$region

mat = 6,

points = 5, 6, 17, 22, 21, 24, 23, 5,

\$end

```
$region
mat = 7,
points = 7, 8, 26, 25, 20, 19, 18, 7,
$end
```

```
$region
mat = 4,
points = 4, 5, 23, 24, 29, 28, 4,
$end
```

```
$region
mat = 5,
points = 8, 9, 27, 30, 25, 26, 8,
$end
```

```
$region
mat = 8,
points = 3, 4, 28, 29, 32, 35, 34, 33, 15, 3,
$end
```

```
$region
mat = 9,
points = 9, 10, 14, 38, 37, 36, 31, 30, 27, 9,
$end
```

```
$region
mat = 10,
points = 2, 3, 15, 16, 2,
$end
```

```
$region
mat = 11,
points = 10, 11, 13, 14, 10,
$end
```

```
$region
mat = 12,
points = 1, 2, 16, 15, 33, 34, 41, 42, 1,
$end
```

```
$region
mat = 13,
points = 14, 13, 11, 12, 39, 40, 37, 38, 14,
$end
```

\$dets

detr(1)=0.0, detz(1)= -11.112, dett(1)=3.7,
detr(2)=0.0, detz(2)= 11.112, dett(2)=3.7,
\$end

\$parts

partr(1) = 7.493, partz(1) = 0.000,
partr(2) = 7.493, partz(2) = 0.381,
partr(3) = 7.493, partz(3) = -2.540,

\$end

MESA

mesa2d (m)
0 , 0.0 , 0.0

\$probsize

heburn= .true. , strength= .true. , jcdfrac=.true., jsfrac=.false. ,
mcr= 260, mcz= 520 ,
mmats= 13 , mcomp= 13, mmix=25000,
\$end

\$options

mlagcyc=1 ,
part=.true.,
clean=.true.,
cleandf(12)=0.6,
cleandf(13)=0.6,
cleandf(4)=0.2,
cleandf(5)=0.2,
dtmin=0.001,
safdtc=0.25,
safdtur=0.25,
safdtuz=0.25,
safdtdiv=0.25,
safdyna=0.25,
\$end

\$mats

\$end

\$ops

ropt = 3.7, 33.7, 37.7, 38.0, 51.0,

```
ropdt = 0.01, 0.01, 0.01, 0.01,
mropsp= 500, 200, 10, 500,
mroplp= 0, 0, 0, 0,
mropdmp= 500, 200, 10, 500,
mroppout= 1, 1, 1, 1,
mtps= 1, 1, 1, 1, 1, 1, 1, 0, 1, 1,
      1, 1, 1, 1, 1, 1, 1, 1, 0, 1,
      0, 0, 0,
```

\$end

GEN

mesa2d (g)

Divergent copper cylinder system w/ jc-strength and jc-frac
L=5", OD=6", t=0.1", mesh=0.05cm

\$probsize

```
heburn= .true. , strength= .true. ,
jsfrac= .false. , jcdfrac=.true.,
mcr= 280, mcz= 360,
mmats= 13 , mcomp= 13 , mmix= 20000,
```

\$end

\$options

```
ibcr1= 0 , ibcr2= 1 , ibcz1= 1 , ibcz2= 1 ,
idgeom= 2 ,
part=.true. ,
t=3.7,
```

\$end

\$mesh

```
ncellr= 280,
coordr= 0.0, 14.0,
rator= 1.0,
ncellz= 360,
coordz= -9.0, 9.0,
ratioz= 1.0,
```

\$end

\$mats

```
matbak= 1 , pribak= 1,
```

```
matname(1)='air', eosform(1)='gas', strform(1)='none',
d0(1)=1.293e-03 , e0(1)=1.9335e-03 , pmin(1)=0.0,
eoscon(1)=1.4 ,
```

```
matname(2) = 'cu', eosform(2) = 'usup', strform(2) = 'j-c',
```


d0(2) = 8.93, e0(2) = 0.0, pmin(2) = -0.100, detvel(2) = 0.0,
eoscon(1,2) = 0.394, 1.489, 0.0, 2.02,
y0(2) = 0.00035, ymax(2) = 0.0064, g0(2) = 0.477, gmax(2) = 2.54,
strcon(1,2) = .00375, 0.0175, 0.30, 1.2, 0.00407, 0., 0.,
fracform(2) = 'j-c-d',
fracon(1,2) = 0.54, 4.89, -3.03, 0.014, 1.12,
0., 0.00407, 0.033, 0.024, 1.0,
priority(2)=3,

matname(3) = '9501', eosform(3) = 'jwl', strform(3) = 'none',
d0(3) = 1.84, e0(3) = 0.05543, pmin(3) = 0.0, detvel(3) = 0.88,
eoscon(1,3) = 0.38, 8.524, 8.46, 0.1802, 2.39,
y0(3) = 0.0, ymax(3) = 0.0, g0(3) = 0.0, gmax(3) = 0.0,
strcon(1,3) = 0.0,
priority(3)=2,

matname(4) = 'polyethylene', eosform(4) = 'usup', strform(4) = 'none',
d0(4) = 0.916, e0(4) = 6.6567e-07, pmin(4) = -0.010, detvel(4) = 0.0,
eoscon(1,4) = 0.266, 1.55, 0.0, 1.64,
priority(4)=6,

matname(5) = 'polyethylene', eosform(5) = 'usup', strform(5) = 'none',
d0(5) = 0.916, e0(5) = 6.6567e-07, pmin(5) = -0.010, detvel(5) = 0.0,
eoscon(1,5) = 0.266, 1.55, 0.0, 1.64,
priority(5)=7,

matname(6) = 'stainless steel(304)', eosform(6) = 'usup', strform(6) = 's-g',
d0(6) = 7.896, e0(6) = 0.0, pmin(6) = -0.10, detvel(6) = 0.0,
eoscon(1,6) = 0.457, 1.49, 0.0, 2.17,
y0(6) = 0.0034, ymax(6) = 0.025, g0(6) = 0.77, gmax(6) = 5.66,
strcon(1,6) = 43.0, 0.0, 0.35, 0.001, 0.00881, 2.26, 2.26,
fracform(6) = 'none', fracon(1,6)= 1.0003, fracon(2,6)= 0.0017,
fracon(3,6)= 0.00001, fracon(4,6)= 0.266
priority(6)=4,

matname(7) = 'stainless steel(304)', eosform(7) = 'usup', strform(7) = 's-g',
d0(7) = 7.896, e0(7) = 0.0, pmin(7) = -0.10, detvel(7) = 0.0,
eoscon(1,7) = 0.457, 1.49, 0.0, 2.17,
y0(7) = 0.0034, ymax(7) = 0.025, g0(7) = 0.77, gmax(7) = 5.66,
strcon(1,7) = 43.0, 0.0, 0.35, 0.001, 0.00881, 2.26, 2.26,
fracform(7) = 'none', fracon(1,7)= 1.0003, fracon(2,7)= 0.0017,
fracon(3,7)= 0.00001, fracon(4,7)= 0.266
priority(7)=5,

matname(8) = '9501', eosform(8) = 'jwl', strform(8) = 'none',

d0(8) = 1.84, e0(8) = 0.05543, pmin(8) = 0.0, detvel(8) = 0.88,
eoscon(1,8) = 0.38, 8.524, 8.46, 0.1802, 2.39,
y0(8) = 0.0, ymax(8) = 0.0, g0(8) = 0.0, gmax(8) = 0.0,
strcon(1,8) = 0.0,
priority(8)=8,

matname(9) = '9501', eosform(9) = 'jwl', strform(9) = 'none',
d0(9) = 1.84, e0(9) = 0.05543, pmin(9) = 0.0, detvel(9) = 0.88,
eoscon(1,9) = 0.38, 8.524, 8.46, 0.1802, 2.39,
y0(9) = 0.0, ymax(9) = 0.0, g0(9) = 0.0, gmax(9) = 0.0,
strcon(1,9) = 0.0,
priority(9)=9,

matname(10) = '9407', eosform(10) = 'jwl', strform(10) = 'none',
d0(10) = 1.6, e0(10) = 0.0538, pmin(10) = 0.0, detvel(10) = 0.791,
eoscon(1,10) = 0.32, 5.7319, 7.4, 0.14639, 2.24,
y0(10) = 0.0, ymax(10) = 0.0, g0(10) = 0.0, gmax(10) = 0.0,
strcon(1,10) = 0.0,
priority(10)=10 ,

matname(11) = '9407', eosform(11) = 'jwl', strform(11) = 'none',
d0(11) = 1.6, e0(11) = 0.0538, pmin(11) = 0.0, detvel(11) = 0.791,
eoscon(1,11) = 0.32, 5.7319, 7.4, 0.14639, 2.24,
y0(11) = 0.0, ymax(11) = 0.0, g0(11) = 0.0, gmax(11) = 0.0,
strcon(1,11) = 0.0,
priority(11)=11 ,

matname(12) = 'polyethylene', eosform(12) = 'gas', strform(12) = 'none',
d0(12) = 0.916, e0(12) = 5.4585e-07, pmin(12) = -0.000, detvel(12) = 0.0,
eoscon(1,12) = 3.0,
priority(12)=12,

matname(13) = 'polyethylene', eosform(13) = 'gas', strform(13) = 'none',
d0(13) = 0.916, e0(13) = 5.4585e-07, pmin(13) = -0.000, detvel(13) = 0.0,
eoscon(1,13) = 3.0,
priority(13)=13,

\$end

\$points

rz=

1 , 0.000 , 7.938 ,
2 , 0.000 , 6.985 ,
3 , 0.000 , 5.715 ,
4 , 0.000 , 5.080 ,
5 , 0.000 , 3.810 ,

6 , 0.000 , 2.540 ,
7 , 0.000 , -2.540 ,
8 , 0.000 , -3.810 ,
9 , 0.000 , -5.080 ,
10 , 0.000 , -5.715 ,
11 , 0.000 , -6.985 ,
12 , 0.000 , -7.938 ,
13 , 0.635 , -6.985 ,
14 , 0.635 , -5.715 ,
15 , 0.635 , 5.715 ,
16 , 0.635 , 6.985 ,
17 , 5.461 , 5.080 ,
18 , 5.461 , 3.810 ,
19 , 5.461 , 2.540 ,
20 , 5.461 , -2.540 ,
21 , 5.461 , -3.810 ,
22 , 5.461 , -5.080 ,
23 , 5.779 , -5.715 ,
24 , 5.779 , -5.080 ,
25 , 5.779 , 5.080 ,
26 , 5.779 , 5.715 ,
27 , 7.366 , 7.938 ,
28 , 7.366 , 6.350 ,
29 , 7.366 , 5.080 ,
30 , 7.366 , -5.080 ,
31 , 7.366 , -6.350 ,
32 , 7.366 , -7.938 ,
33 , 7.620 , -6.350 ,
34 , 7.620 , 6.350 ,

\$end

\$region

mat = 2,
points = 28, 29, 30, 31, 33, 34, 28,
\$end

\$region

mat = 3,
points = 17, 18, 19, 20, 21, 22, 24, 30, 29, 25, 17,
\$end

\$region

mat = 6,
points = 5, 6, 19, 18, 5,
\$end

\$region
mat = 7,
points = 7, 8, 21, 20, 7,
\$end

\$region
mat = 4,
points = 4, 5, 18, 17, 4,
\$end

\$region
mat = 5,
points = 8, 9, 22, 21, 8,
\$end

\$region
mat = 8,
points = 3, 4, 17, 25, 26, 15, 3,
\$end

\$region
mat = 9,
points = 9, 10, 14, 23, 24, 22, 9,
\$end

\$region
mat = 10,
points = 2, 3, 15, 16, 2,
\$end

\$region
mat = 11,
points = 10, 11, 13, 14, 10,
\$end

\$region
mat = 12,
points = 1, 2, 16, 15, 26, 25, 29, 28, 27, 1,
\$end

\$region
mat = 13,
points = 14, 13, 11, 12, 32, 31, 30, 24, 23, 14,
\$end

```
$dets
detr(1)=0.0, detz(1)= -6.984, dett(1)=3.7,
detr(2)=0.0, detz(2)= 6.984, dett(2)=3.7,
$end
```

```
$parts
partr(1) = 7.493, partz(1) = 0.000,
partr(2) = 7.493, partz(2) = 0.381,
partr(3) = 7.493, partz(3) = -2.540,
```

```
$end
```

MESA

```
mesa2d (m)
0 , 0.0 , 0.0
```

```
$probsize
heburn= .true. , strength= .true. , jcdfrac=.true., jsfrac=.false. ,
mcr= 280, mcz= 360 ,
mmats= 13 , mcomp= 13 , mmix=20000,
$end
```

```
$options
mlagcyc=1 ,
part=.true.,
clean=.true.,
cleandf(12)=0.6,
cleandf(13)=0.6,
cleandf(4)=0.2,
cleandf(5)=0.2,
dtmin=0.001,
safdtc=0.25,
safdtur=0.25,
safdtuz=0.25,
safdtdiv=0.25,
safdyna=0.25,
$end
```

```
$mats
$end
```

```
$ops
ropt = 3.7, 28.7, 30.3, 30.34, 42.0,
ropdt = 0.01, 0.01, 0.01, 0.01,
```

```
mrovsp=    500,   80,   2,   500,
mrovlp=     0,    0,   0,    0,
mrovdmp=   500,   80,   2,   500,
mrovpout=   1,    1,   1,    1,
  mtps= 1, 1, 1, 1, 1,  1, 1, 0, 1, 1,
        1, 1, 1, 1, 1,  1, 1, 1, 0, 1,
        0, 0, 0,
$end
```